TRANSIENT ANALYSIS OF PROPENE PARTIAL OXIDATION OVER IRON ANTIMONY OXIDE

Mgcini Tshwaku
BSc (UFH), BSc. Eng. (Chem) (UCT).

Submitted to University of Cape Town

In fulfilment of the requirements for

Master of Science.

Department of Chemical Engineering
University of Cape Town
Rondebosch
Cape Town
South Africa

June 2000

This thesis is dedicated to my beloved uncle, ***Valithuba Tshwaku.***

Your mother, Nosithile Tshwaku, family and I will always miss you.

Rest in peace, Hlathi, the great one.

ACKNOWLEDGEMENTS

To my supervisor Dr. Klaus Möller and co-supervisor Dr. Eric van Steen, thank you for sharing wisdom and advice with me. It will not be forgotten.

Many thanks to Peter Dobias, Joachim Macke and Granville de la Cruz for being there when I needed the materials of construction and electrical equipment. Thanks to Dr Michael Claeys for helping me with the G.C. Not forgetting Nelli Dili for her help with the administration and support. Her jokes cheered my days during the doldrum of research. Also many thanks to Pam and Lorna for making sure that the Catalysis unit administration side runs smoothly. To my sister Dr Noxolo Tshwaku and her fiancée Mr Simphiwe Makasi, thanks for making sure that my stay in Cape Town is pleasant, you guys are the best. A special word of gratitude goes to Gigi Mthembu, thank you so very much. To my great friends: Sandile Roro, Xolile Khahla and Phuthuma Khahla, point taken, you all stay real.

Last but certainly not the least, to my family Mandisa Tshwaku (Mother), Nosithile Tshwaku (Grandma), Dr Novuyise Tshwaku (aunt) and Vuyokazi Tshwaku(aunt), thank you for loving and taking care of me all these years, until I changed from a boy to man. I love you all. Not forgetting my uncle Mr Valithuba Tshwaku, who passed away recently, to whom this thesis is dedicated.

To God and Jesus my Lord and saviour I give thanks.

SYNOPSIS

The main purpose of this work was to investigate propene partial oxidation at steady state and transient mode over an iron antimonate catalyst of Sb/Fe=1.5:1 and to formulate a transient kinetic simulation for the reaction. The literature review revealed that propene partial oxidation over $FeSbO_4$ on a cyclic fixed bed operation should be beneficial. The prepared $FeSbO_4$ catalyst contained the rutile $FeSbO_4$, α-Sb_2O_4, β-Sb_2O_4 and Fe_2O_3 phases and had a surface area of $6.8m^2/g$ with a mean pore size of 200 Å.

The experiments were carried out in a fixed bed reactor at 375°C at a WHSV of $1.2hr^{-1}$ using a 1min sampling interval which allowed resolution of all time dependent behaviour. The cyclic experiments were carried out by switching propene in and out of the reactor. A single site mechanism along with a CSTR assumption was developed to qualitatively simulate steady state and cyclic behaviour. Experimental results show that the initial acrolein yield was always lower than that of CO_x. However, acrolein yield improved with time on stream to exceed that of CO_x. In all cases yields of all the products decreased with time on stream to reach steady state after 20 min. Cyclic experiments showed the same qualitative trends. However, long oxidation times were beneficial in re-oxidising the catalyst and thus producing a high yield of acrolein, as for the steady state operation, however, this increase was only marginal.

The reactor model was qualitatively able to reproduce the trends observed in the experimental data. It was also shown qualitatively that many O_2 layers of the lattice are involved in the oxidation of propene and that the oxidation of these layers was responsible for the slow decrease of the yield with time on stream.

TABLE OF CONTENTS

LIST OF FIGURES

LIST OF TABLES

1 INTRODUCTION

Selective hydrocarbon oxidation reactions involve the insertion of oxygen into the hydrocarbon chain in the presence of a catalyst. These reactions take place mainly on olefins and aromatics and constituents more than half the worlds organic chemical production.

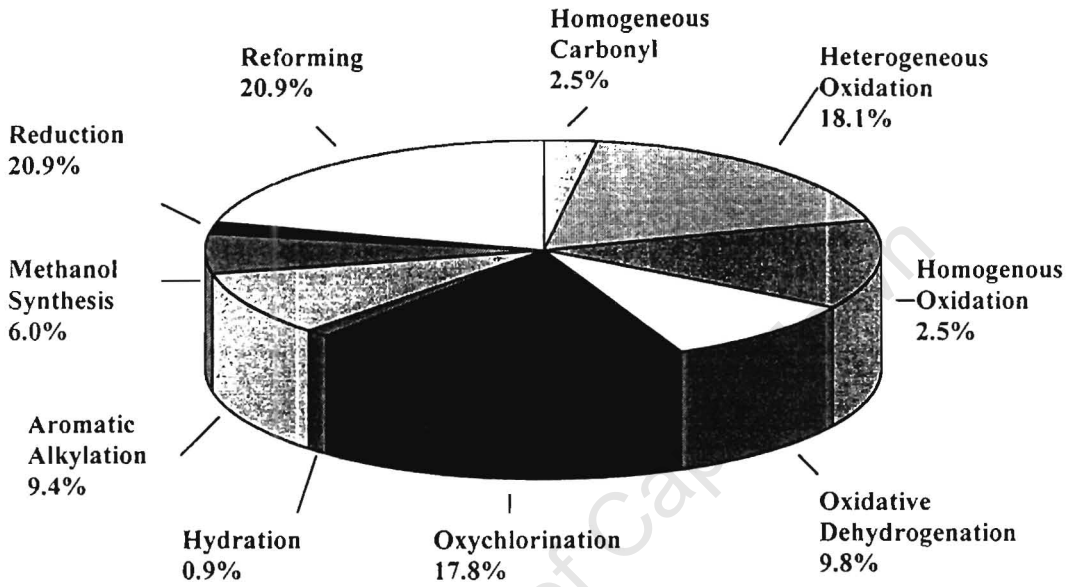

Figure 1.1 Production of major organic chemicals in the United States in 1991 [Oyama et al.1993]

The oxidation catalyst promotes the reactivity of oxygen, such that reactions can take place under mild, easily controlled conditions. Above all, the catalyst introduces selectivity and reduces the amount of carbon dioxide formed. It is easy to lose control of the oxidation process so that the carbon dioxide and water are the only significant products formed. The free energy and the enthalpy for total oxidation are favourably large such that the balance between a selective oxidation process and more complete oxidative degradation is controlled by kinetics. Catalytic oxidation reactions are carried out in the homogeneous liquid phase, the heterogeneous liquid phase and the heterogeneous gas phase reaction.

Oxidation reactions can be classified into four types.

(i) The introduction of oxygen as a functional group.

$$CH_3\text{-}CH{=}CH_2 + O_2 \rightarrow CH_2{=}CH\text{-}CHO + H_2O \qquad 1.1$$

(ii) The oxidative removal of hydrogen.

CH_2=CH-CH_2 -CH_3 + O_2 → CH_2=CH-CH_2=CH_3 + H_2O 1.2

(iii) Formation of nitriles through oxidative coupling with ammonia.

CH_2-$CHCH_2$ + NH_3 + 1.5 O_2 → CH_2 CH-CHN +3 H_2O 1.3

(iv) Complex oxidation to carbon dioxide/monoxide and water as the major or only products.

In the partial oxidation of hydrocarbons it becomes desirable to substitute olefins with paraffin as a raw material because of their low price e.g. production of maleic anhydride from oxidation of n-butane over vanadium-phosphate–oxide (VPO)), and the production of aldehydes, alcohols and ketones. However, South Africa produces large amounts of olefins from syngas by the Fischer-Tropsch process [Schnobel et al 1997]. These α-olefins are either sold as chemicals or converted into gasoline and diesel. The process would become more profitable if the α-olefins were converted into higher value chemicals. Partial oxidation of α-olefins is one route to produce these high value chemicals.

2 LITERATURE REVIEW

2.1 INDUSTRIAL PRODUCTION OF ACROLEIN.

Deggussa developed the first industrial acrolein synthesis in the early 1930's, and began production in 1942. In 1991, the capacity for acrolein manufacture world-wide was about 128000 tonnes per year 54000,23000, and 11000 tonnes per year were produced in Western Europe, United States of America, and Japan, respectively. The classical process was based on the condensation of acetaldehyde with formaldehyde [Weissermel et al. 1997].

$$CH_3CHO + HCHO \rightarrow H_2C = CH\text{-}CHO + H_2O \quad \Delta H_R\,(298K) = -84\ kJ/mol \qquad (2.1)$$

Reaction 2.1 occurs at 300-320°C in the gas phase over silica. Currently the production of acrolein is obtained by the catalytic oxidation of propene (Reaction 2.2).

$$CH_2CHCH_2 + O_2 \rightarrow H_2CCH\text{-}CHO + H_2O \quad \Delta H_R\,(298K) = -368\ kJ/mol \qquad (2.2)$$

Shell was the first company to practice this gas phase oxidation in a commercial unit (1958-1980). The reaction was carried out at 350 – 400°C over Cu_2O/SiC with I_2 as the promoter. The unit operates at 20% conversion and 70- 85% selectivity to acrolein.

[Weissermel et al.1997].

In 1957 Standard Oil of Ohio discovered the bismuthmolybdate and phosphomolybdate catalysts which enable the company to produce high yields of acrolein at high propene conversions (>90%) and pressures close to atmospheric conditions [Callahan et al. 1990]. Many key improvements and enhancements to the bismuth molybdate based propylene oxidation catalysts have occurred over the past thirty years. Other catalysts have also received attention, these include tin-antimony oxide, uranium–antimony oxide and iron antimony oxide [Aso et al 1980]. The iron antimony oxide catalyst is a preferred industrial catalyst for the manufacture of acrolein [Weissermel et al. 1997].

2.2 REACTOR TECHNOLOGY FOR PRODUCTION OF ACROLEIN

2.2.1 Industrial steady state reactors.

Propene is oxidised to acrolein in the presence of steam and air at 330-370°C and 1- 2 bar. The reaction is exothermic and is conducted in a fixed bed reactor with up to 22000 tube per reactor. Sohio in 1959 – 1960 used a supported bismuth phospho-molybdate catalyst in a fluidised bed operated at 425°C. The feed stream was propylene/air/steam at a WHSV of 3 sec^{-1}. A conversion of 57% was measured at acrolein selectivity of 72%. Thus the advantage of this catalyst was that the reaction could be run at high single pass yields. Now the catalyst performance has been improved over the years and the present-day bismuth molybdate catalysts are very complex and are suitable for fixed-bed or fluidised bed applications. The latter is preferred for large capacity installations. The catalyst lifetime can be as long as three years.

The industrial Sohio process uses approximately stoichiometric feeds of propene and ammonia and a slight excess of air and water in a fluidised reactor operated at 450°C and 1.5 bar to produce acrolein and acrylonitrile. During partial oxidation of propene a lot of heat is released and is removed from the reactor by heat exchangers i.e. perpendicularly arranged coiled pipes through which the water is circulated are used to generate steam. BP (Distillers) oxidise propene in the presence of Se/ CuO catalyst to acrolein and convert this to acrylonitrile in a second stage by the addition of NH_3 and air over MoO_3 fixed-bed catalyst. An acrolein selectivity of about 90% is obtained on this process.

In the Montedison process, propene is oxidised in a fluidised bed reactor at 420°C over a catalyst consisting of Te, Ce and Mo-oxide on SiO_2. The acrolein yield attained was 80% at a propene conversion of about 95% [Weissermel et al. 1997].

2.2.2 Conceptual industrial transient reactors.

This section describes a forced unsteady-state operation technique as employed for continuous processes, which represent the majority of heterogeneous catalysis applications. The catalyst life in these processes often lasts several years. Traditional operation is steady state, and automatic control systems are needed to eliminate any fluctuations in performance parameters.

The main goal of a traditional design is to obtain the optimal steady-state conditions, which provide maximum use of catalyst properties as constrained by the process economy. The reactor at optimal steady-state conditions does not determine a potential limit for a heterogeneous catalytic system. This performance can be improved further by using forced unsteady-state operation. Various schemes of reactor operation under forced unsteady state conditions are shown in figure 2.1and 2.2.

An unsteady-state in a fixed bed reactor can be created by oscillations in the inlet composition or temperature. A stepwise periodic control is preferred as compared to other types of inlet parameter forcing (e.g. sine wave) due to its simplicity to be performed and can affect the system more strongly than any other smooth type of control.

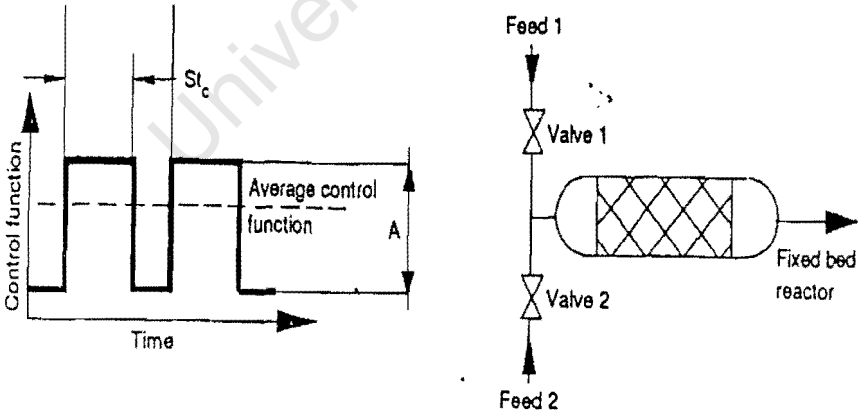

A = amplitude t_c= time of cycle S = split of inlet signal

Figure 2.1 (a) Step-wise of inlet parameters change. (b) Fixed-bed reactor operated at periodic switching between two different feeds that provide for step-wise control.

A most widely used applied technique in a fixed bed reactor is a periodical flow reversal (Figure 2.2(a)), four switching valves are used to provide control for the operation. In a rotatory reactor (Figure 2.2(b)) with plate type catalyst, the catalyst bed position is continuously changed relative to the stationary direction of flow, thereby achieving an effect similar to a flow reversal reactor. Reactor (a) and (b) provide for a continuous migration of temperature or adsorption zone along the catalyst bed. The direction of this zone is changed periodically. Figure2.2(c) provides the possibility of moving zone in one direction through a system with two catalyst beds.

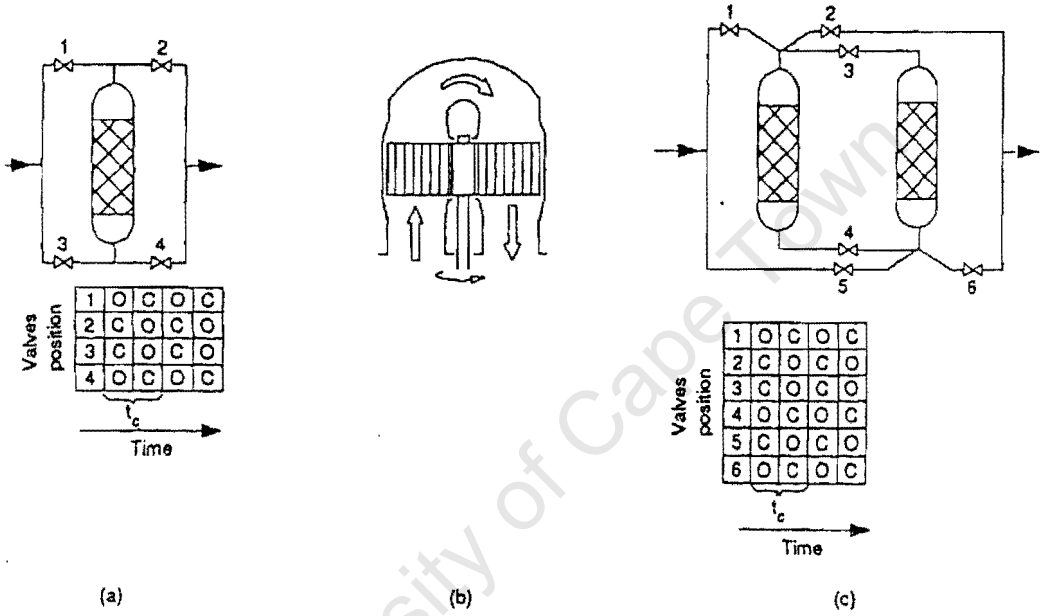

Figure 2.2 Schemes of fixed bed reactors operated under forced unsteady-state conditions: (a) Reverse flow reactor; (b) Rotary reactor; (c) Reactor system with periodic changes between the inlet and outlet ports of two fixed beds.

Lewis et al. [1949] proposed a system of two fluidised beds and a catalyst transfer via a pneumatic lift as shown in figure 2.3.

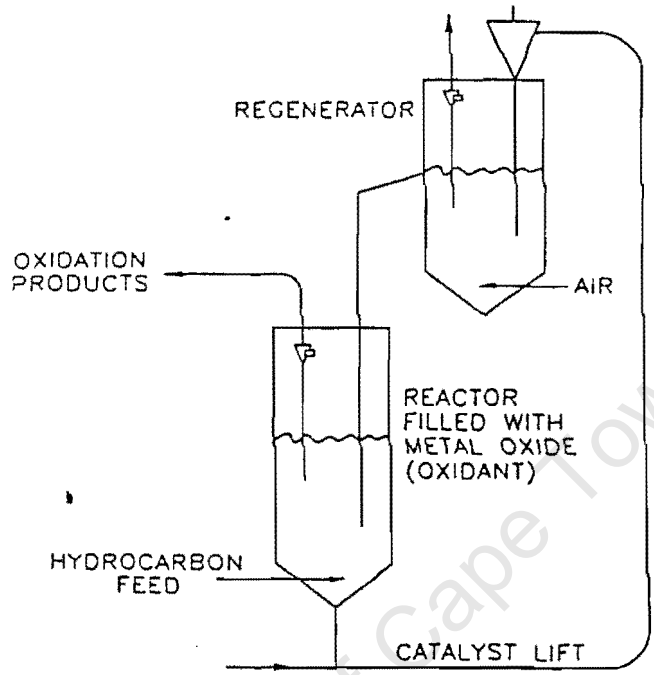

Figure 2.3 Conceptual system for composition forcing of partial oxidation reactions using fluidised beds with catalyst transfer between the beds [Lewis et al. 1949].

On one of the beds the hydrocarbon is selectively oxidised while the catalyst is reduced. The second bed is fluidised with air/O_2 and re-oxidises the catalyst. Increased hydrocarbon concentrations are possible, hence the formation of hot spots leading to temperature runaways is minimised. Furthermore, the catalyst oxidation and reduction steps are carried out at different temperatures to minimise contact times, because each step occurs in a different reactor. The amount of heat released is lower than when carried out on a single reactor system. Using the technique described above Du Pont Company commissioned a two bed circulating catalyst scheme, for maleic anhydride production as shown in figure 2.4.

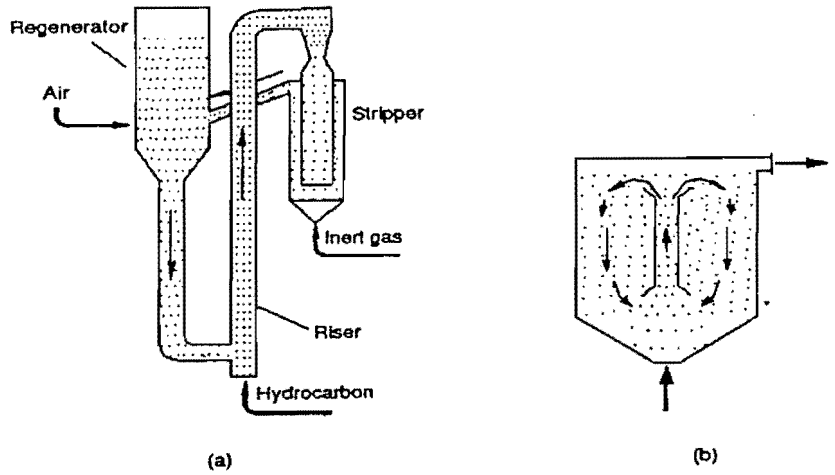

Figure 2.4 Reactors with fluidised bed for partial oxidation process: Du Pont system for maleic anhydride production combining riser, fluidise bed regenerator, and stripper;(b) fluidised-bed reactor with internal catalyst circulation. [Contractor et al. 1997]

Chang et al. [1999] Investigated superiority of reverse-flow catalytic oxidation reactor against a conventional single pass fixed bed reactor for the combustion of volatile organic compounds in gaseous industrial effluents. The investigation was carried out by allowing a step input of temperature into the system as shown in Figure 2.5. Auto-thermal operation, through periodic reversal of flow direction in the reactor, traps the heat of reaction within the catalyst bed and the insulated regenerator regions present on either side of the reactor, removing the need for preheating and maintaining the entire bed in an ignited state.

Reverse flow reactor operation can be thermally unstable at longer periods of time and can lead to concentrated energy accumulation within very localised hot spots in the bed. Figure 2.5 depicts that imbedding metal rods in the reactor eventually stabilises the bed against hot spot formation.

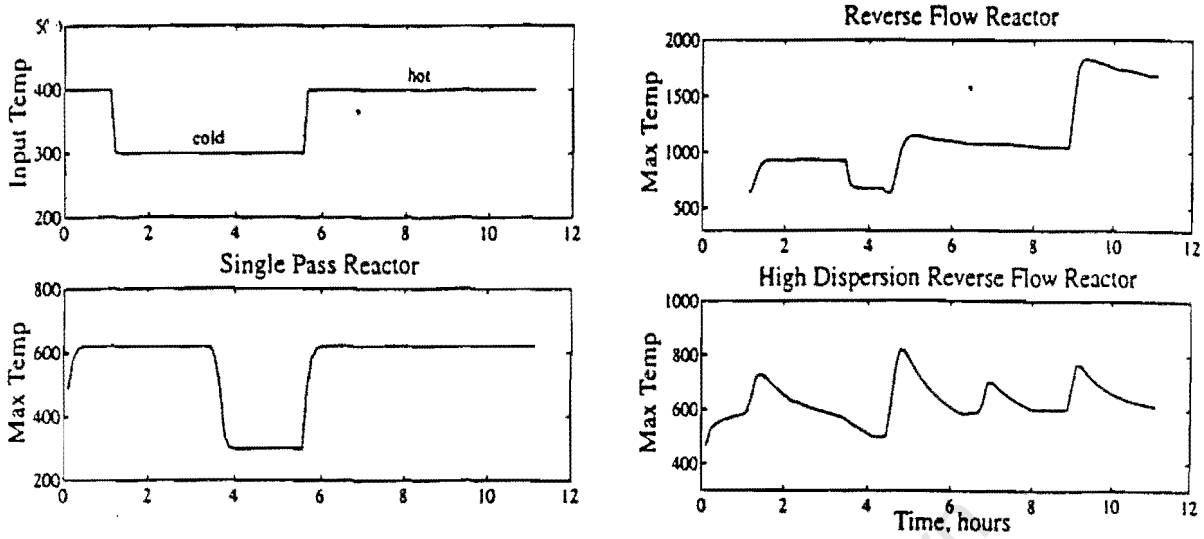

Figure 2.5 Responses of three types of reactor designs to a step-in temperature feed. Under these conditions the single pass catalytic reactor extinguishes, the reverse-flow reactor exhibits thermal runaway, and the high dispersion reactor remains stable. [Chang et al. 1999]

Pak et al. [1986] designed a multi-tubular circulating solid fluidised bed reactor, figure.2.6, in which the hydrocarbon and air are contacting in a single step.

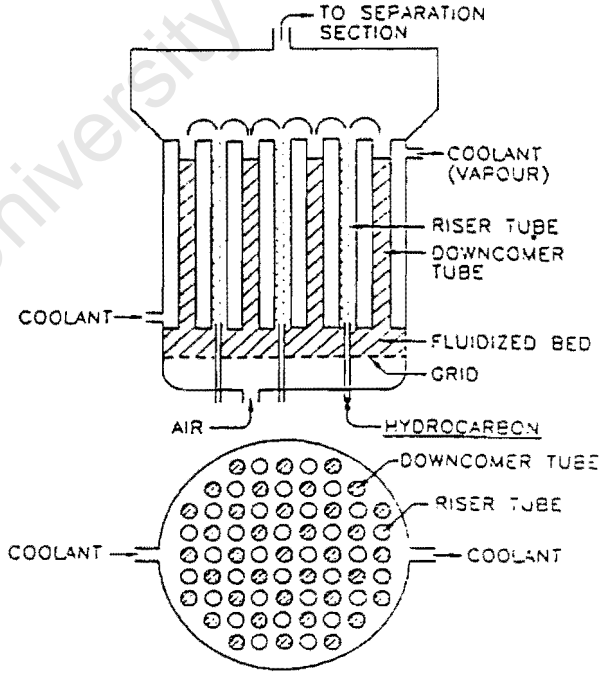

Figure 2.6 Multi-tubular reactor proposed for partial oxidation under periodic operation. [Pak et al. 1986]

On the design the hydrocarbon feed carries the catalyst upward in one group of tubes and it descends in airflow in the second group of tubes into a fluidised bed of air, where the catalyst is deoxidised. The design offers the advantage of a single vessel but at the expense of downstream separation steps, because the oxidant streams mix in the reactor effluent. It is also disadvantageous that there is a high possibility of a detonation zone.

2.3 COMMERCIAL APPLICATION OF ACROLEIN

Acrolein has several reactive sites, the aldehyde group, the olefinic double bond and the conjugated double bond system, and thus a number of reactions are possible. For example, the reduction of acrolein to ally alcohol and its further conversion to glycol is a commercial process. The formation of Pyridine and 3-picoline are from acrolein reacting with ammonia over multicomponent catalysts Al_2O_3 or $Al_2O_3 \bullet SiO_2$. Acrolein is used for the manufacturing of methionine, the essential amino acid used for supplementing the protein concentrate in animal feed, in particular for feed optimisation in poultry breeding. Acrolein is an important building block in the pharmaceutical industry. It is also used in the manufacture of a new polyester, poly (trimethylene terephthalate).

2.3.1 Acrylic acid production

Japan, USA, England and France, developed a two step process for the production of acrylic acid and ester derivatives. Propene is oxidised to acrolein in the presence of steam and oxygen and the products are further processed to acrylic acid. In the last few years acrylic acid and ester derivatives have been ranked first in growth among the unsaturated organic acids and esters. The world production in 1994 was estimated to be 2×10^6 tonnes per year. The largest producer is BASF in Germany. In a single step, propene is directly oxidised with air or oxygen (sometimes with steam) at 10 bar and 200- 250^{0}C, depending on the catalyst employed. Acrolein and acrylic acid are formed together [Wesseirmel et al. 1997].

$$H_2CCHCH_3 + O_2 \rightarrow H_2CCHCHO + H_2O \quad (\Delta H = -368 \text{ kJ/mol}) \qquad (2.3)$$

$$H_2CCHCHO + 0.5\ O_2 \rightarrow H_2CCHCOOH + H_2O \quad (\Delta H = -266 \text{ kJ/mol}) \qquad (2.4)$$

Acrylic acid and its ester derivatives are used mainly for the manufacturing of paints, adhesives, paper and textile finishing, super-absorbent and in leather finishing. The flowsheet below shows a typical scheme for acrolein and acrylic acid production.

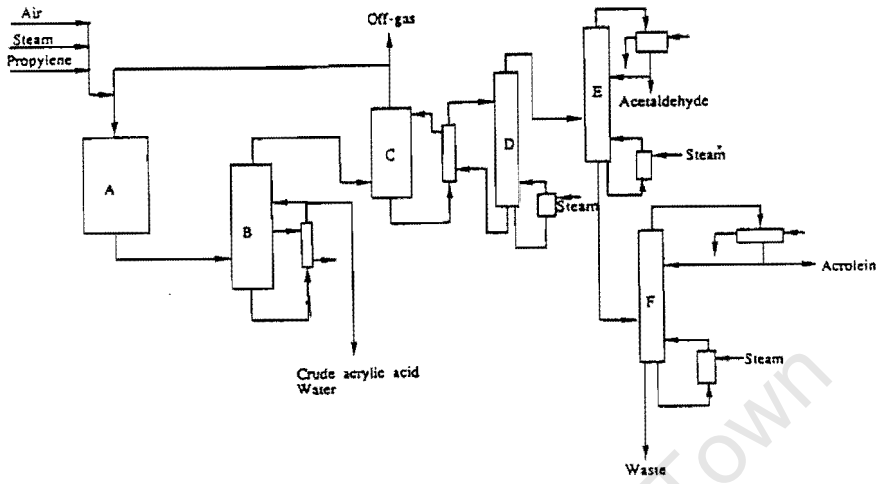

Figure 2.7 Typical process flowsheet for acrolein and acrylic acid manufacture. [Dever et al. 1995]

The aqueous acrylic acid and acrolein are condensed from the reactor effluent and adsorbed in the water–based stream, to separate propene, nitrogen, oxygen and carbon dioxide. Distillation is used for the separation of water and acetaldehyde from crude acrylic acid and acrolein is recovered as an azeotrope with water.

2.4 THERMODYNAMIC ANALYSIS

The Table 2.1 below shows the standard Gibbs Free Energy for the compounds that might be formed during propene oxidation at typical reaction conditions (350^0C – 400^0C and 1 bar).

Table 2.1 Standard Gibbs Free Energy for possible reactions during partial oxidation of propene. [Schnobel et al. 1997]

Reactions	**ΔG^0_R (kJ/mol)**		
	327^0C	**427°C**	**527°C**
$C_3H_6 + O_2 \rightarrow C_3H_4O$(Acrolein) $+ H_2O$	-399	-418	-439
$C_3H_6 + 3/2O_2 \rightarrow C_3H_4O_2$ (Acrylic acid)$+ H_2O$	-557	-550	-543
$C_3H_6 + O_2 \rightarrow C_3H_4$ (Allene) $+ H_2O$	-109	-117	-124
$C_3H_6 + 4.5\ O_2 \rightarrow 3CO_2 + 3\ H_2O$	-1938	-1942	-1944
$C_3H_6 + 3\ O_2 \rightarrow 3CO + 3\ H_2O$	-1248	-1277	-1305
$C_3H_4O + 7/2\ O_2 \rightarrow 3CO_2 + 2\ H_2O$	-1539	-1524	-1505

Total oxidation products are thermodynamically more favoured than the formation of any other compounds. The formation of total oxidation products from acrolein is also thermodynamically favoured. Double bond isomerisation (allene) reaction is the least thermodynamically favoured reaction, hence only trace amounts are expected to be formed.

According to the thermodynamic analysis, temperature rise favours the formation of most of the compounds listed, including acrolein. Since the Gibbs free energy for the CO_2 formation increases negatively as the temperature increases implies, the reaction is favoured at higher reaction temperatures.

2.5 CATALYSTS FOR PARTIAL OXIDATION.

Mixed metal oxides, such as Bi- Mo-Sn –Sb have been found to be an efficient catalyst for the selective oxidation of propene to acrolein. A number of different mono, bi and multicomponent oxide systems have been studied. Metals (mainly Ag for ethylene epoxidation), zeolites (TS-1

for phenol oxidation) and heteropolyoxometallates ($H_4PMO_{11}VO_{40}$) for isobutene oxidation to methacrolein) may also be used. In the following section iron antimony oxide will be discussed. The Bismuth molybdate will also be discussed briefly due to its commercial importance.

2.5.1 Iron antimony oxide catalyst.

2.5.1.(i) Prepared by precipitation method.

The catalyst can be prepared by an impregnation method as described by [Ellen et al. 1996]. In this method $Fe(NO_3)_3$. H_2O is heated to 60^0C to form iron nitrate and its water of crystallisation. Sb_2O_4 in powder form was added and the temperature raised to 80^0C. The pH was adjusted to 3 using aqueous ammonia. The solid was then dried for 16h at 120°C and calcined in air for 7hrs at 900°C. [Carbucicchio et al. 1985] employed $FeCl_3.6H_2O$ and $SbCl_5$ with the latter as being the antimony source and former the Fe source.

2.5.1.(ii) Structure of iron antimony oxide catalyst.

The antimony oxide and iron antimonates were investigated by [Vitaliano et al. 1955]. They suggested the chemical formula to be $FeSbO_4$ rather than $Fe_3Sb_3O_{12}$ $Fe_2Sb_2O_7$ or $Fe_2Sb_2O_8$. $FeSbO_4$ has a tetragonal, rutile-type structure, Figure2.8 having XRD characteristic peaks at 27.1^0, 35.6^0, and 53.2^0.

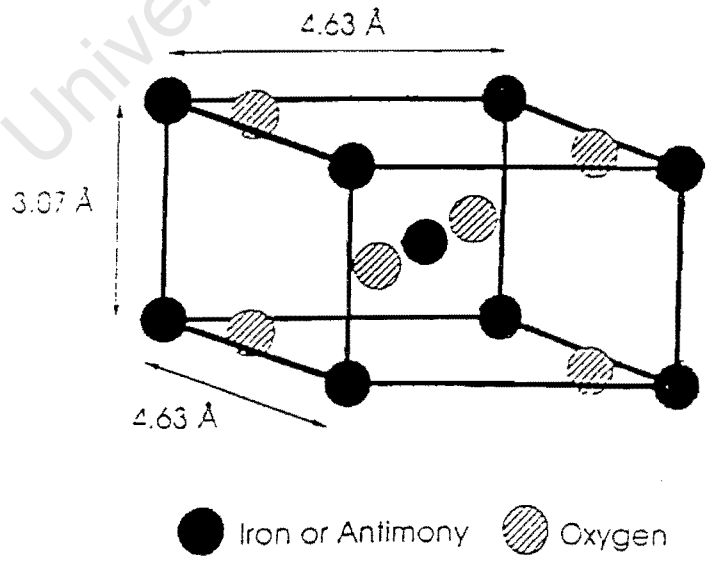

Figure 2.8 Ideal rutile structure of $FeSbO_4$ [Allen et al. 1996].

Table 2.2 Lattice parameters determined using different techniques.

Experimental Technique	a/Å	b/Å	References
X-ray diffraction	4.6388	3.0773	Amador and Rasines [1981]
X-ray diffraction	4.633	3.072	Burriesci et al [1982]
Neautron diffraction	4.6365	3.0742	Teller et al [1985]

X-ray diffraction techniques [Amador and Rasines, 1981] and neutron diffraction techniques [Teller et al. 1985] indicated that the Sb and Fe ions are randomly distributed in the octahedral sites within the oxygen lattice. However [Berry et al. 1987], proposed that $FeSbO_4$ has a trirutile structure consisting of three tetragonal cells stacked along the c-axis, resulting in lattice parameters a=b=4.63Å and c=9.21Å. The authors claimed that they were able to detect superlattices reflections that were not possible using conventional X-ray and neutron diffraction techniques as used by the other authors. It should be noted also that these superlattice were detected on the samples calcined in air and not on samples calcined under vacuum conditions as suggested by other authors [Ellen and Bowker, 1996] using X-ray diffraction.

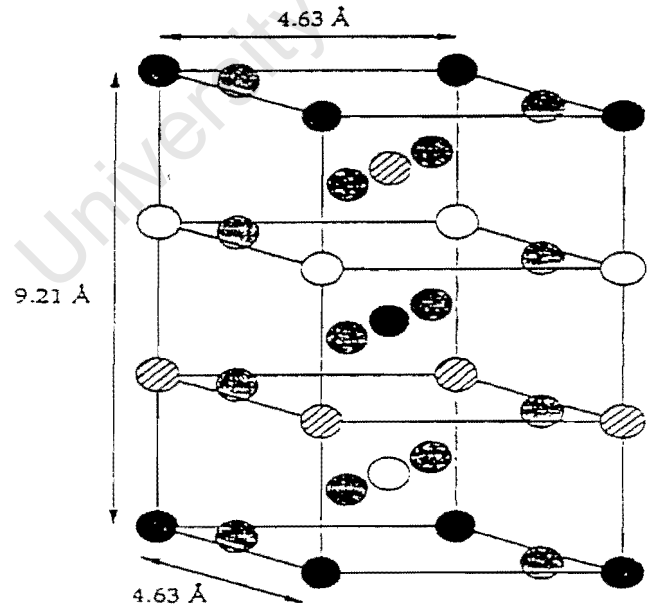

Figure 2.9 Trirutile structure of Iron antimonate [Berry et al. 1987].

2.5.1.(iii) Influence of calcination temperatures on the phase and structure of iron antimony oxide catalyst.

Carbucicchio et al. [1985] studied the influence of calcination temperature for iron antimonate containing ratio Sb/Fe = 1: 1 and Sb/Fe = 2:1 synthesised by the method described by Ellen et al. [1985]. Figure 2.10 below shows that increasing the calcination temperature to 900^{0}C causes a decreased in the linewidth because of sintering.

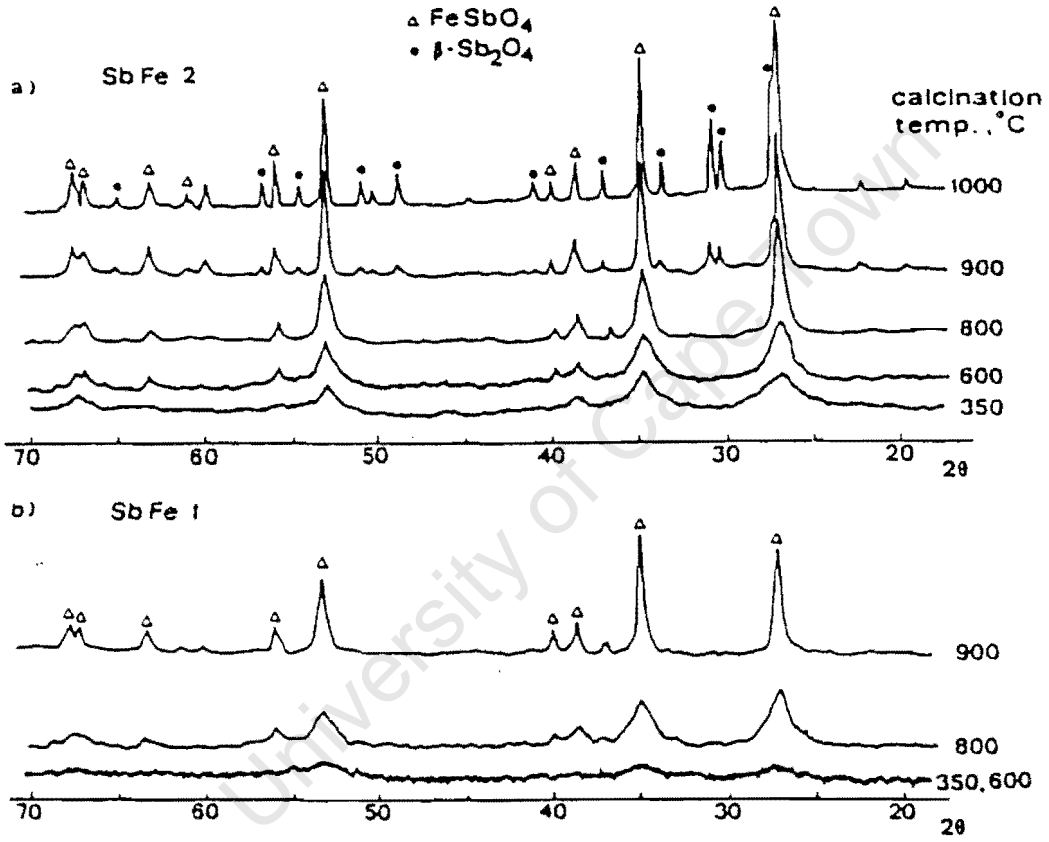

Figure 2.10 X-ray diffraction patterns of Sb/Fe=1:1 and Sb/Fe=2:1 as a function of calcination temperature. [Carbucicchio et al. 1985]

For Sb/Fe=1:1 and Sb/Fe=2:1 samples only β-Sb_2O_4 and $FeSbO_4$ phases were detected. The authors also noted that the cell volumes of the unit cell for Sb/Fe=1:1 and Sb/Fe=2:1 were larger than the unit cell of $FeSbO_4$ for calcination temperatures of 800°C and 900°C. It was concluded that the excess antimony is held within the non-stoichiometric rutile structure of the catalyst.

Teller et al. [1985] observed from neutron diffraction data that calcination temperature had no effect on the cell volume of rutile $FeSbO_4$ based. This was also supported by van [Steen et al. 1997] using X-ray diffraction experiments.

Burriesci et al. [1982] using X-ray powder diffraction investigated the phase composition of the iron antimony oxide catalyst (Sb/Fe=1:1 and Sb/Fe=1:2) prepared from iron nitrate with Sb_2O_3 as a function of calcination temperature.

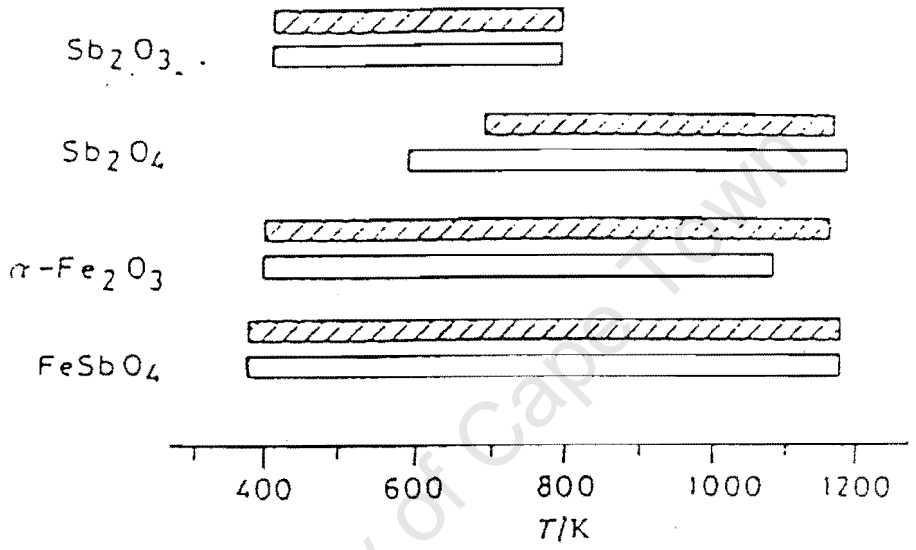

Figure 2.11 Occurrence of different phases as a function of calcination temperature for Sb/Fe=1:1 (dashed bars) and Sb/Fe=1:2 (empty bars) [Burriesci et al 1982]

These results can be compared to those of Carbucicchio et al. [1985], the main differences are the presence of Sb_2O_3 and α-Fe_2O_3 for calcination temperature up to 500°C and 850°C respectively.

2.5.1.(iv) Influence of Sb-enrichment on catalytic properties

There is a general agreement in the literature that the rutile-based catalyst has to be prepared with an excess of antimony oxide to obtain a catalyst, which is both selective and active. The role of excess antimony has been a subject of many investigations and the hypothesis of the active sites on the rutile structure fall in four categories (i) a solid solution of Sb in the rutile

structure (ii) an oriented film or crystals of Sb_2O_4 grown on the surface of the rutile phase (iii) surface modification and $Sb^{(v)}$=O surface sites and (iv) phase interface effects

Aso et al. [1980] studied the influence of the antimony content in iron antimonate in the catalytic oxidation of propene. The antimony content was varied from 0% (pure Fe_2O_3) and 100% (pure Sb_2O_4). Figure 2.12 depicts that Fe_2O_3 favoured the formation of deep oxidation products while pure Sb_2O_4 favoured high selectivities of acrolein and 1,5 hexadiene at low reaction rates.

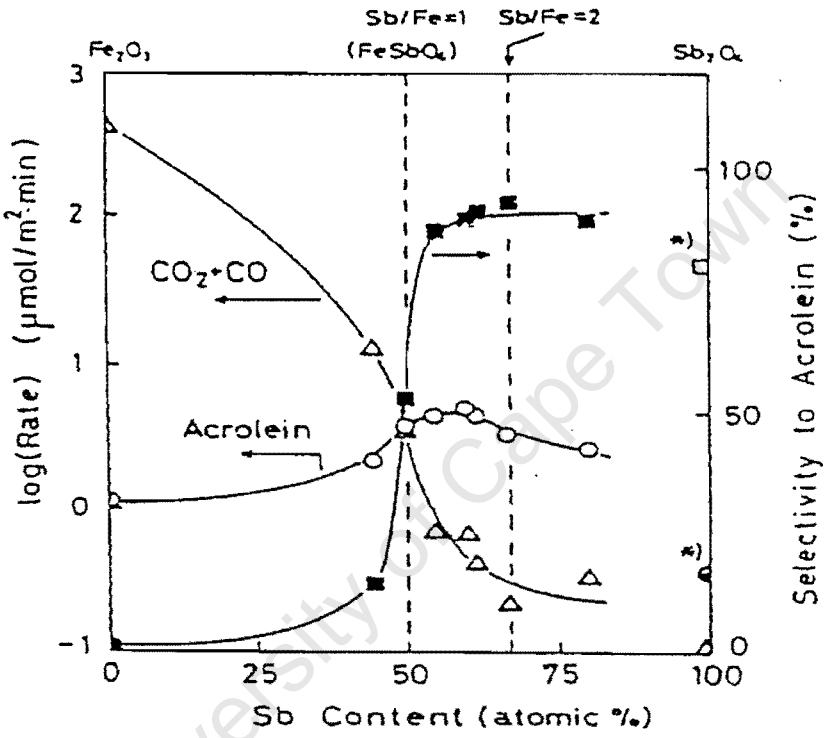

Figure 2.12 Rate of formation and selectivity for the formation of acrolein as a function of antimony content [Aso et al. 1980].

Figure 2.12 shows that at an antimony content of 50% ($FeSbO_4$) selectivity to acrolein increased sharply, while the rate of formation of acrolein goes through a maximum at an antimony content ca. 60%. The explanation of the dependency of the catalytic selectivity on the antimony content is not well understood, but various postulates have been brought forward.

Fattore et al. [1975b] suggested that the increase in the catalytic selectivity as a result of an increase in the antimony content is due to phase co-operation between the $FeSbO_4$ and Sb_2O_4. This involves:

(a) The migration of either oxide ions or an allyl intermediate between the two phases.

(b) The formation of highly selective islands on top of the $FeSbO_4$ particles

(c) The inhibition of the formation of free Fe_2O_3 and suppression of total oxidation.

Sala and Trifiro [1976] proposed that the formation of $FeSbO_6$ or $Fe_2Sb_2O_7$ is responsible for the increased selectivity of the catalyst and the active oxidation site is related somehow to Sb^{5+} ion. The role of iron is to catalyse the re-oxidation of the antimony ions, which are reduced during the reaction with the olefin. It is also responsible for the activation of gaseous oxygen, a property that is lacking in Sb_2O_4 where Sb^{5+} is present. The infrared spectra led to the identification of the two Sb^{5+}=O groups Sb_2O_4 and Sb_2O_3. They are presented by two connected Sb^{5+}ions and can play an important role in the hydrogen allylic abstraction from olefins. The second Sb^{5+}=O group makes a second hydrogen abstraction possible, without movement of the hydrogen molecule on the catalyst surface.

Allen and Bowker [1995] investigated the properties of $FeSbO_4$ (Sb/Fe=1) using X-ray photoelectron spectroscopy, temperature programmed desorption (TPD) and Transmission Electron microscopy. The authors found that $Sb^{(0)}$ was present after reducing the fresh catalyst with 4 to 10 Torr of ammonia at 550K for 20min. A structure which was proposed consists of Sb enriched skin. After reduction it was coated with Sb metal, which after thermal desorption leaves an iron oxide rich skin. The nature of this skin is crucial for the selectivity in propene oxidation.

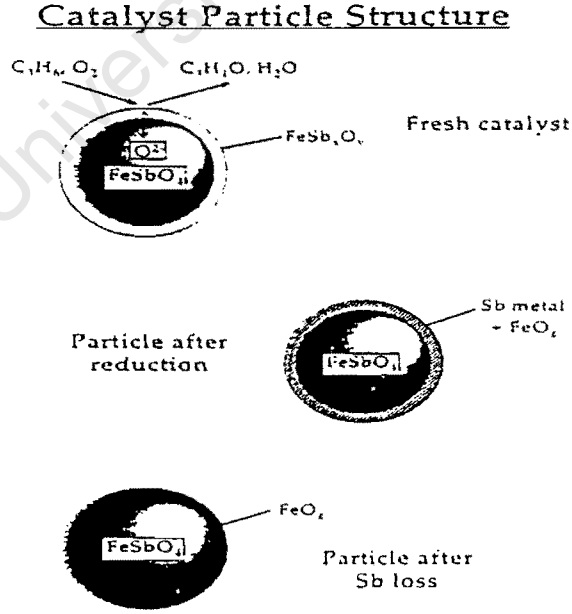

Figure 2.13 Schematic diagram of the structure of $FeSbO_4$ catalysts after different treatments [Allen et al. 1996]

2.5.2 Bismuth - molybdate catalyst

The Bishmuth molybdate catalyst comes in three catalytic active phases:
α-$Bi_2(MoO_4)_3$, β-$Bi_2Mo_2O_9$,γ-Bi_2MoO_6 . It has been reported that these phases possess enhanced stability relative to the binary oxides. The pulse reduction studies revealed the importance of catalyst structure on the redox processes in Bismuth Molybdate catalyst. Among the above phases the selectivity decreases according to the following order, β-$Bi_2Mo_2O_9$ > α-$Bi_2(MoO_4)_3$ > γ-Bi_2MoO_6. The β-$Bi_2Mo_2O_9$ has the surface structure and active–site configuration that is best suited for selective ammoxidation. Partial reduction under reaction conditions can improve the selectivity, but complete depletion of active oxygen from the lattice will result on the catalyst deactivation. The kinetics of the reoxidation of the catalyst can be influenced by the solid state properties of the catalyst depending on the location of the oxygen vacancies. At all degrees of initial reduction studied, the rates of reoxidation decrease as follows: γ-Bi_2MoO_6 >β-$Bi_2Mo_2O_9$ > α-$Bi_2(MoO_4)_3$. Oyama et al [1996] reported that the reoxidation for γ-Bi_2MoO_6 and α-$Bi_2(MoO_4)_3$ occurs both at the surface and in bulk of the catalysts.
The β-$Bi_2Mo_2O_9$ is the most active and selective because it possesses a stoichiometry which maximises the bismuth-molybdenum pair. The presence of the layers provides low energy pathways for the diffusion of oxygen vacancies, which makes the reoxidation of the catalyst proceed with the activation energy of only 8-9-kcal/mol.

2.5.3 Surface oxygen species in partial oxidation catalysts.

It is assumed that the oxidising agent is O^{2-} from the lattice, which is abstracted by a reducing agent as electrons are donated to a lattice cation. Reoxidation by O_2 is usually assumed to lead to a formation of O^{2-} in the lattice gain:

$$O_2 + 2\,* \rightarrow 2O^{2-}*$$

Figure 2.14 Formation of the lattice oxygen [Haber et al. 1996].

The reaction is assumed to take place with the simultaneous transfer of four electrons. It might be expected that a stepwise donation of electrons take place. Figure 2.15 shows the enthalpy data for the formation of mono- and dioxygen species in the gas phase.

			ΔH (kJ/mol)
$O_2 + * + 2e^-$	→	O_2^{2-}	646.4
$O_2^- + e^-$	→	O_2^{2-}	688.9
$O^- + e^-$	→	O^{2-}	752.7

Figure 2.15 Enthalpy data for the formation of mono and dioxygen species [Chen et al. 1983].

The superoxide ion was found to be the stable ion in the gas phase and it is formed according to the above reactions shown in Figure 2.15. These negative ion species might be stabilised by the Madelung potential in the bulk of solid oxides or as adsorbed species [Haber and Bielanski]. The following scheme was suggested for the oxygen incorporation in the oxide layer:

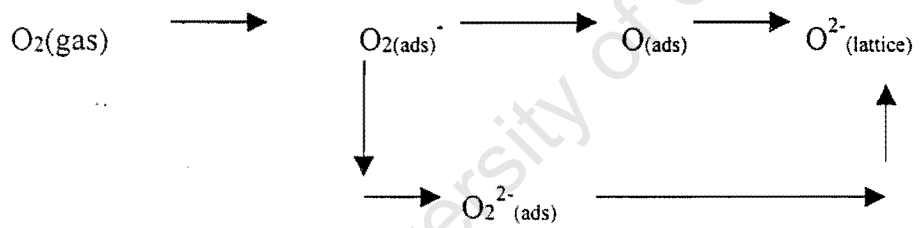

Figure 2.16 Oxygen incorporation in the oxide layer [Oyama et al. 1996]

Chen et al. [1983] stated that the transformation of $O_2^-{}_{(ads)}$ (oxygen species is responsible for the formation of partial oxidation products) to $O^-{}_{(ads)}$ (oxygen species responsible for the formation of total oxidation products) is energetically favoured than via $O_2^{2-}{}_{(ads)}$, as shown by the enthalpy values presented by the reactions shown in Figure 2.15

Haber et al. [1996] suggested that nucleophilic oxygen e.g. O^{2-} is responsible for the selectivity of partial oxidation products and electrophilic oxygen [e.g. O_2^- and O_2^{2-}] for the total oxidation products. These oxygen species are formed as intermediates during catalyst reoxidation process. In the case of antimony-enriched catalysts, the surface is reduced to a lesser extent than the case

of catalyst prepared with Sb/Fe ≤ 1. Fewer electrophilic oxygen are formed, implying higher selectivity to partial oxidation products over antimony enriched catalyst.

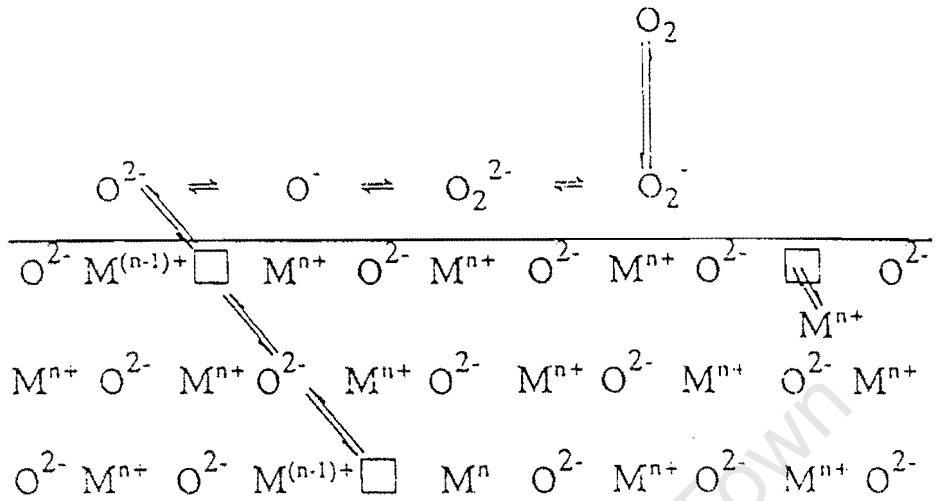

Figure 2.17 Formation of electrophilic oxygen species at the oxide surface [Haber et al. 1996].

2.6 OXIDATION REACTION MECHANISM

2.6.1 Redox mechanism

Mars and van Krevelen [1954] derived the rates for the reduction and re-oxidation of the catalyst for partial oxidation of aromatics over vanadium oxide catalysts. Figure 2.18 shows a scheme for redox mechanism according to Mars and van Krevelen [1954].

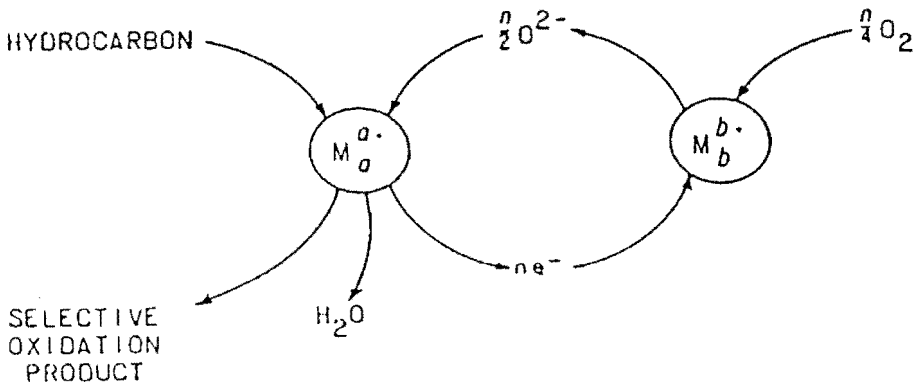

Figure 2.18: Scheme of the Mars van Krevelen mechanism [Vedrine et al 1997]

Figure 2.18 shows that the role of the gaseous oxygen is to maintain the oxidation state of the catalyst. The catalyst has two different sites, the active cationic site, which oxidises the hydrocarbon, and another site for the reduction of gaseous oxygen. Thus it can be concluded that the reaction takes place in two steps:

(i) the reaction between the hydrocarbon and the oxide in which the hydrocarbon is oxidised and the oxide is reduced.

(ii) the reaction of the reduced oxide with O_2 to give back its initial state.

2.6.2 Reaction mechanism over iron antimonate catalyst.

The species that is directly responsible for the oxidation is assumed to be the O^{2-} ion on the surface of the oxide catalyst, and the reaction is therefore an example of the non-insertion type. The formation of partial and total oxidation products is independent of the presence of oxygen in the feed and is the evidence of the incorporation of lattice oxygen (O^{2-}) [Aso et al. 1980] and [Fattore et al. 1975b]

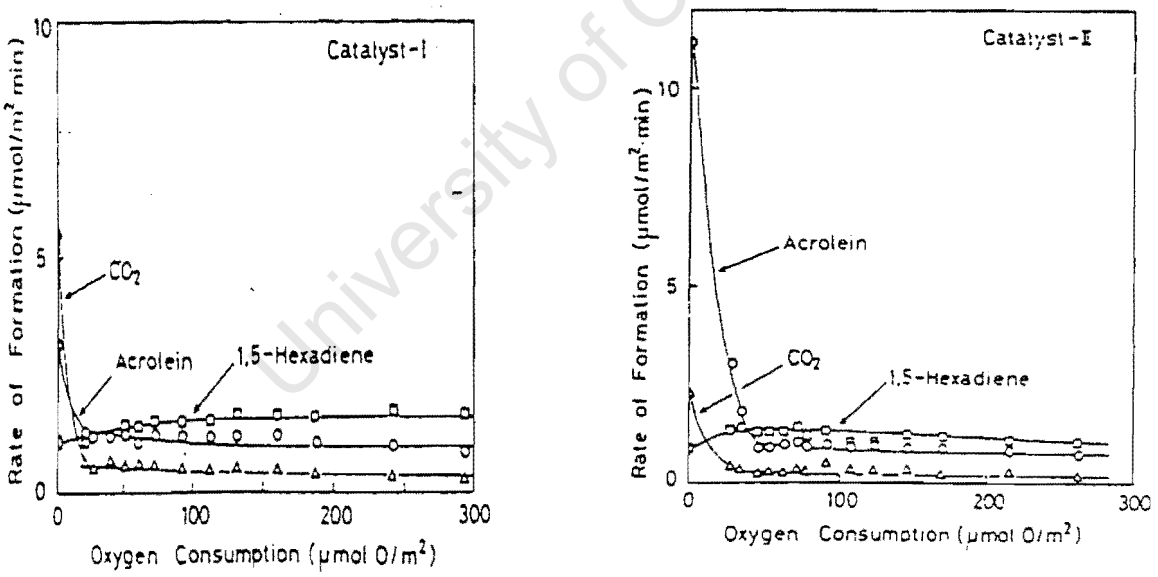

(a) (b)

Figure2.19 Rate of formation of oxidised products in the absence of gas-phase oxygen over iron antimony catalysts as a function of the amount of catalyst oxygen consumed. [Aso et al 1980]

Figure 2.19(a) and (b) indicate that the lattice oxygen is involved in the oxidation process. Fe_2O_3 reacts with propene at 400°C, to produce exclusively CO_2. In contrast Sb_2O_4 reacts with propene

producing selectively 1,5 hexadiene and acrolein at nearly constant rates over the reduction period. In contrast to Sb/Fe=1:1 and Sb/Fe =2:1, the rate of reduction is observed to decline sharply after an initial period of high activity. This was also confirmed by van Steen et al. [1997] using a catalyst with Sb/Fe between 0.25:1 and 2:1. It was suggested that the high initial activity period is due to the removal of the surface monolayer, and the period of stationery oxygen consumption is due to the reduction into the bulk of the catalyst [Allen et al. 1986]. It was also suggested that the surface oxygen is more reactive than the bulk oxygen because of the diffusion of oxygen from the bulk to the surface of the catalyst.

2.6.2. (i) Active sites for propene oxidation.

Carbucchicio et al. [1985] and Sala and Trifiro [1976] using infra-red spectroscopy detected the presence of O=Sb=O groups at the surface of iron antimony catalyst which play an important role in the allylic oxidation of propene and also the formation of acrolein. Burrington et al. [1984] proposed the existence of bridging oxygen species, which connect two Sb^{5+} and two Sb^{3+} cations. The Sb^{5+} is thought to be responsible for propene adsorption and oxygen insertion into the allylic intermediate. The Sb^{3+} is thought to be responsible for the initial abstraction of α-hydrogen.

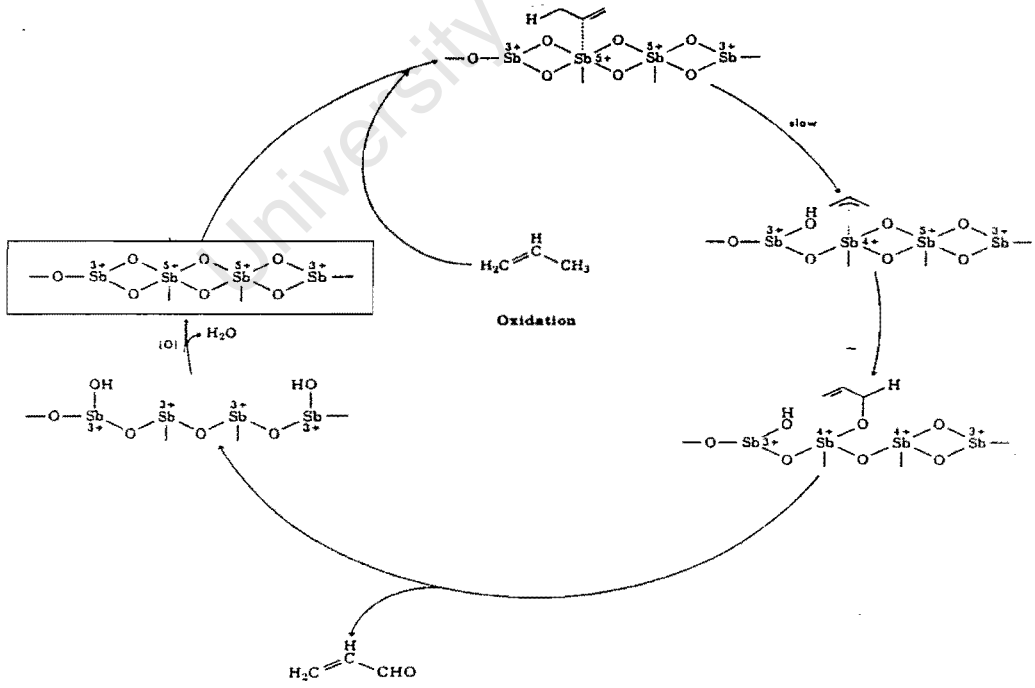

Figure 2.20 Proposed reaction mechanism of propene oxidation over antimony catalysts [Burrington et al. 1984]

The proposed mechanism presented in Figure 2.20 is consistent with that of Teller et al. [1985], who proposed that the Sb^{3+}sites are responsible for the formation of allylic intermediate, while Sb^{5+}sites are associated with the insertion of oxygen to form acrolein. In the process Sb^{5+}ions are reduced to Sb^{3+} ions. The catalyst reoxidation was postulated to proceed via the redox couple (Fe^{3+}+ e^{-}→ Fe). The mechanistic scheme as proposed by Teller et al [1985] is shown in Figure 2.21.

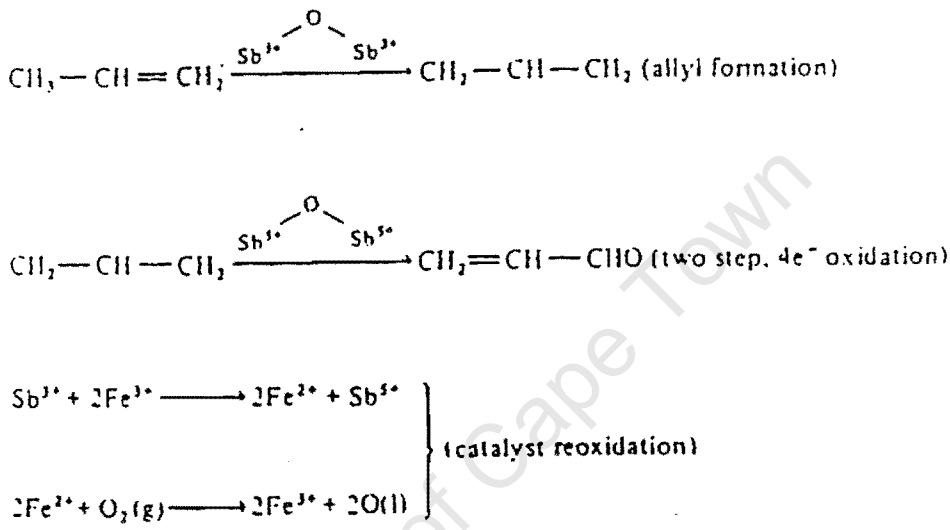

Figure 2.21 Propene oxidation mechanism over iron antimony oxide as proposed by Teller et al [1985]

2.6.2. (ii) Formation of total oxidation products.

Davydov et al [1978] investigated propene adsorption over various metal oxide catalysts using infrared spectroscopy and thermal-desorption techniques. They noted that adsorbed propene had weakly and reversibly bound forms and strongly and irreversibly bound forms. The propene, which was weakly bound, gave rise to pi and sigma allylic complexes respectively, leading to the formation of partial oxidation products. While the strongly bound forms gave rise to carbonate and carboxylate structures and pi complexes lead to the formation of total oxidation products (Figure 2.22).

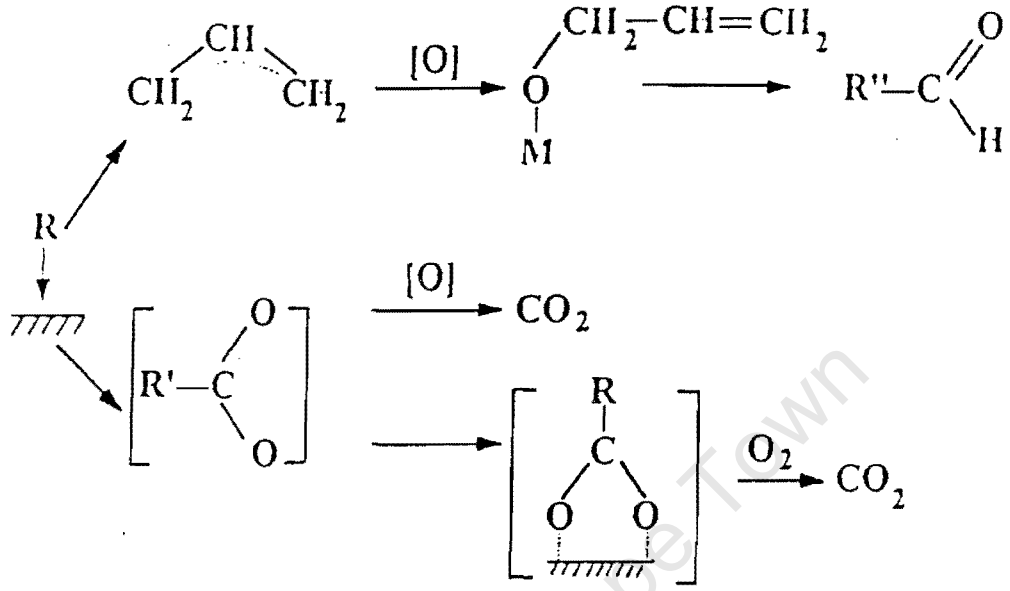

Figure 2.22 Formation of total oxidation products [Davydov et al. 1978]

2.6.3 Reaction mechanism over Bismuth molydate catalyst.

Bettahar et al [1996] claimed that propene oxidation over bismuth molybdate occurs via nucleophilic addition of oxygen to the allylic species which results in the formation of a σ-bond between the allyl, initially π-bonded to the metal cation, and the lattice oxygen, situated at the surface of the catalyst. This adsorbed complex must now get rid of one hydrogen atom linked to the carbon atom of the C=O group, before it can be adsorbed in the form of acrolein. The second abstraction of hydrogen proceeds and is followed by the addition of oxygen, then desorption of acrolein and formation of an oxygen vacancy at the catalyst surface.

Adams and Jennings [1964] investigated the mechanism of propene oxidation over bismuth molybdate catalysts and found that the abstraction of hydrogen takes place prior to the insertion of oxygen. Their results were confirmed by Monnier and Keulks [1981] using two deuterated propenes: propene-1, 1, 2-d_3: CD_2=CD-CH_3 and propene-2,3 ,3 ,3-d_4 : CH_2=CD-CD_3. The main

difference in the mechanism of acrolein formation over iron antimony oxide and bismuth molybdate is the order of hydrogen abstraction. For iron antimonate the hydrogen abstraction occurs after the oxygen insertion and vice versa for bismuth molybdate.

2.6.4 Reaction kinetic models.

Mars and Van Krevelen [1954] suggested a redox kinetic model for the steady-state reduction of the catalyst by the hydrocarbon feed. The rate of reduction and rate of oxidation can be expressed as follows:

$$r_{reduction} = k_{red} \times P_{olefin}^{m} \times \theta_{ox} \tag{2.4}$$

$$r_{oxidation} = k_{ox} \times P_{O_2}^{n} \times (1-\theta_{ox}) \tag{2.5}$$

where θ_{ox} is the fraction of the oxidised active sites of the catalyst. At steady state the rate of oxidation equals the rate of reduction. Then the olefin consumption can be written as:

$$-r_{olefin} = \frac{k_{red} \times P_{olefin}^{nn} \times k_{ox} \times P_{O_2}^{m}}{\beta \times k_{red.} \times P_{olefin}^{n} + k_{ox} P_{O_2}^{m}} \tag{2.6}$$

where β is the stoichiometric number depending on the type of product formed.

van Steen et al [1997] investigated the kinetics of selective partial oxidation of C_3 to C_6 α-olefins over an iron antimony oxide catalyst. Two different mechanisms were considered, single site mechanism and oxidative mechanism. On the single site mechanism it is assumed that all catalytic sites are energetically equal and can be occupied by either olefin or oxygen. It is also assumed that the adsorption of an olefin and oxygen are at equilibrium and the rate determining step is the reaction between adsorbed olefin and an adjacent oxygen species. The following reaction mechanism was derived:

$$Olefin + * \leftrightarrow Olefin*$$
$$O_2 + * \leftrightarrow 2O*$$
$$Olefin* + O* \leftrightarrow .....(products)(rds)$$

Figure 2.23 Single site mechanism [van Steen et al.1997]

In the oxidation mechanism, the surface is thought to consist of only antimony and oxygen species as proposed by Burrington et al. [1984]. To incorporate the involvement of $Sb^{(5+)}$=O groups [Carbucicchio et al. 1985], the proposed mechanism is summarised below:

$$step1: Sb + O_2 \leftrightarrow SbOO$$
$$step2: SbOO + *,a \leftrightarrow Sb = O + O^{*,a}$$
$$step3: Sb = O + *,a \leftrightarrow Sb + O^{*,a}$$
$$step4: SbOO + olefin \rightarrow Sb - O - O - olefin$$
$$step5: Sb - O - O - olefin + *,a \rightarrow combustion/cracking$$
$$step6: Sb = O + olefin \leftrightarrow Sb - O - olefin$$
$$step7: Sb - O - olefin + O^{*,a} \rightarrow partial - oxidation/dehydrogenation$$
$$step8: Sb - O - olefin + O^{*,a} \rightarrow double - isomerers$$
$$step9: Sb + olefin \leftrightarrow Sb - olefin$$
$$step10: Sb - olefin + O^{*,a} \rightarrow combustion/cracking$$
$$step11: Sb - olefin + O^{*,a} \rightarrow double - bond.isomers$$

Figure 2.24 Oxidation of olefins according to the oxidation model [Schnobel et al. 1997].

$O^{*,a}$ and *,a are the oxygen species and vacancies in the bridging positions in the crystallite surface respectively.

Antimony at the surface can adsorb molecular oxygen yielding a peroxo complex, which decomposes yielding oxygen in the bridging position and a Sb=O species. The adsorption of an olefin onto the peroxo group results in its decomposition. The co-ordination of the olefin to Sb=O results in the formation of partial oxidation products. The following assumptions were imposed:

(i) The transformation of Sb=O to Sb was not favoured.

(ii) The rate constant for the olefin adsorption into the peroxo complex was smaller than that for the subsequent decomposition i.e. step four of the rate determining step.

Formation of partial oxidation, oxydehydrogenated, cracking and combustion products are expressed as follows:

$$-r_{POX+ODH} = \frac{a_i P_{olefin} P_{O_2}^{0.5}}{(1 + c_1 P_{olefin} + c_2 P_{O_2} + c_3 P_{O_2}^{0.5})} \quad (2.7)$$

$$-r_{Crack+Combustion} = \frac{P_{olefin}(a_i P_{O_2}^{0.5} + b_i)}{(1 + c_1 P_{olefin} + c_2 P_{O_2} + c_3 P_{O_2}^{0.5})} \quad (2.8)$$

2.6.5 The power - law rate model.

Keulks et al [1980b] and Aso et al [1979] have shown that partial reaction orders were changing with temperature, suggesting that the overall kinetics are a composite of the re-oxidation and reduction kinetics. Table 2.3 shows the reported activation energies of acrolein and carbon dioxide formation and were observed to differ by 1 kJ/mol at T=375°C. The small difference between the activation energy of acrolein and that of carbon dioxide was attributed to presence of high antimony content on the surface of the catalyst thus suppressing the formation of carbon dioxide. Table 2.3 also suggests that the kinetic parameters for the reduction of iron antimonate catalyst are controlled primarily by catalyst reduction at high temperatures and are re-oxidation limited at lower temperatures. This was later confirmed by van Steen et al [1997] for Sb/Fe=1.5:1 on Table 2.4.

Table 2.3 Overview of the kinetics parameters obtained using the power- law rate model

$$r_{reduction} = k_{red} \times P_{olefin}^{m} \times P_{O_2}^{n}$$

Catalyst FeSbO4	E_a(kJ/mol) Acrolein	E_a(kJ/mol) CO_2	T^{0}C	Acrolein Formation.		CO_2 Formation		References
				N	m	n	M	
(Sb/Fe=4)	82.1	81.6	350 375 450	0.5 0.5 0.8	0.4 0.3 0.3	0.4 0.6 0.7	0.6 0.7 0.7	Keulks et.al [1986]
Sb/Fe=2 Sb/Fe=1	-	-	400 400	0.12 0.23	0.89 0.8	0.21	0.65	Aso et al [1980]
Sb/Fe=1.5	60	100	375	0.7	0.5	0.5	0.6	van Steen et al [1997]

Table 2.4 Rate constants for the rate of consumption of propene [Schnobel et al. 1997].

$$-r_{olefin} = \frac{k_{red} \times P_{olefin}^{nn} \times k_{ox} \times P_{O_2}^{m}}{\beta \times k_{red.} \times P_{olefin}^{n} + k_{ox} P_{O_2}^{m}}$$

Feed	$T_{reaction}$	$k_{reduction}$	$k_{oxidation}$
	(°C)	mol olefin/ $kg_{cat.}$.s.Pa	mol O_2/ $kg_{cat.}$.s.Pa
Propene	350	1.21×10^{-4}	1.76×10^{-4}
	375	2.43×10^{-4}	2.60×10^{-4}
	400	3.10×10^{-4}	4.00×10^{-4}

2.7 INFLUENCE OF REACTION PARAMETERS ON PROPENE PARTIAL OXIDATION OVER IRON ANTIMONY OXIDE UNDER STEADY-STATE CONDITIONS.

2.7.1 Influence of temperature.

All oxidation processes are highly exothermic. The temperature profile along the bed length achieves a well-pronounced maximum, the region of high temperature is known as the hot spot as shown by figure 2.25. If the temperature in the hot spot rises above a critical value total oxidation occurs. If there is inefficient heat removal in the reactor the reaction "runs away."

Marengo et al [1997] investigated transient thermal effects during catalytic oxidation of propane in a packed bed reactor, using Rh on γ-alumina catalyst. Figure 2.25 shows the temperature profiles during ignition of the C_3H_8-O_2 reaction over 3% Rh/Al_2O_3 and a reaction front forming near the reactor inlet due to the release of heat of reaction. Upon ignition the reaction front developed slowly, holding its position and showing no dynamics.

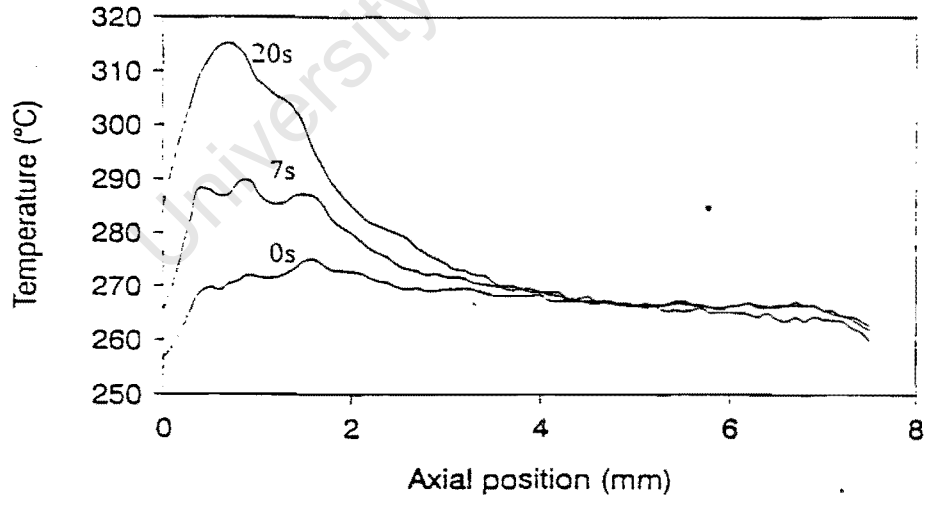

Figure 2.25 Temperature profiles during ignition of the C_3H_8-O_2 reaction over 3% Rh/Al_2O_3 [Marengo et al. 1997]

The selectivity of an oxidation reaction can depend on the properties of the catalyst. It is understood that electrophilic oxygen is responsible for the total oxidation and that it may be generated

at the surface of an oxide either as a result of its dissociation a high temperatures or during the adsorption of gaseous oxygen at lower temperatures. Schnobel et al [1997] observed that the yield of the reaction products, acrolein and carbon dioxide, increased with an increase in temperature when a mechanical mixture of $Fe_2.O_3$ / $Sb_2.O_4$ with Sb/Fe = 2 was used. Figure2.26 shows the yields of acrolein and carbon oxides as a function of reaction temperature. The yield of carbon dioxide increases faster compared to yields of acrolein with increase in temperature

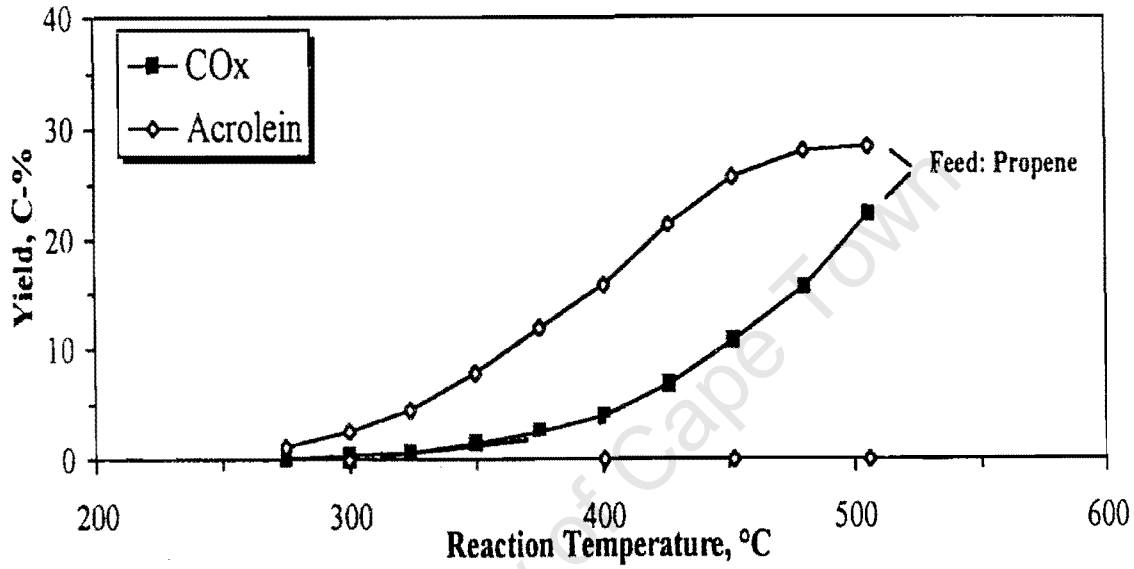

implying that the activation energy for total oxidation is higher than for selective oxidation.

Figures 2.26 Yields of Acrolein and Carbon oxides for the partial oxidation propene over iron antimony oxide (Sb/Fe=1.5:1) as function of reaction temperature and calcination temperature [Schnobel et al. 1997].

2.7.2 Influence of partial pressure

Schnobel et al [1997] conducted experiments by varying the inlet partial pressure at constant space times and at different temperatures. Figure 2.27 shows that increasing the partial pressure of propene, decreased the conversion of propene. No effect was observed on the partial and complete oxidation products. It was suggested that the reaction order of the olefin was less than zero. If the rate-determining step involves an adsorbed olefin, reaction orders less than one are expected (Figures 2.27(a)). An increased in oxygen pressure resulted in an increase in propene conversion. The selectivity to total oxidation products increased slightly while the partial oxidation selectivity declined slightly (Figure2.27 (b)).

Feed: Propene:

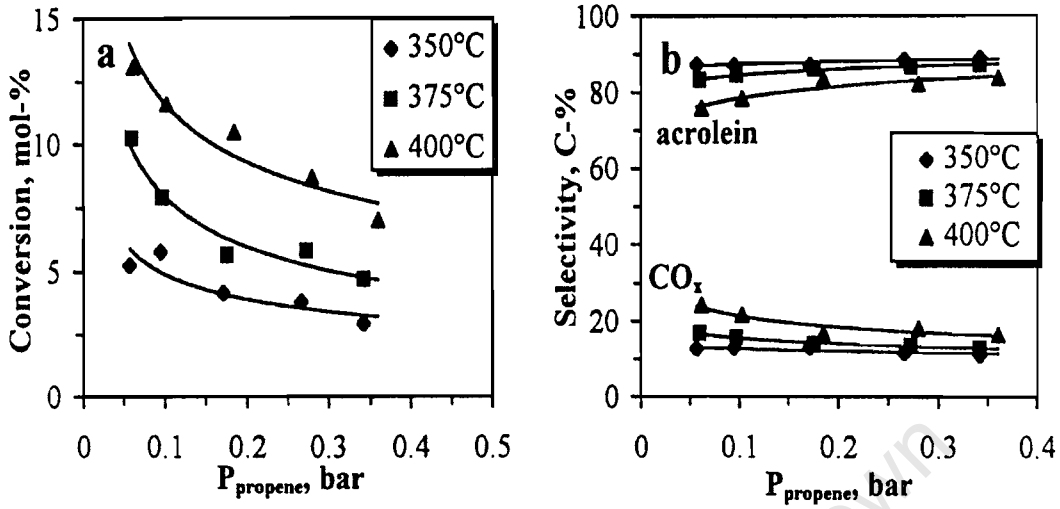

(a)

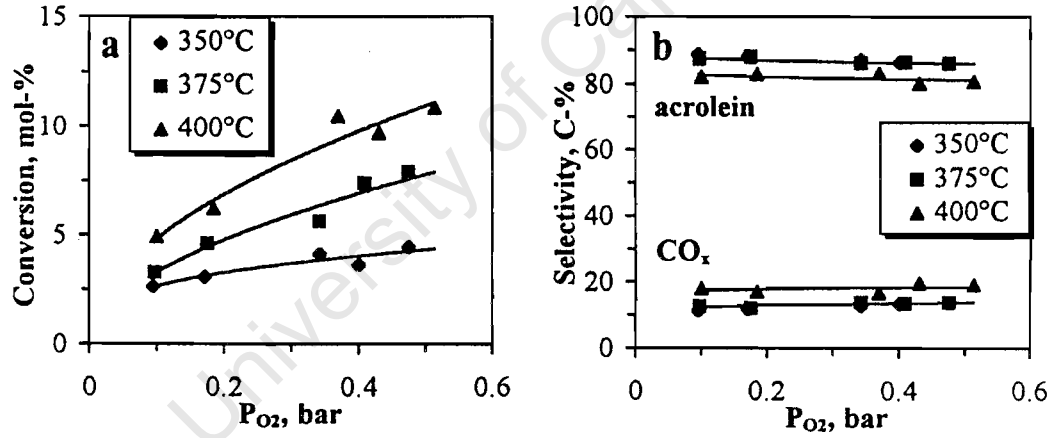

(b)

Figure 2.27 Effect of the (a) inlet propene partial pressure (b) inlet oxygen partial pressure on the selectivity of oxidative conversion of propene [Schnobel et al 1997].

2.7.3 Influence of space time.

Schnobel et al [1997] has shown that increasing the space-time increases the conversion but decreases the selectivity .The authors suggested that this was an indication of consecutive reaction of acrolein to carbon dioxide at high space velocities. Since there was no change in the CO content of the total oxidation products with changing space-time, it was then concluded that there was a parallel formation of CO and CO_2 from acrolein.

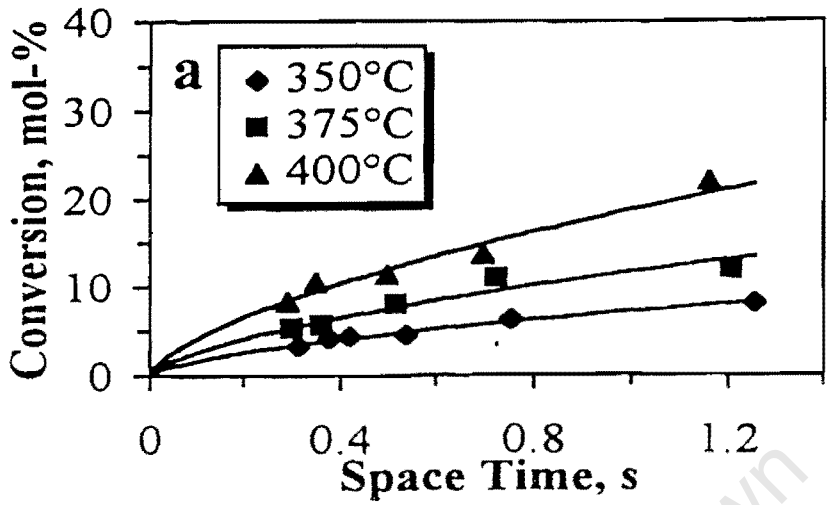

Figure 2.28 Influence of space-time on oxidative conversion of propene [Schnobel et al 1997]

2.7.4 Influence of time on stream

It is now well understood that the oxygen contained in the solid catalyst –so called "lattice oxygen has an active role in selective hydrocarbon oxidation. For a variety of oxidation reactions, the catalyst will continue to operate with the same steady-state yield, if the oxygen supply is discontinued. The activity declines as the catalyst is reduced by the olefin. Under steady-state conditions the catalyst is operating under partially reduced conditions. The optimum level of partial reduction depends mainly on the catalyst and reaction.

Schnobel et al [1997] observed that the conversion and the selectivity of the partial oxidation of propene over iron antimony oxide catalysts decreases rapidly in the first few minutes of reaction (0-2min) as shown in Figure 2.29. Pre-reduction of the catalysts led to a lower maximum initial activity. Schnobel et al [1997] concluded that the fully oxidised catalyst is the most active and most selective.

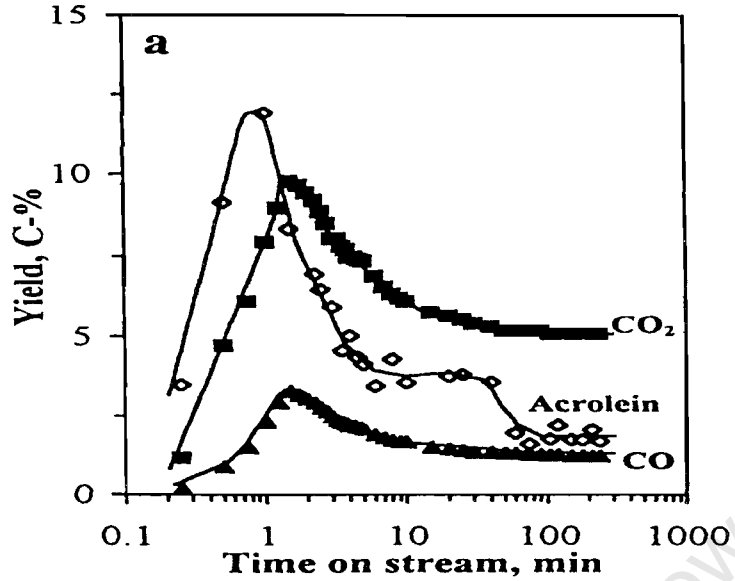

Figure 2.29 Yield of Acrolein during partial oxidation of propene as a function of time on stream [Schnobel et al. 1997]

van Steen et al [1997] investigated the time on stream behaviour of propene oxidation over iron antimony oxide in the presence and absence of gas phase oxygen using a temperature programmed reduction. Figure 2.30 shows that the conversion of propene in the absence of oxygen decreases sharply with 5 min time on stream with acrolein attaining a maximum. This shows that the activity is dependent on the amount of available lattice oxygen, which is depleted as the reaction progresses.

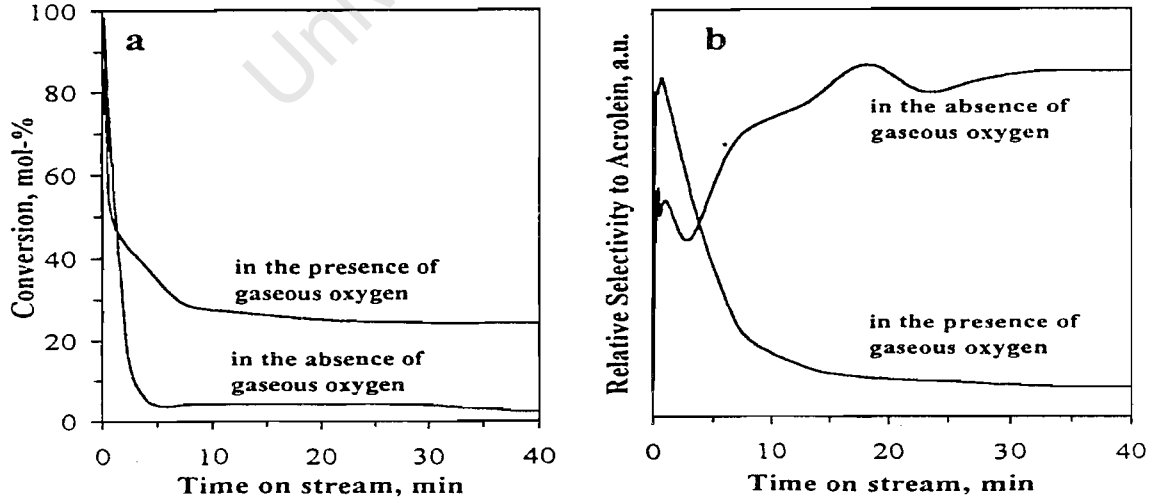

Figure 2.30 Formation of CO_2 and Acrolein during propene oxidation in the presence and absence of O_2 [Schnobel et al. 1997].

In the presence of oxygen the catalyst loses its initial high activity showing that the initial high oxidation state cannot be maintained by the presence of gaseous oxygen. Now since the electrophilic oxygen species are intermediates in the reoxidation of the catalyst with gaseous oxygen, the relative selectivity to acrolein decreases in the case where gaseous oxygen is present. In the absence of gaseous oxygen, vacancies are formed on the catalyst surface, which cannot be refilled from the gas phase. Therefore fewer electrophilic oxygen species are present to form combustion products. Keulks et al [1983] observed the same phenomenon for the bismuth molybdate catalyst while investigating the reaction mechanism using isotopic measurements Figure 2.31.

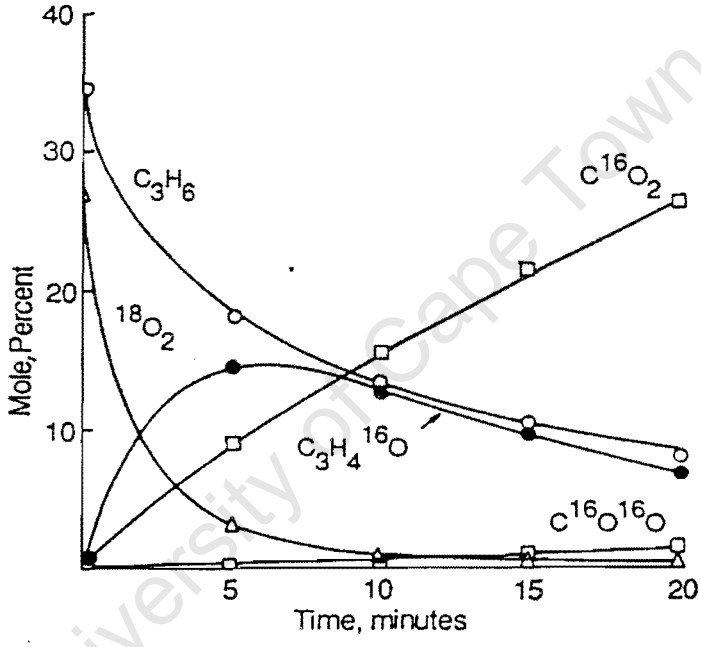

Figure 2.31 Yield plotted as a function of time on stream for bismuth molybdate catalyst at 425°C [Keulks et al 1986]

The maximum yield of acrolein occurred at 5 minutes over bismuth molybdate and less than 0.1 minutes over iron antimony oxide catalyst. This means that for the antimony oxide catalyst, reduction occurs on the surface layer whereas for bismuth molybdate it occurs from the bulk oxygen layers [Grasselli et al. 1981]. In bismuth molybdate the lattice oxygen is much more mobile than in iron antimony oxide. The lattice oxygen on the iron antimony oxide is more reactive than that of bismuth molybdate catalyst [Magagula et al 1998]. Iron antimony oxide needs to be maintained at high oxidation state so as to maintain its high initial activity thus favouring the formation of partial oxidation products. Since the decrease in initial activity is rapid for antimony oxide, reducing and oxidising the catalyst at short switching times is required.

This can be achieved by performing the reaction in two separate reactors as discussed by [Callahan et al. 1960]. Another alternative is to periodically alter the feed from a reducing atmosphere to the oxidising atmosphere.

2.8 PERIODIC OPERATION

Transient operation is a way to control conversion or selectivity in a chemical reactor. Periodic operation is hardly new, all process whereby the catalyst is regenerated in situ operate periodically. Catalytic cracking of gas oil is a well-known example that employs cycles of the order of minutes. The reason for periodic operation is to increase the catalyst conversion or rate of reaction. It is probably more expensive than steady-state operation. If an increase in conversion is desired, this could be achieved by simply increasing the size of the reactor and the amount of catalyst. When it is desired to increase the capacity of an existing reactor, periodic operation could be attractive [Silveston et al. 1995].

2.8.1 Why consider periodic operation?

Non-steady-state experiments have become a tool for investigating mechanisms of heterogeneous catalysed reactions. This is necessary, since reaction kinetics measured under steady-state conditions yield models unable to predict dynamic behaviour [Silveston et al. 1995].

Matros et al [1975] pointed out that improvement in reactor performance under periodic operation resulted from favourable changes in catalyst activity through a variety of mechanisms, often changes in the composition of the catalyst surface. When the catalyst is altered in response to adsorbate composition and /or temperature, both activation energy and the frequency factor change. Moreover, since periodic operation is sensitive to amplitude and the shape of the forcing function, the true kinetics of a catalytic process can be investigated and it becomes possible to separate the model parameters that would be lumped if determined under steady-state conditions.

2.8.2 Laboratory – scale reactors for transient experiments

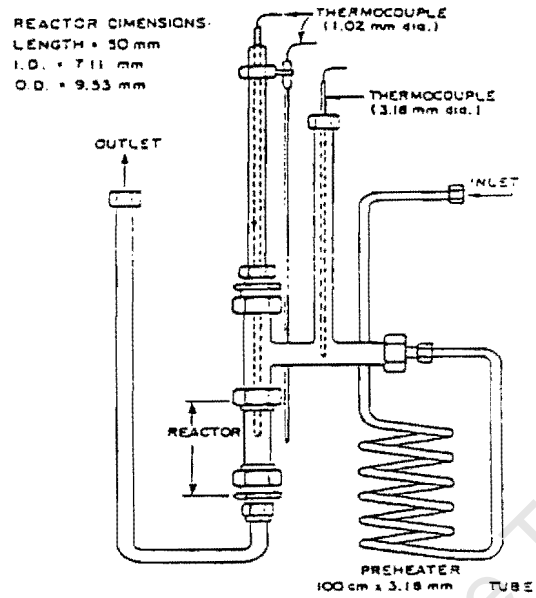

Figure 2.32 Microreactor for use in component forcing studies [Chanchlani et al. 1994]

A microreactor reactor that requires just milligram samples of catalyst can be used and provide differential parameters as shown in figure 2.32 [Chanchlani et al 1994]. This type of reactor permits the observation of reaction dynamics by means of an infra-red spectrometer attached to the reactor. Now, if the reactor is replaced by an optical cell, an IR transparent wafer containing the catalyst, the dynamics of the catalyst surface can be observed. The disadvantage of a catalyst wafer is that the catalyst is modified during pressing of the disk and that additional diffusional interference can occur. Furthermore the flow patterns in the cell are not well defined. This problem can be minimised by using DRIFTS (Diffuse Reflectance Infrared Fourier Transform spectroscopy)

Vamling et al. [1987] studied the production of ethanolamines from ethylene oxide and ammonia over an ion exchange resin catalyst using an integral reactor. The non-uniform temperature distribution makes data difficult to interpret. Silveston et al. [1980] used an internal recirculation reactor instead of a fixed bed reactor to overcome non-uniform temperature distributions.

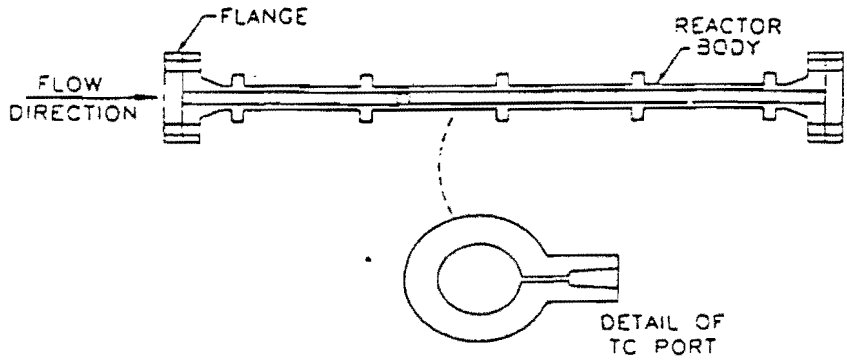

Figure 2.33 Integral reactor used for composition modulation of ethanolamine formation from ethylene oxide and ammonia [Vamling et al. 1987]

A membrane reactor can also be used to suppress or limit the total oxidation reaction. In this reactor an O^{2-} conducting membrane separates the hydrocarbon containing and oxygen containing mixtures. The hydrocarbon containing mixture is exposed essentially to the ' selective oxygen', i.e. O^{2-} ions, while the ' unselective forms of oxygen (O_2 , $O_{2,ads}$, O_2^-, O^-) are less abundant [Genser et al. 1999].

Transient studies can also be performed using temporarily analysis of products reactor (TAP reactor) [Gleaves et al. 1999]. It consists of the following: a gas mixing station, microreactor with high-speed pulse valves, and a mass spectrometer .The TAP-1 reactor has been used to investigate the systematic formation of acrylonitrile from the adsorbed acrolein and NH_x species. There has been an improvement on the TAP-1.

The advantage of the new TAP-2 reactor is that the mass spectroscopy is located under the microreactor. Thereby the detection limit is increased by a factor of 1000-10000, which implies that the required pulse size can be decreased, thus enabling operation in the Knudsen diffusion zone [Hinz et al. 1996]. Instead of minimising diffusion effects, as in PFR or CSTR, the strategy is to use a TAP reactor operated in the Knudsen diffusion regime. In this regime the transport of individual species is independent of the gas concentration.

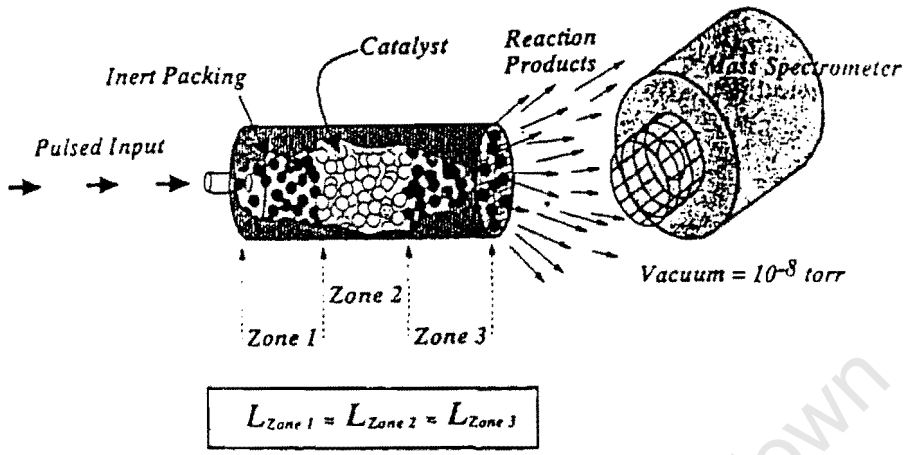

Figure 2.34 TAP reactor set-up [Gleaves et al. 1999]

2.8.3 Selectivity enhancement and catalyst surface transient conditions.

Partial oxidation of propene to acrolein over iron antimony catalyst is thought to proceed via redox mechanism [Keulks et al. 1983]. The oxidation and reduction are generally performed simultaneously, but can be physically separated by performing the reaction in two separate reactors [Callahan et al. 1970]. The feed can be alternated from a reduction environment to an oxidising environment. This would lead to a higher activity and selectivity over iron antimony catalyst. The concept of alternating feed to enhance activity and/or selectivity has been discussed by Silveston et al [1985].

van Steen et al [1999] showed that the selectivity and yield towards acrolein can be improved by operating the partial oxidation in a cyclic mode i.e. alternating the feed from reducing (hydrocarbon/air) to oxidising (air) atmospheres. The authors observed during the 30 min reaction cycle that activity and selectivity decreased in a relatively short space of time on stream. During the re-oxidation cycle some activity was regained. They concluded that to obtain higher original oxidation states of the catalyst, longer re-oxidation times, and higher re-oxidation temperatures are needed.

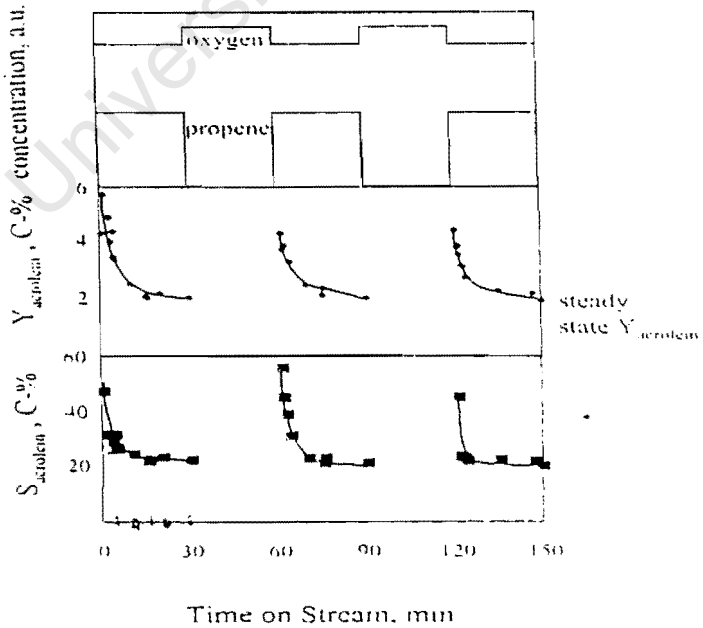

Figure 2.35 Partial oxidation of propene over iron antimony oxide catalyst (Sb/Fe=1:1) at 350°C with alternating feed [van Steen et al. 1999].

Saleh-Alhamed et al [1996] investigated periodic operation on partial oxidation of propylene to acrolein and acrylic acid over antimony tin vanadium oxide catalyst Sb/Sn/V with an ratio of Sb/Sn/V=2/1/2. Periodic experiments were carried out by cycling propene and steam. It was observed that the selectivity to acrylic acid increases with a suitable choice of mode, split and period but exceeded the highest steady-state selectivity [Lang et al. 1989b] by no more than 5%. Selectivity to Acrylic acid was observed to decline when steam cycling was used. When cycling propene, an improvement in selectivity as high as 75% towards acrolein and acrylic acid was achieved. The oxygenates and carbon dioxide were not greatly affected by cycle period. Figure 2.36 shows the improvement in time-average rate for acrolein acrylic acid at different cycling periods. The curve attained a maximum between cycle periods 1 to 2. This effect can be explained by the source of oxygen species concerned for the formation of each product.

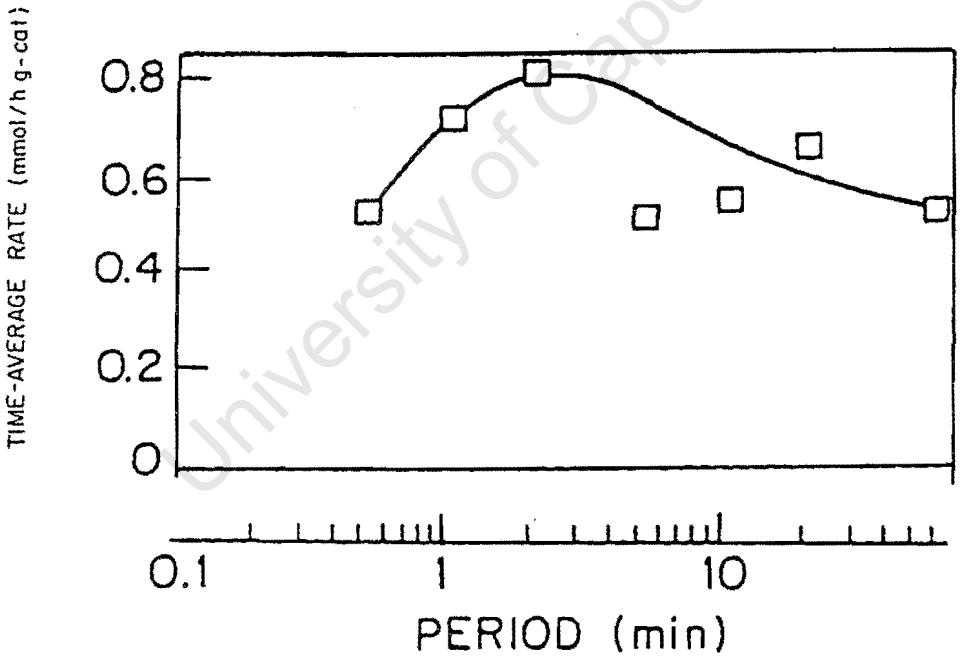

Figure 2.36 Effect of period on the time average rate of formation of products [Saleh-Alhamed et al. 1992]

According to Haber et al [1996] lattice oxygen is involved in selective oxidation whereas adsorbed oxygen radicals are responsible for total oxidation. Therefore cycling improves acrolein and acrylic acid selectivity, because it seems to keep the catalyst at high oxidation state, thus, more lattice oxygen is available for reaction.

Renken et al. [1997] investigated the oxidative coupling of toluene under periodic conditions on Pb/Li/MgO catalyst for a selective pathway to 1,2-diphenylethane. Periodic operation presented changes in product distribution in comparison with steady state through alternation of toluene oxidation in absence of oxygen in the feed and regeneration of the catalyst by oxygen. Figure 2.37 shows that the selectivity of 1,2-diphenylethane is increased from 0.6 to 0.9 by increasing the cycle period i.e. by suppressing gas phase oxygen. This is attributed to interaction between the catalyst and the toluene methyl group, which produces benzyl intermediates which react selectively to form 1,2-diphenylethane and benzene.

Figure 2.37 shows that the yield of 1,2-diphenylethane is higher under periodic operation compared to the steady-state experiment. The catalyst is observed to be more active at short periods due to short reaction intervals, which leads to less deactivation. Renken et al [1997] investigated the effect of the ratio of reaction and regeneration intervals i.e. split varying from 1:1 to 6.8:1.

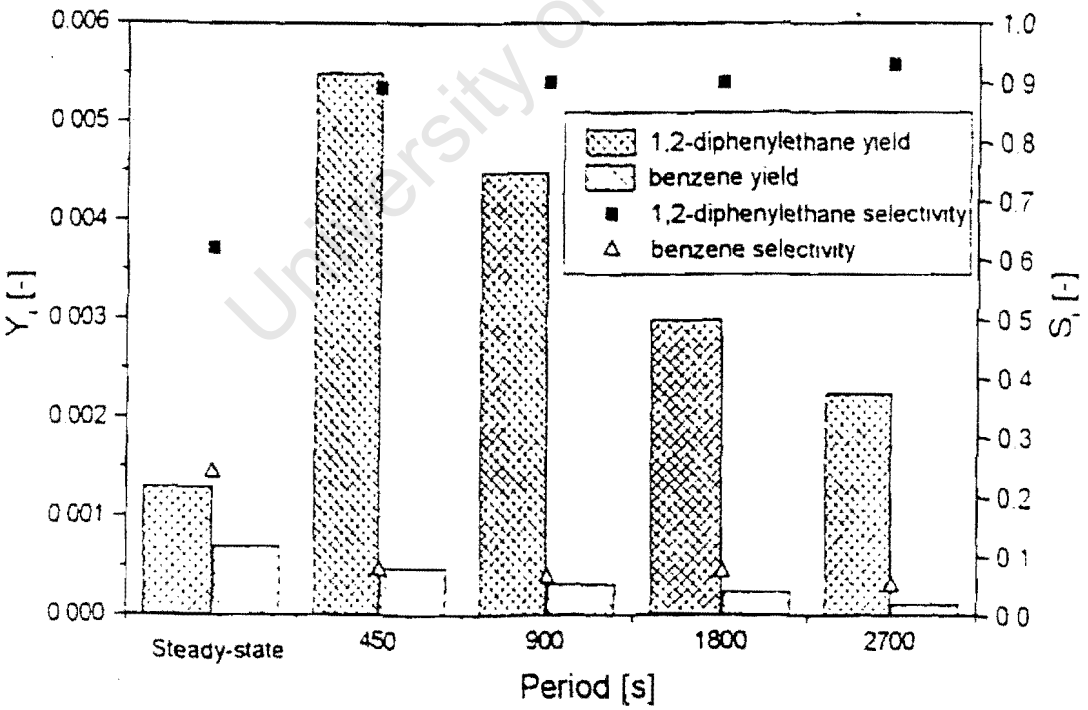

Figure 2.37 Comparison of periodic and steady-state yield and selectivity [Renken et al. 1997]

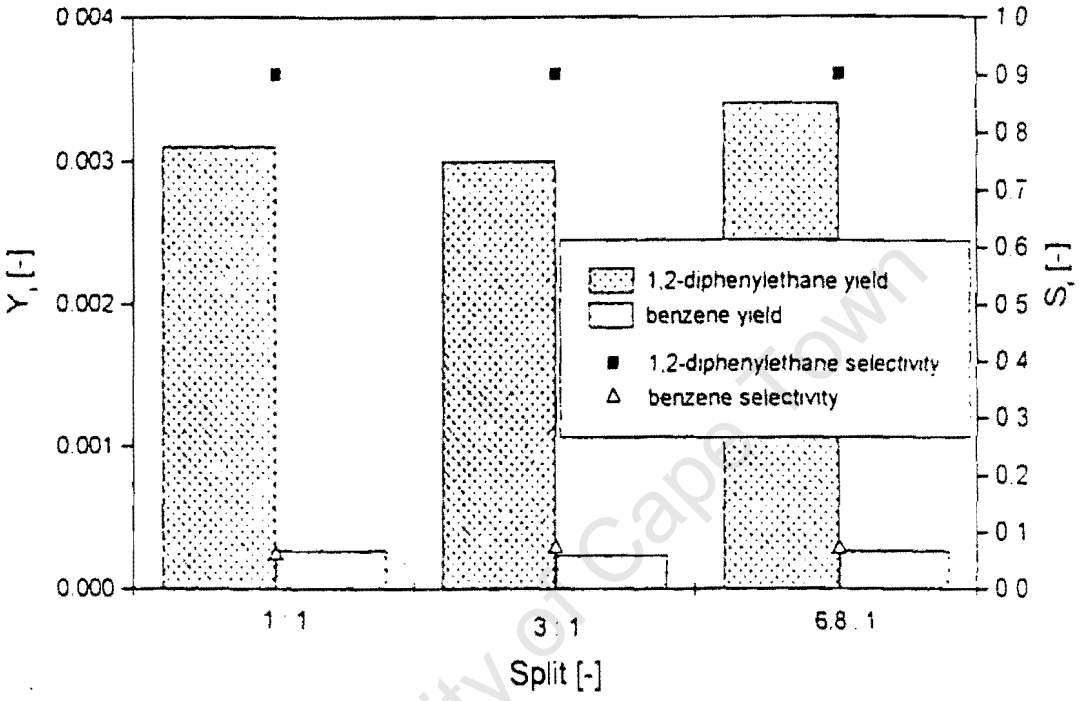

Figure 2.38 Yield and selectivity at different split ratios [Renken et al. 1997]

Figure 2.38 shows that higher toluene concentration during the 1:1 experiment induces faster deactivation while a similar effect was observed for 3:1. At lower toluene concentration ratio of 6.8:1 slowe deactivation is encountered during a longer reaction interval, thus leading to higher yields of 1,2 –diphenylethane.

Contractor et al [1997] investigated the effect steam cycling on butane oxidation over vanadyl pyrophosphate on a riser reactor. Figure 2.39 shows that the maleic anhydride yield is increased by 4%. The improvement was attributed to the competitive adsorption between steam and oxygen, hence fewer sites are available for oxygen activation and the contribution of the gas-phase –oxygen to maleic anhydride production is suppressed.

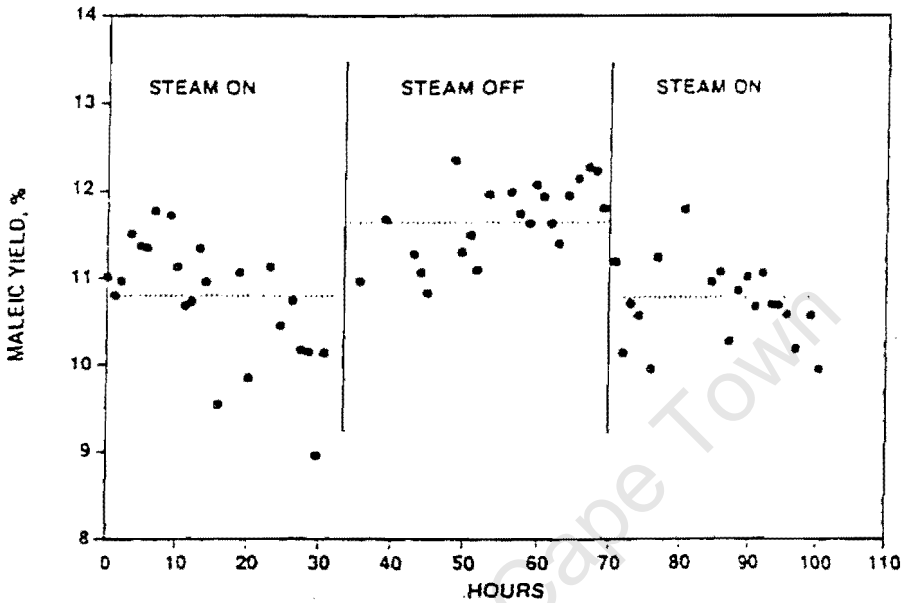

Figure 2.39 The effect of steam fed to the riser on maleic anhydride yield. Oxygen has been co-fed with steam [Contractor et al. 1997].

Cordova et al [1983] investigated transient kinetics of benzene oxidation to maleic anhydride in an automated periodic pulse reactor and the response of ($V_2O_5 - MoO_3$) to reduction and oxidation. The experimental results showed that the average reaction rate is $r_{MA}=0.466\times10^{-4}$ mol/g.h, against 0.342×10^{-4} mol/g.h in steady-state experiment. This corresponds to a 36% increase at a temperature of 370^0C with m_{sand}=3-4g and m_{cat}= 0.5g.

Lang et al [1991] investigated selectivity improvement, by alternately contacting the catalyst with butane and oxygen with an inert gas pulse between them at 350°C. Maleic anhydride (MA), furan, acrolein and total oxidation products (H_2O and CO_x) were formed as products. Short cycle periods between reactants decreased the production rate of all products except furan. At longer switching times, all products decreased as the period increased. However, the ratio of total oxidation and partial oxidation products remain unchanged by this operating mode.

It was concluded the short cycling periods do have an effect on the partial /total oxidation pathways and that an important reaction path to maleic anhydride and acrolein must be the oxidation

of furan either by gaseous or lattice oxygen. Further oxidation of MA and acrolein to CO_2 was not significant. The authors also noted that the split, defined as the duration of butadiene exposures on the catalyst before reoxidation had a little effect on the formation of oxygenates. Increasing the split increased furan production while small but similar production of maleic anhydride and acrolein were observed. Carbon dioxide production was not affected.

Creasar et al [1999] investigated the cyclic period of the oxidative dehydrogenation of propane over a V-Mg-O catalyst, alternating propane and oxygen gas mixtures. The split notation used corresponds to the propane/oxygen ratio. Thus a 1:0.4 split means the cycle consisted of 50s exposure to propane followed by 20s exposure to oxygen. Propane and oxygen conversion, selectivity and yield for periodic operation with propene to oxygen ratios are shown in figure 2.40.

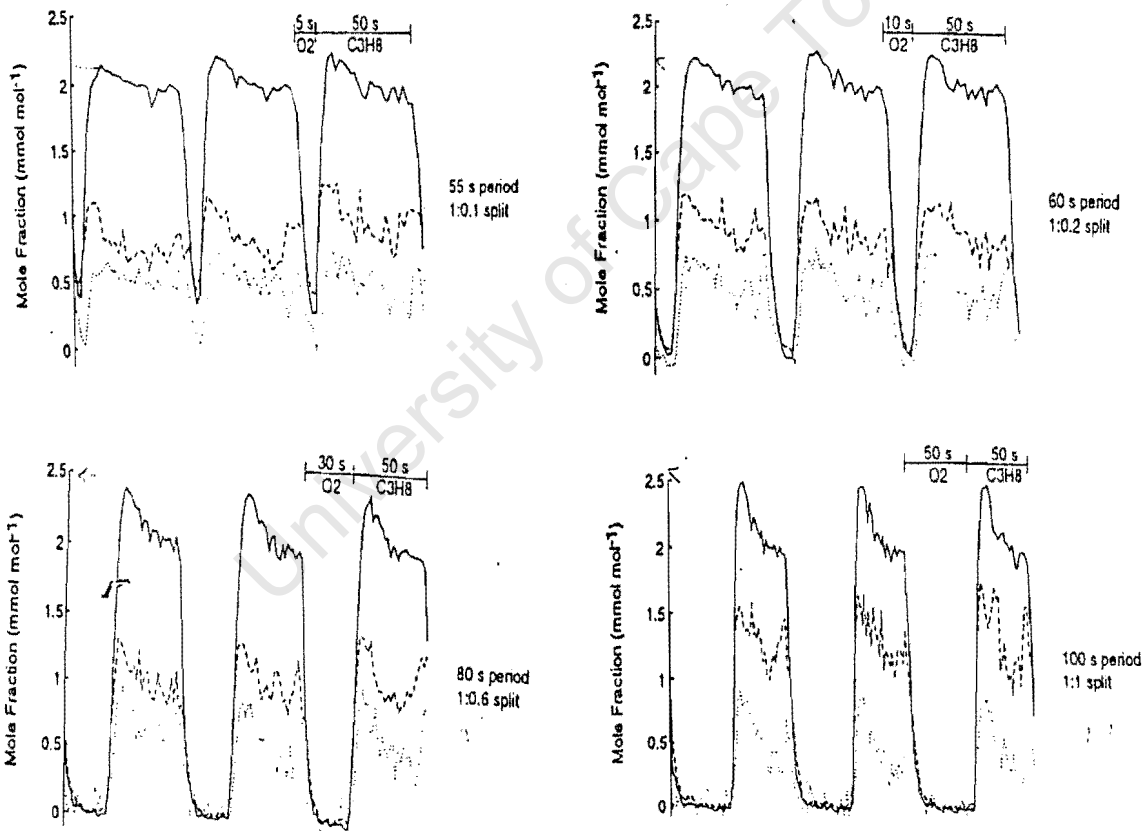

Figure 2.40 Product concentration transients over three cycles for cycling operations with a constant 50s exposure to propane and exposures to oxygen at different duration. [Creaser et al. 1999]

Propene selectivity is always higher for cycling than for steady state. The oxygen exposures could be shortened to as little as 5s, meaning that catalyst re-oxidation must be rapid. At reducedpropene to oxygen exposures, the propene yield remains constant except at shorter times.

At short oxygen exposures the change in composition was not apparent. The authors suggested that short oxygen exposures preventing 'full oxidation' of the catalyst might improve the initial selectivity after exposure to propane.

Tamilov et al [1999] investigated the transient kinetic modelling of oxidative dehydrogenation of butene-1 over Sb-Sn oxide catalyst on the basis of experimental data obtained by Shukin et al [1970]. The influence of residence time, amplitude and duration of periodic cycles, ratio of reagent concentrations within the cycle and the process parameters were simulated. An isothermal unsteady-state CSTR model was used. The suggested mechanism and the fitted parameters describe the experimental data satisfactory. Figure 2.41 shows the typical dependency of overall yield of butadiene on residence time and cycle duration.

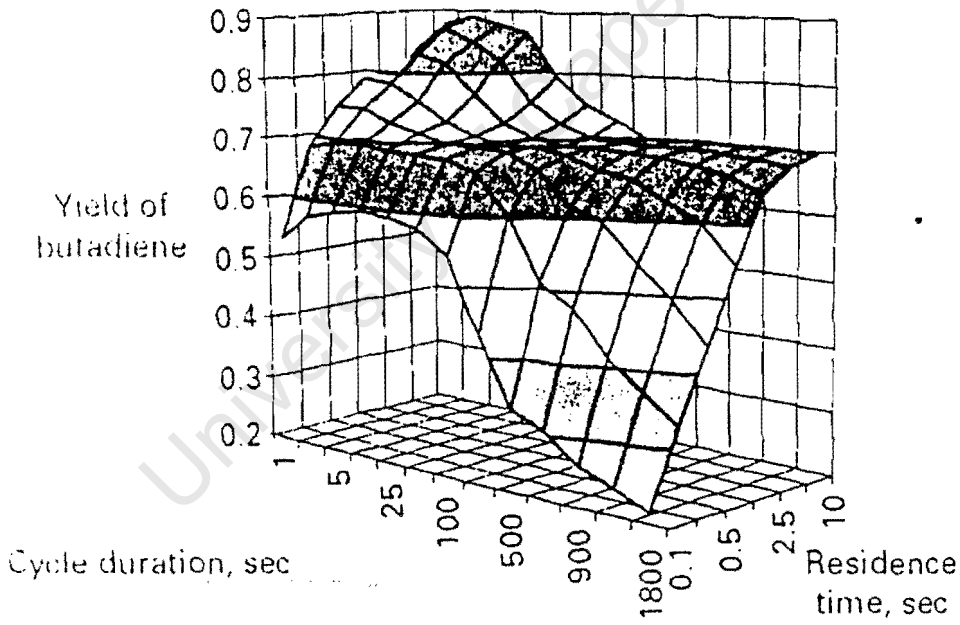

Figure 2.41 Dependency of the averaged per cycle yield of Butadiene on residence and cycle duration in the established cyclic regime [Tamilov et al 1999].

The curve also shows that butadiene yield attains a maximum at short cycles while longer cycles show characteristics of the steady-state process performance. Thus it was concluded that simulation of cycling behaviour showed that forced composition cycling makes it possible to achieve

improve process performance compared to the steady-state, resulting in the increase in butadiene yield.

2.9 KINETIC MODELLING OF OXIDATION REACTIONS

Pietrzyk et al [1999] simulated the oxydehydrogenation of propane on V_2O_5/TiO_2 under transient conditions assuming a differential plug flow reactor model in a concentration step mode. The surface coverage and partial pressure were expressed by the following ordinary differential equations:

$$\frac{dP_i}{dt} = (u/L\varepsilon)(p^0{}_j - p_j) + (RT/\varepsilon\rho)r_j(\theta, P) \tag{2.10}$$

$$\frac{d\theta_j}{dt} = \sum_j \nu_j r_j \tag{2.11}$$

Mass and heat transport phenomena were analysed to ensure that the results are not distorted. The theoretical model agreed very well with the experimental data points.

Lynch [1983] modelled resonant behaviour during cycling of catalytic reactors. The author showed that a mathematical model, which is based on a Langmuir- Hinshelwood type of mechanism, could predict the resonant behaviour of the species in the catalytic oxidation of carbon monoxide over platinum. The reaction was assumed to occur in an isothermal, well-mixed reactor operated at constant pressure. The author showed that the model predictions are in substantial qualitative agreement with a published experimental report concerning resonant behaviour of CO oxidation on platinum.

Literature has extensive information on the kinetic modelling of the reactions and transient kinetic studies, not necessarily on oxidation reactions viz. Turek et al [1999], N_2O decomposition over Cu-ZSM-5; Marin et al [1999], Transient kinetic study on conversion of methanol to olefins: Razon et al [1987], Ammonia synthesis over Rh catalyst. Silveston et al [1995] have supplied an outline of the developments made in transient studies over the years dating from the 70's to the 90's.

2.10 PROBLEM STATEMENT

The $FeSbO_4$ catalyst shows high a yield and activity in the initial few minutes of reaction. The good performance, however, decreases rapidly with time on stream to a much lower yield and activity. It is believed that this effect is due to the changing oxidation state of the catalyst as the reaction proceeds. Transient reactors provide means by which the yield and selectivity and hence the properties of the active sites can be controlled. Hence, this work will investigate the cyclic behaviour of a $FeSbO_4$ catalyst for the oxidation of propene. The transient response and the variation of the cycle times will enable a better understanding of the active site and its role in the catalytic reaction.

2.10.1 HYPOTHESIS

(a) Single site redox mechanism model qualitatively predicts the trends.

2.10.2 KEY QUESTIONS

(a) What effect do the reactants, operated on a periodic mode, have on the acrolein yield and activity?
(b) What effect does the cycle time have in acrolein yield?
(c) Does the model qualitatively predict the trends?

2.10.3 AIMS AND OBJECTIVES.

(a) To study the steady state and transient cyclic behaviour of the $FeSbO_4$-propene system.
(b) To formulate a transient single site redox model.
(c) To provide qualitative interpretation of the reaction behaviour.

3 MODEL DEVELOPMENT

3.1 Introduction

A 'lumped mechanism' approach has been used in this study. It means that a generalised mechanism (kinetic-scheme) is proposed, which contains a small number of quasi-elementary stages. The kinetic model and mechanism are developed using observed information and reasonable assumptions.

The qualitative analysis of literature data yields the following information:

(a) Reaction occurs via chemisorption of propene at the surface of the catalyst surface leading to the formation of stable surface intermediates.

(b) The surface intermediates are converted into acrolein (desired product) and undesired side products CO/CO_2 .

(c) The reduced active sites after the desorption of products are reoxidised by the oxygen from the gas phase.

3.2 Proposed reaction mechanism.

Using the following assumptions:

(a) Isothermal differential reactor. This was achieved by diluting the catalyst highly with silicon carbide on ratio of 1:20 and conversions less than 10%

(b) Constant pressure across the bed.

(c) Reoxidation and reduction occur on the same site.

(d) All the elementary reaction steps are irreversible.

(e) Propene chemisorption at the catalyst surface occurs on the fixed number of oxidised active sites

(f) Acrolein is produced directly from the surface product of propene, consuming one oxygen atom and delivering all other sites after acrolein desorption.

(g) Deep oxidation of surface intermediates to carbon oxides requires consumption of neighbouring oxygen atoms from the catalyst surface and leads to the formation of reduced active sites.

(h) Kinetic equations corresponding to the stages of propene chemisorption and oxidation are linear with respect to gas and surface concentration.

(i) Reduced sites are oxidised by oxygen from the gas phase.

On the basis of the above assumptions the following mechanism was proposed:

$$Step1: C_3H_{6(g)} + 2OV \leftrightarrow C_3H_5(OV) + OHV \quad 3.1$$

$$Step2: C_3H_5(OV) \rightarrow C_3H_5O(V) \quad 3.2$$

$$Step3: C_3H_5O(V) + OV \rightarrow C_3H_4O(V) + OHV \quad 3.3$$

$$Step4: C_3H_4O(V) \rightarrow C_3H_4O_{(g)} + V \quad 3.4$$

$$Step5: 2OHV \rightarrow H_2O_{(g)} + V + OV \quad 3.5$$

$$Step6: C_3H_5(OV) + (3x+4)OV \rightarrow 3CO_{x(g)} + 5OHV + 3xV \quad 3.6$$

$$Step7: O_{2(g)} + 2V \rightarrow 2OV \quad 3.7$$

(a) Step1: The hydride is abstracted from propene, forming a sigma allyl complex. which can lead to the formation carbon di/monoxide.

(b) Step2: The sigma allyl complex rearranges itself to a pi allyl complex.

(c) Step3: Second hydride is abstracted from the complex leading to the formation an adsorbed acrolein and hydroxyl group.

(d) Step4: The adsorbed acrolein desorbes to form gaseous acrolein.

(e) Step5: the hydroxyl groups formed in steps 1 and 3 combine to form water.

(f) Step5: Formation of CO_x from the sigma allyl complex.

(g) Step6: The gaseous oxygen from the feed replenishes the used lattice oxygen sites.

The reaction rates for equations 3.1 to 3.7 can expressed as follows:

$$r_1 = k_1 C_{C3H6} \theta_{OV} \quad 3.8$$

$$r_2 = k_2 \ \theta_{C3H5(OV)} \quad 3.9$$

$$r_3 = k_3 \theta_{C3H5O(V)} \theta_{OV} \quad 3.10$$

$$r_4 = k_4 \theta_{C3H4O(V)} \quad 3.11$$

$$r_5 = k_5 \theta_{OHV}^2 \quad 3.12$$

$$r_6 = k_6 \theta_{C3H5(OV)} \theta_{OV}^{3x+4} \quad 3.13$$

$$r_7 = k_7 C_{O_2} \theta_V \quad 3.14$$

3.3 Reactor model.

The analysis of the evolution of bulk concentration was performed using a model. The basis for the mathematical description is the mass balance for a CSTR to analyse the evolution of the bulk concentration species. The surface coverage and bulk concentration are in this approach given by a set of differential equations written below:

Equations 3.17 and 3.18 were normalised with respect to concentration and position by using the following equations.

$$x_i = \frac{C_i}{C_t} \quad 3.15$$

$$\theta_i = \frac{S_i}{N} \quad 3.16$$

Gas-phase equation:

$$\frac{dx_i}{dt} = (x_i^0 - x_i)/\tau\varepsilon - \frac{V_{cat}}{C_t V_{reactor}} \sum_i \nu_i r_i . \quad 3.17$$

Solid-phase equation:

$$\frac{d\theta_j}{dt} = \frac{m}{N} \sum_j \nu_j r_j . \quad 3.18$$

where N denotes the molar concentration of active sites per kilogram of catalyst m, denotes the mass of the catalyst. The fraction of the vacant sites is obtained from

$$\theta_V = 1 - \theta_{OV} - \theta_{C3H5(OV)} - \theta_{C3H5O(V)} - \theta_{C3H4O(V)} - \theta_{OHV} \quad 3.19$$

For each species the mass balance equation is as follows:

Bulk Concentrations expressions:

$$\frac{dx_{C3H6}}{dt} = (x^0_{C3H6} - x_{C3H6})/\tau\varepsilon - \frac{V_{cat}}{C_t V_{reactor}} r_1 \quad 3.20$$

$$\frac{dx_{O2}}{dt} = (x^0_{O2} - x_{O2})/\tau\varepsilon - \frac{V_{cat}}{C_t V_{reactor}} r_7 \quad 3.21$$

$$\frac{dx_{C3H4O}}{dt} = (x^0_{C3H4O} - x_{C3H4O})/\tau\varepsilon + \frac{V_{cat}}{C_t V_{reactor}} r_4 \quad 3.22$$

$$\frac{dx_{H2O}}{dt} = (x^0_{H2O} - x_{H2O})/\tau\varepsilon + \frac{V_{cat}}{C_t V_{reactor}} r_5 \quad 3.23$$

$$\frac{dx_{COx}}{dt} = (x^0_{COx} - x_{COx})/\tau\varepsilon + \frac{\tau V_{cat}}{C_t V_{reactor}} 3r_6 \quad 3.24$$

Surface coverage expressions:

$$\frac{d\theta_{C3H5(OV)}}{dt} = \frac{m}{N}(r_1 - r_2) \quad 3.25$$

$$\frac{d\theta_{C3H5O(V)}}{dt} = \frac{m}{N}(r_2 - r_3) \quad 3.26$$

$$\frac{d\theta_{C3H4O(V)}}{dt} = \frac{m}{N}(r_3 - r_4) \quad 3.27$$

$$\frac{d\theta_{OHV}}{dt} = \frac{m}{N}(r_1 + r_3 + 5r_6 - 2r_5) \quad 3.28$$

$$\frac{d\theta_{OV}}{dt} = \frac{m}{N}(-2r_1 - r_3 - (3x+4)r_5 + r_5 + 2r_7) \quad 3.29$$

Surface constancy expression:

$$\theta_V + \theta_{OV} + \theta_{C3H5(OV)} + \theta_{C3H5O(V)} + \theta_{C3H4O(V)} + \theta_{OHV} = 1 \quad 3.30$$

3.3.1 Initial conditions.

The resulting system of differential equations were integrated using <ODE23s> for stiff differential equations in the Matlab software package with a tolerance of tol<1×10^{-6}. The software was programmed in such a way that concentration steps of propene are obtained as follows:

$x_{propene}=0$ between t=0 and 3600seconds in the feed

$\theta_i=0$ between t=0 and 3600 except for θ_{O2} and θ_v .

Initially the catalyst was assumed to have θ_O = 0.2 and θ_v =0.8 and the simulation was carried out allowing the reaction to reach steady state before turning the propene on. The pretreatment with oxygen was taken to be 3600 seconds; similar to the time used in the laboratory experiments. The structure of the program is presented in appendix 5.

4 EXPERIMENTAL

4.1 Materials

4.1.1 Gases

The gases used are listed in Table 4.1 and were filtered before feeding them into the reactor. Silicon carbide (270micron) was supplied by Aldrich and was used as a diluent.

Table 4.1 Gas specifications

Gases	Molar-mass	Manufacturer	Purity%
Propene	42.081	Fedgas	99.9
Oxygen	31.999	Fedgas	9.999
Helium	4.003	Fedgas	99.99
Methane	15.999	Air products	99.99

4.2 Catalyst

4.2.1 Catalyst preparation

The iron antimony oxide catalyst was prepared by the method described by Allen et al [1996]. A catalyst of Sb/Fe =1.5:1 required a mass of 10.55g and 8.55 g of iron nitrate and antimony oxide respectively. Fe $(NO_3)_3.9H_2O$ was heated to 60°C and a solution of iron nitrate was formed in water of crystallisation. The corresponding mass of Sb_2O_3 was added to the solution and the pH of the solution was approximately one. The temperature was raised to 80°C. An aqueous solution of NH_3 (approximately 10 ml) was added to raise the pH to 3. The catalyst was dried at 120°C for 16hrs to allow interdiffusion of ions and subsequently calcined in air at 900°C for 7hrs.

4.2.2 Catalyst characterisation.

4.2.2.(i) X-ray diffraction measurements

The catalyst structure was analysed using X-ray diffraction (XRD). Phillips X-ray diffractometer generated Cu-Kα radiation at 40 kV, 30mV with a wavelength of 1.54Å. Approximately 0.5 g was placed on to the sampler holder and the surface was carefully levelled out. A scan range of $20^0 < 2\theta < 70^0$ with a step size of 0.1^0 was used. The XRD pattern was then compared with values obtained from the literature [JCPDS, 1980].

4.2.2.(ii) Infrared measurements.

FT-IR spectra of the catalyst (ca. 1% in KBr) were recorded at room temperature using a Nicolet 5ZDX FT-IR spectrometer at a resolution of $4cm^{-1}$ over the wave-number range of 400 to $4000cm^{-1}$. The sample and the KBr were predried in air an oven at 100°C for 2hrs and prior to the wafer preparation.

4.2.2.(iii) BET characterisation

N_2-BET surface area measurements were determined using an Accelerated Surface Area and Porosimetry (ASAP) 2000 system from Micromeritics. About 1g of $FeSbO_4$ sample was dried for 120 minutes in situ at 150^0C under vacuum conditions (5μmHg). Nitrogen was then adsorbed at the boiling temperature of liquid nitrogen (77K) using an extended pressure table with 150 pressure points ranging from 0.65kPa to ambient pressure.

4.3 Experimental apparatus

All reactions were carried out in the apparatus as shown in figure 4.1. The apparatus consisted of four mass flow controllers, each for propene, oxygen helium and methane. The feed gas was passed through a mixer before entering the reactor or going through the bypass line. The reactor was situated inside the furnace to minimise temperature gradients. The details of the reactor are given in section 4.3.1. The actual temperature of the bed was monitored by a thermocouple housed in ¼ " graphite ferrule and it protruded into the catalyst packing.

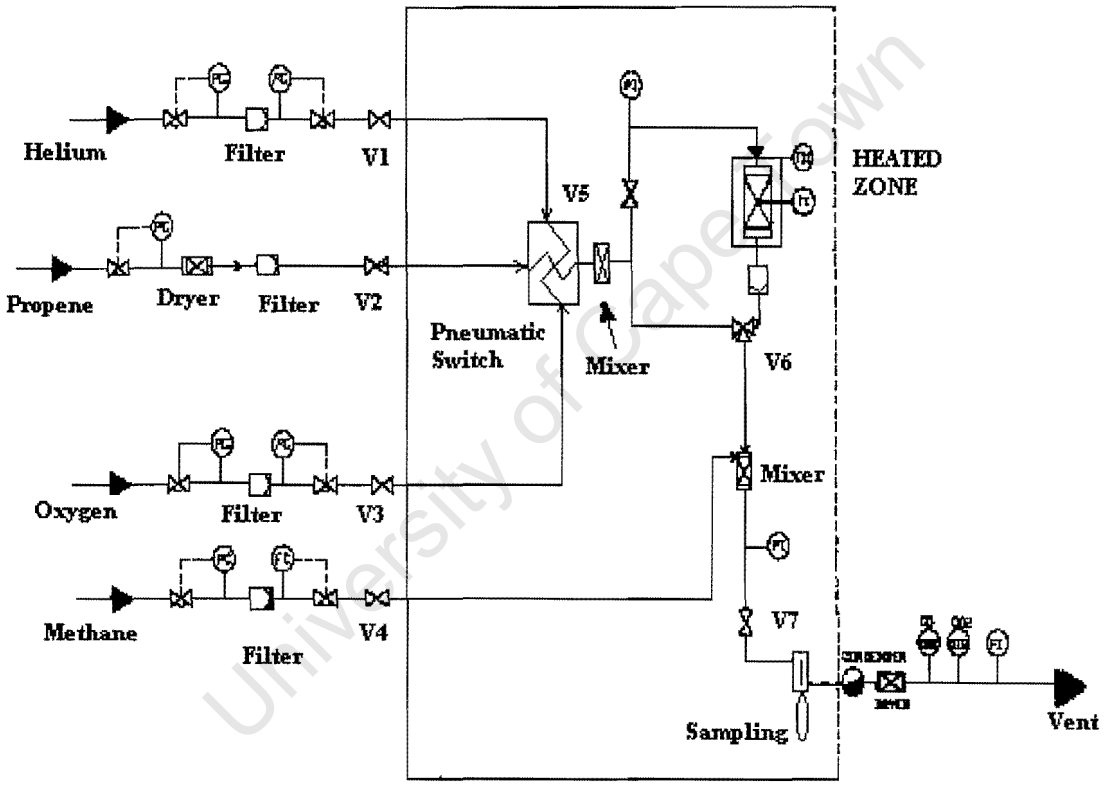

Figure 4.1 Flowsheet of the experimental rig

An internal standard was fed into the gas stream using a mass flow controller to facilitate product analysis. After passing through the mixer, the final gas steam flowed through the ampoule sampler (Schulz et al [1986]) and passed through the bubble flow meter before it was vented. The product and internal standard lines were heated to 180^0C. The details of the pneumatic switch for the oxidation and the reduction phase are shown in figure 4.2(a) and (b).

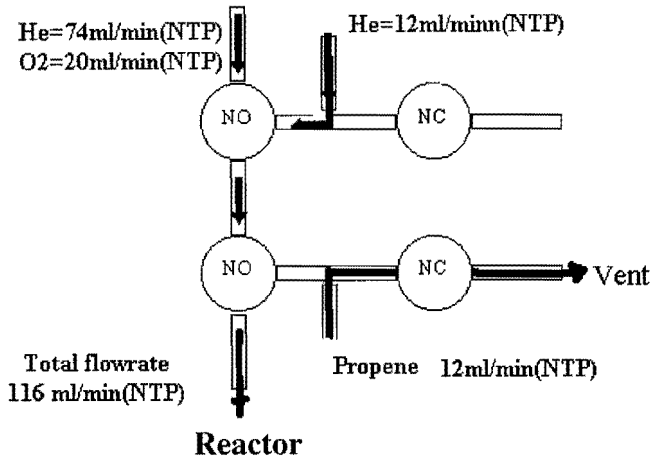

NO = Normally open **NC** = Normally closed

Figure 4.2 (a) Pneumatic switch for the **oxidation phase**

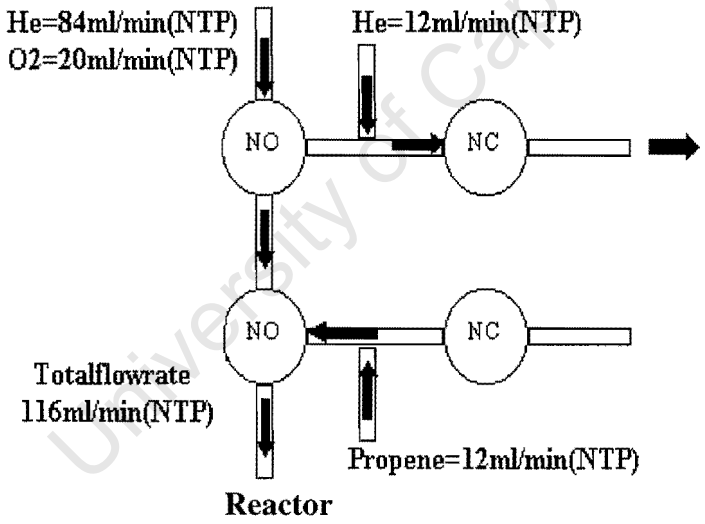

NO = Normally open **NC** = Normally closed

Figure 4.2(b) Pneumatic switch for the **reduction phase.**

The normally closed or open magnetic switches were electrically operated and have an aperture, which is controlled by the flow of nitrogen, so as to direct the flow of propene (12ml/minNTP) and that of make up helium (12ml/minNTP) online or to vent depending on the reduction or oxidation environment. The flow of helium (84ml/minNTP) and oxygen (20ml/minNTP) was kept flowing throughout the experiment. The total

volumetric flow was always kept constant at all times, by switching the make up gas on during the oxidation phase.

4.3.1 Reactor

Figure 4.3 shows a schematic diagram of the fixed bed reactor which consisted of a stainless steel tube with internal diameter of 4mm and an outer diameter of 5 mm and a length of 360 mm.. From top to bottom the reactor was connected via the VCR fittings to a head and bottom piece, which were welded to the feed and product line respectively and was operated in down flow mode.

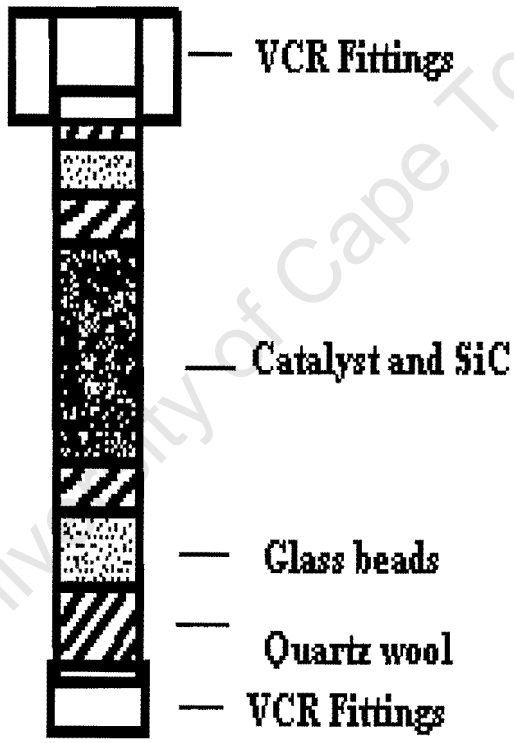

Figure 4.3 Fixed bed reactor used for partial oxidation of propene.

4.3.2 Ampoule sampler.

Figure 4.4 shows the sketch of an ampoule sampler. This method of analysis was developed by Schulz et al [1986] and is described in detail in this reference.

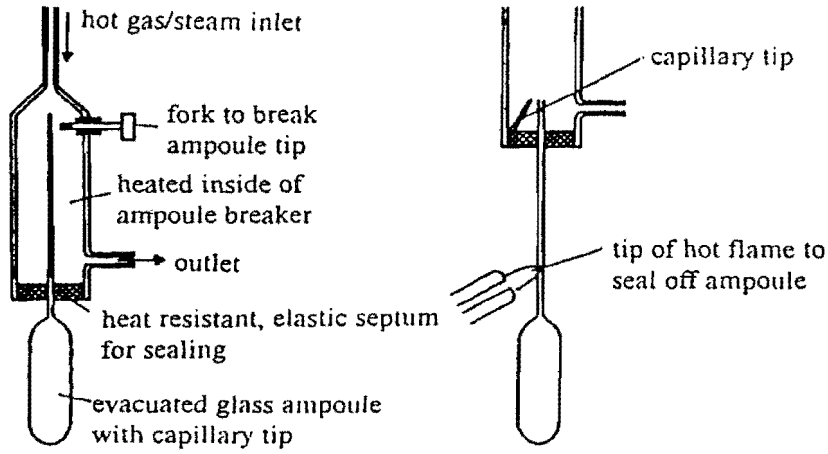

Figure 4.4 Ampoule sampler [Schulz et al. 1986]

4.4 Experimental procedure.

A blank run was carried out using silicon carbide (270micron) before loading the catalyst. The purpose of the blank run was to ensure that there are no traces of the catalyst that are in the rig other than in the reactor.

4.4.1 Steady-state experiment.

The reactor was loaded with a mixture of 1g catalyst and 20g of silicon carbide to minimise temperature gradients in the reactor. The packing was stabilised by plugs of quartz wool at both the reactor top and bottom. After each loading the reactor was leak tested before each run. The catalyst was then treated with 20ml/min (NTP) of oxygen and 84ml/min (NTP) of helium at reaction temperature ($T_r = 375^0C$) for an hour. This is the process whereby the reduced catalyst is transformed into an active form by the catalytic transformation of bulk oxygen by the ferric ions in the catalyst into nucleophilic and electrophilic oxygen.

Then 12ml/min (NTP) of propene and 30ml/min (NTP) methane were introduced while bypassing the reactor. The flows were allowed to stabilise for 4hrs. In the process sam-

ples were taken to determine if the flows have stabilised. A bypass sample was then taken to determine the initial conditions. The propene was then introduced into the reactor and samples were taken every 2 minutes for the first 20 minutes, and the catalyst was then pretreated with oxygen at different time. High frequency sampling was required since the iron antimonate catalyst reduces rapidly with time on stream [Schnobel et al 1997].

A bubble-flowmeter, which was connected to a vent, was used to measure the total flow. Methane served as an internal standard for the evaluation of carbon balance and the calculation of the yield, conversion and selectivity. Table 4.2 shows the summary for the reaction conditions:

Table 4.2 Summary of reaction conditions.

Reaction temperature	370°C
Catalyst mass	1g
WHSV	0.02g/g_{cat}min
Propene flow	12ml/min(NTP)
Oxygen flow	20ml/min(NTP)
Helium flow	84ml/min(NTP)

The heating tapes were used to maintain the lines at 180°C. Their purpose was to ensure that acrolein does not condense along the lines since acrolein boils at 54°C, as this would affect the mass balance.

4.4.2 Unsteady-state experiment.

The concentration forcing of propene was carried out using electro-operated pneumatic switches . 84ml/min (NTP) helium and 20ml/min (NTP) oxygen were used to pretreat the catalyst for 1hr at 375°C while propene was vented. Thereafter propene was passed

through the bypass to evaluate initial condition. Using a two way valve the mixture of 12ml/min (NNTP) propene, 20ml/min (NTP) oxygen and 84ml/min (NTP) of helium was passed through the reactor. The reaction was carried out at different switching times of propene varied from 5min, 10min, 20min and 30min. For each experiment propene cycling was carried out three times. The moment when the reactor was switched on line with the feed was defined as zero. The dead time of the reactor and the experimental rig was 3.5 s. Table 4.3 depicts the overview of the experiments carried out.

Table 4.3 Overview of the experiments conducted.

Duration of oxygen treatment.	Time on stream (min)	No of cycles
30	120	3
20	120	3
10	120	3
5	120	3

4.4.3 Product analysis

The capillary and the ampoule were preheated in heated flame of a butane torch to avoid condensation of the product gas. The ampoule was push into the septum of the ampoule sampler until it was fully housed. The tip of the capillary was broken and the product gas filled the pre-evacuated ampoule. The ampoule was sealed off immediately using a butane torch flame. The ampoule sampling technique completely decouples the sampling from the analysis and thus samples can be stored over a long period of time and data points with a frequency of up to one sample every 20 seconds can be achieved.

4.4.3.(i) Gas chromatography analysis

The ampoules containing the product was then broken in a heated ampoule breaker, which was connected to the gas chromatograph via a six port sampling valve. The GC carrier gas could thus bypass the ampoule breaker or transport the product sample to the column when both were switched in-line. The analysis of the products from the conver-

sion of propene was performed using a SGE-BP5 capillary column (100 m long and film thickness 0.5 micron) connected into a Varian 3400 gas chromatograph. The GC was equipped with a flame ionisation detector. Table 4.4 shows the specification and temperature program.

Table 4.4 GC flowrates and settings.

GC parameter	Settings
Nitrogen Flowrate (Make up gas)	30 ml/min(NTP)
Hydrogen Flowrate (FID)	30ml/min(NTP)
Temperature program	35°C for t=10min
split	1:100
Column head pressure	30psig
Column length	50m
Inner diameter	0.2mm
Stationary phase	Phenyl dimethyl Siloxane
Film thickness	0.5μm
Flame ionisation detector range	7
Flame ionisation detector attenuation	2

4.4.4 Analysis of data

When the ampoule technique is used, carbon balance can only be determined with the help of the internal standard, methane. The internal standard does not react with the products and does not interfere with the product peaks in the gas chromatography.

The molar flowrates of the products and reactants F_i were calculated using the formula below based on the known peak areas A_i.

$$F_i = F_{istd} \frac{N_{c,istd} A_i RF_i}{N_{c,i} A_{istd} RF_{istd}} \qquad 4.1$$

Carbon balance around the reactor was performed by comparing the incoming flow of carbon to the out flowing carbon in the product stream. Using the bypass the amount of carbon coming in could be evaluated before the reactants are switch into the reactor.

$$C-balance = \frac{\sum F_{i,out} N_{ci} + F_{feed,out} N_{c,feed}}{F_{feed,in} N_{c,feed}} \qquad 4.2$$

Using the peak areas from the chromatographic analysis the % balance is calculated as shown below:

$$C-balance = \frac{\sum \frac{A_{i,out} RF_i}{A_{istd} RF_{istd}}}{\frac{A_{feed,in} RF_{feed}}{A_{Istd} RF_{Istd}}} \times 100\% \qquad 4.3$$

Conversion based on the reactant was calculated as follows:

$$X = \frac{F_{feed,in} - F_{feed,out}}{F_{feed,in}} \qquad 4.4$$

The peak areas A_i from the GC analysis enable the conversion to be calculated as follows:

$$X = 1 - \frac{\frac{A_{feed,out} RF_{feed}}{A_{istd} RF_{istd}}}{\frac{A_{feed,in} RF_{feed}}{A_{Istd} RF_{Istd}}} \qquad 4.5$$

4.4.5 Linear velocity.

It is defined as the gas velocity at reactor conditions in an empty reactor and was quantified assuming constant density system:

$$u = \frac{FRT_{reactor}}{P_t} \qquad 4.6$$

4.4.6 Mass and heat transport in transient partial oxidation of propene.

It was then necessary to investigate heat and mass transport so that the results do not become distorted. Moulijn et al [1991] gave a detailed general analysis of intra and inter heat and mass transport for transient experiments for a reaction of general order. The estimations of the mass transport and thermodynamic properties of the gas mixture were obtained from Perry et al [1984]. Gas phase was considered as ternary-mixture of propene, helium and oxygen. The product partial pressures were ignored. A complete outline of the mass and heat transfer limitation is entailed in appendix 3. It was found that intra and inter mass transfer and intra particle heat transfer limitations were absent while the inter particle heat transfer limitations were existing. The maximum temperature difference ($T_{surface} - T_{bulk}$) between the catalyst surface and the bulk temperature was evaluated to be 123 K , assuming that the mass-transfer controls the global reaction rate by equation 4.7.

$$T_{surface} - T_{bulk} = \frac{-\Delta H}{C_p \rho} C_b \qquad 4.7$$

4 EXPERIMENTAL

4.1 Materials

4.1.1 Gases

The gases used are listed in Table 4.1 and were filtered before feeding them into the reactor. Silicon carbide (270micron) was supplied by Aldrich and was used as a diluent.

Table 4.1 Gas specifications

Gases	Molar-mass	Manufacturer	Purity%
Propene	42.081	Fedgas	99.9
Oxygen	31.999	Fedgas	9.999
Helium	4.003	Fedgas	99.99
Methane	15.999	Air products	99.99

4.2 Catalyst

4.2.1 Catalyst preparation

The iron antimony oxide catalyst was prepared by the method described by Allen et al [1996]. A catalyst of Sb/Fe =1.5:1 required a mass of 10.55g and 8.55 g of iron nitrate and antimony oxide respectively. Fe $(NO_3)_3.9H_2O$ was heated to 60°C and a solution of iron nitrate was formed in water of crystallisation. The corresponding mass of Sb_2O_3 was added to the solution and the pH of the solution was approximately one. The temperature was raised to 80°C. An aqueous solution of NH_3 (approximately 10 ml) was added to raise the pH to 3. The catalyst was dried at 120°C for 16hrs to allow interdiffusion of ions and subsequently calcined in air at 900°C for 7hrs.

4.2.2 Catalyst characterisation.

4.2.2.(i) X-ray diffraction measurements

The catalyst structure was analysed using X-ray diffraction (XRD). Phillips X-ray diffractometer generated Cu-Kα radiation at 40 kV, 30mV with a wavelength of 1.54Å. Approximately 0.5 g was placed on to the sampler holder and the surface was carefully levelled out. A scan range of $20^0 < 2\theta < 70^0$ with a step size of 0.1^0 was used. The XRD pattern was then compared with values obtained from the literature [JCPDS, 1980].

4.2.2.(ii) Infrared measurements.

FT-IR spectra of the catalyst (ca. 1% in KBr) were recorded at room temperature using a Nicolet 5ZDX FT-IR spectrometer at a resolution of $4cm^{-1}$ over the wave-number range of 400 to $4000cm^{-1}$. The sample and the KBr were predried in air an oven at 100°C for 2hrs and prior to the wafer preparation.

4.2.2.(iii) BET characterisation

N_2-BET surface area measurements were determined using an Accelerated Surface Area and Porosimetry (ASAP) 2000 system from Micromeritics. About 1g of $FeSbO_4$ sample was dried for 120 minutes in situ at 150^0C under vacuum conditions (5μmHg). Nitrogen was then adsorbed at the boiling temperature of liquid nitrogen (77K) using an extended pressure table with 150 pressure points ranging from 0.65kPa to ambient pressure.

4.3 Experimental apparatus

All reactions were carried out in the apparatus as shown in figure 4.1. The apparatus consisted of four mass flow controllers, each for propene, oxygen helium and methane. The feed gas was passed through a mixer before entering the reactor or going through the bypass line. The reactor was situated inside the furnace to minimise temperature gradients. The details of the reactor are given in section 4.3.1. The actual temperature of the bed was monitored by a thermocouple housed in ¼ " graphite ferrule and it protruded into the catalyst packing.

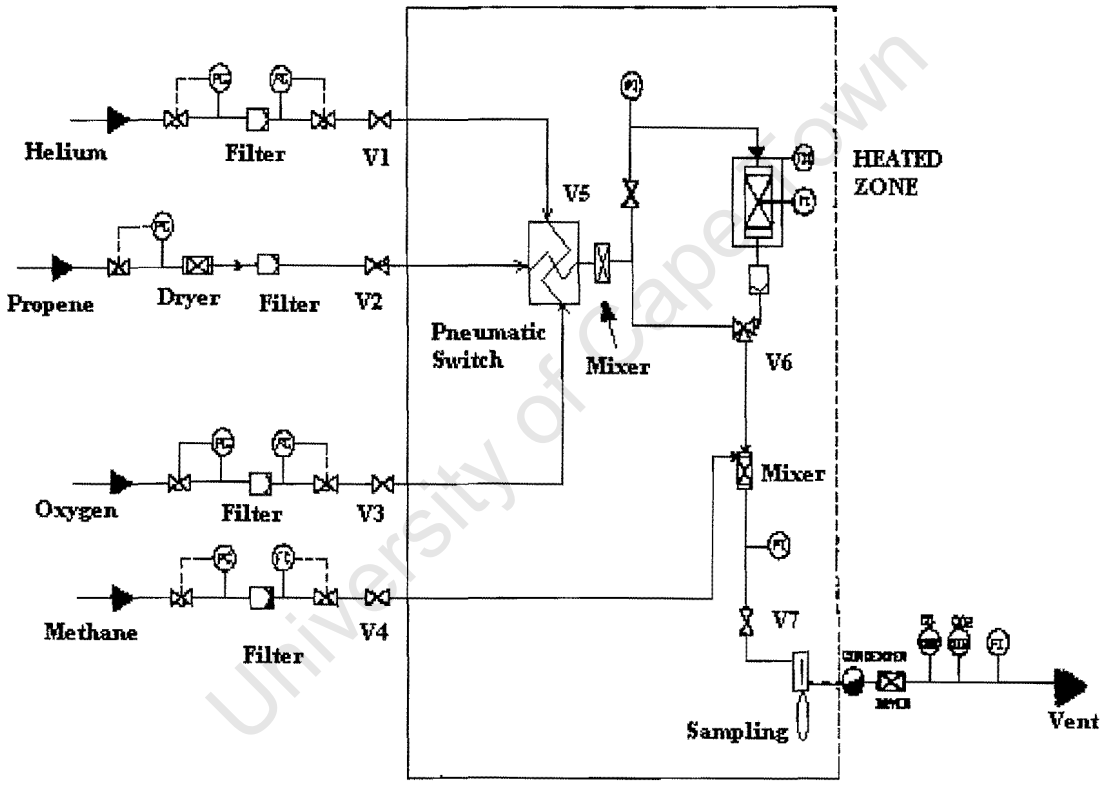

Figure 4.1 Flowsheet of the experimental rig

An internal standard was fed into the gas stream using a mass flow controller to facilitate product analysis. After passing through the mixer, the final gas steam flowed through the ampoule sampler (Schulz et al [1986]) and passed through the bubble flow meter before it was vented. The product and internal standard lines were heated to 180^0C. The details of the pneumatic switch for the oxidation and the reduction phase are shown in figure 4.2(a) and (b).

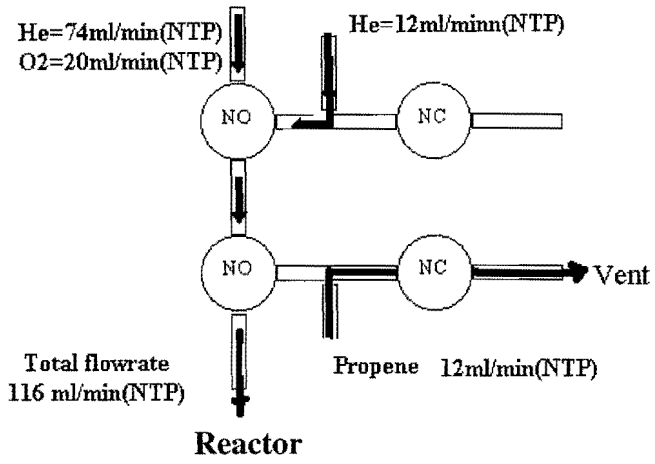

NO = Normally open **NC** = Normally closed

Figure 4.2 (a) Pneumatic switch for the **oxidation phase**

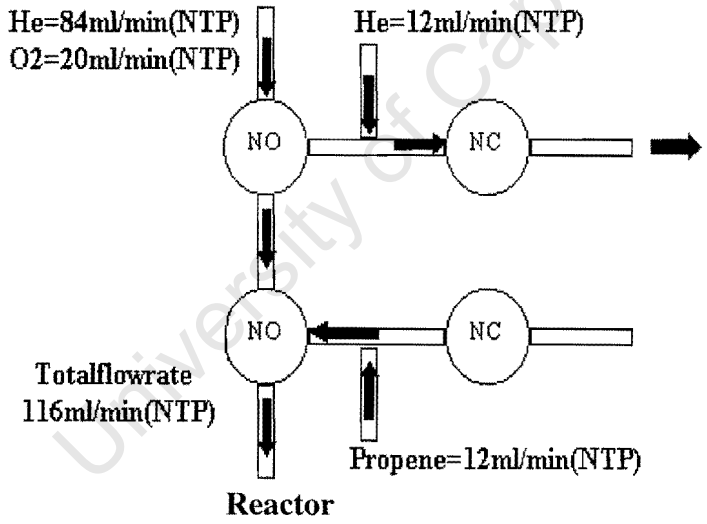

NO = Normally open **NC** = Normally closed

Figure 4.2(b) Pneumatic switch for the **reduction phase.**

The normally closed or open magnetic switches were electrically operated and have an aperture, which is controlled by the flow of nitrogen, so as to direct the flow of propene (12ml/minNTP) and that of make up helium (12ml/minNTP) online or to vent depending on the reduction or oxidation environment. The flow of helium (84ml/minNTP) and oxygen (20ml/minNTP) was kept flowing throughout the experiment. The total

volumetric flow was always kept constant at all times, by switching the make up gas on during the oxidation phase.

4.3.1 Reactor

Figure 4.3 shows a schematic diagram of the fixed bed reactor which consisted of a stainless steel tube with internal diameter of 4mm and an outer diameter of 5 mm and a length of 360 mm.. From top to bottom the reactor was connected via the VCR fittings to a head and bottom piece, which were welded to the feed and product line respectively and was operated in down flow mode.

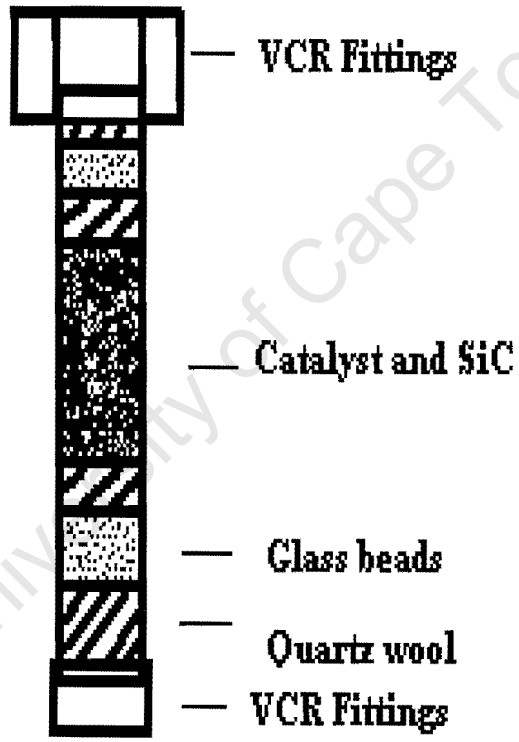

Figure 4.3 Fixed bed reactor used for partial oxidation of propene.

4.3.2 Ampoule sampler.

Figure 4.4 shows the sketch of an ampoule sampler. This method of analysis was developed by Schulz et al [1986] and is described in detail in this reference.

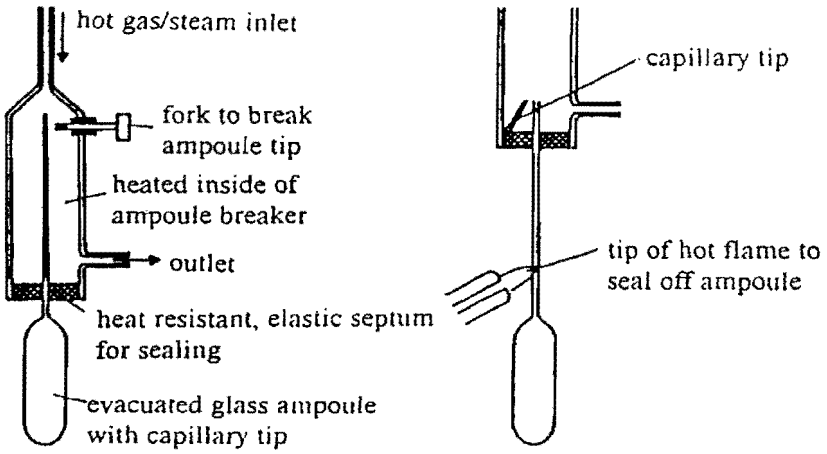

Figure 4.4 Ampoule sampler [Schulz et al. 1986]

4.4 Experimental procedure.

A blank run was carried out using silicon carbide (270micron) before loading the catalyst. The purpose of the blank run was to ensure that there are no traces of the catalyst that are in the rig other than in the reactor.

4.4.1 Steady-state experiment.

The reactor was loaded with a mixture of 1g catalyst and 20g of silicon carbide to minimise temperature gradients in the reactor. The packing was stabilised by plugs of quartz wool at both the reactor top and bottom. After each loading the reactor was leak tested before each run. The catalyst was then treated with 20ml/min (NTP) of oxygen and 84ml/min (NTP) of helium at reaction temperature ($T_r = 375^0C$) for an hour. This is the process whereby the reduced catalyst is transformed into an active form by the catalytic transformation of bulk oxygen by the ferric ions in the catalyst into nucleophilic and electrophilic oxygen.

Then 12ml/min (NTP) of propene and 30ml/min (NTP) methane were introduced while bypassing the reactor. The flows were allowed to stabilise for 4hrs. In the process sam-

ples were taken to determine if the flows have stabilised. A bypass sample was then taken to determine the initial conditions. The propene was then introduced into the reactor and samples were taken every 2 minutes for the first 20 minutes, and the catalyst was then pretreated with oxygen at different time. High frequency sampling was required since the iron antimonate catalyst reduces rapidly with time on stream [Schnobel et al 1997].

A bubble-flowmeter, which was connected to a vent, was used to measure the total flow. Methane served as an internal standard for the evaluation of carbon balance and the calculation of the yield, conversion and selectivity. Table 4.2 shows the summary for the reaction conditions:

Table 4.2 Summary of reaction conditions.

Reaction temperature	370°C
Catalyst mass	1g
WHSV	0.02g/g_{cat}min
Propene flow	12ml/min(NTP)
Oxygen flow	20ml/min(NTP)
Helium flow	84ml/min(NTP)

The heating tapes were used to maintain the lines at 180°C. Their purpose was to ensure that acrolein does not condense along the lines since acrolein boils at 54°C, as this would affect the mass balance.

4.4.2 Unsteady-state experiment.

The concentration forcing of propene was carried out using electro-operated pneumatic switches . 84ml/min (NTP) helium and 20ml/min (NTP) oxygen were used to pretreat the catalyst for 1hr at 375°C while propene was vented. Thereafter propene was passed

through the bypass to evaluate initial condition. Using a two way valve the mixture of 12ml/min (NNTP) propene, 20ml/min (NTP) oxygen and 84ml/min (NTP) of helium was passed through the reactor. The reaction was carried out at different switching times of propene varied from 5min, 10min, 20min and 30min. For each experiment propene cycling was carried out three times. The moment when the reactor was switched on line with the feed was defined as zero. The dead time of the reactor and the experimental rig was 3.5 s. Table 4.3 depicts the overview of the experiments carried out.

Table 4.3 Overview of the experiments conducted.

Duration of oxygen treatment.	Time on stream (min)	No of cycles
30	120	3
20	120	3
10	120	3
5	120	3

4.4.3 Product analysis

The capillary and the ampoule were preheated in heated flame of a butane torch to avoid condensation of the product gas. The ampoule was push into the septum of the ampoule sampler until it was fully housed. The tip of the capillary was broken and the product gas filled the pre-evacuated ampoule. The ampoule was sealed off immediately using a butane torch flame. The ampoule sampling technique completely decouples the sampling from the analysis and thus samples can be stored over a long period of time and data points with a frequency of up to one sample every 20 seconds can be achieved.

4.4.3.(i) Gas chromatography analysis

The ampoules containing the product was then broken in a heated ampoule breaker, which was connected to the gas chromatograph via a six port sampling valve. The GC carrier gas could thus bypass the ampoule breaker or transport the product sample to the column when both were switched in-line. The analysis of the products from the conver-

sion of propene was performed using a SGE-BP5 capillary column (100 m long and film thickness 0.5 micron) connected into a Varian 3400 gas chromatograph. The GC was equipped with a flame ionisation detector. Table 4.4 shows the specification and temperature program.

Table 4.4 GC flowrates and settings.

GC parameter	Settings
Nitrogen Flowrate (Make up gas)	30 ml/min(NTP)
Hydrogen Flowrate (FID)	30ml/min(NTP)
Temperature program	35°C for t=10min
split	1:100
Column head pressure	30psig
Column length	50m
Inner diameter	0.2mm
Stationary phase	Phenyl dimethyl Siloxane
Film thickness	0.5µm
Flame ionisation detector range	7
Flame ionisation detector attenuation	2

4.4.4 Analysis of data

When the ampoule technique is used, carbon balance can only be determined with the help of the internal standard, methane. The internal standard does not react with the products and does not interfere with the product peaks in the gas chromatography.

The molar flowrates of the products and reactants F_i were calculated using the formula below based on the known peak areas A_i.

$$F_i = F_{istd} \frac{N_{c,istd} A_i RF_i}{N_{c,i} A_{istd} RF_{istd}} \qquad 4.1$$

Carbon balance around the reactor was performed by comparing the incoming flow of carbon to the out flowing carbon in the product stream. Using the bypass the amount of carbon coming in could be evaluated before the reactants are switch into the reactor.

$$C - balance = \frac{\sum F_{i,out} N_{ci} + F_{feed,out} N_{c,feed}}{F_{feed,in} N_{c,feed}} \qquad 4.2$$

Using the peak areas from the chromatographic analysis the % balance is calculated as shown below:

$$C - balance = \frac{\sum \frac{A_{i,out} RF_i}{A_{istd} RF_{istd}}}{\frac{A_{feed,in} RF_{feed}}{A_{Istd} RF_{Istd}}} \times 100\% \qquad 4.3$$

Conversion based on the reactant was calculated as follows:

$$X = \frac{F_{feed,in} - F_{feed,out}}{F_{feed,in}} \qquad 4.4$$

The peak areas A_i from the GC analysis enable the conversion to be calculated as follows:

$$X = 1 - \frac{\frac{A_{feed,out} RF_{feed}}{A_{istd} RF_{istd}}}{\frac{A_{feed,in} RF_{feed}}{A_{Istd} RF_{Istd}}} \qquad 4.5$$

4.4.5 Linear velocity.

It is defined as the gas velocity at reactor conditions in an empty reactor and was quantified assuming constant density system:

$$u = \frac{FRT_{reactor}}{P_t} \qquad 4.6$$

4.4.6 Mass and heat transport in transient partial oxidation of propene.

It was then necessary to investigate heat and mass transport so that the results do not become distorted. Moulijn et al [1991] gave a detailed general analysis of intra and inter heat and mass transport for transient experiments for a reaction of general order. The estimations of the mass transport and thermodynamic properties of the gas mixture were obtained from Perry et al [1984]. Gas phase was considered as ternary-mixture of propene, helium and oxygen. The product partial pressures were ignored. A complete outline of the mass and heat transfer limitation is entailed in appendix 3. It was found that intra and inter mass transfer and intra particle heat transfer limitations were absent while the inter particle heat transfer limitations were existing. The maximum temperature difference ($T_{surface} - T_{bulk}$) between the catalyst surface and the bulk temperature was evaluated to be 123 K , assuming that the mass-transfer controls the global reaction rate by equation 4.7.

$$T_{surface} - T_{bulk} = \frac{-\Delta H}{C_p \rho} C_b \qquad 4.7$$

5 RESULTS:

5.1 Catalyst characterisation.

5.1.1 X-ray diffraction

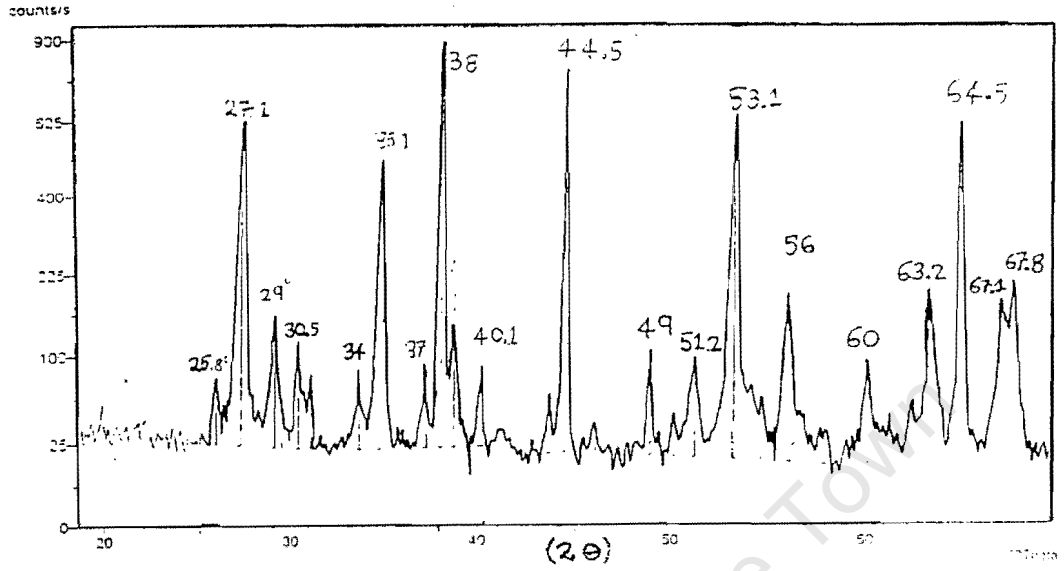

Figure 5.1: X-ray diffractogram for $FeSbO_4$ [Sb/Fe =1.5]

Figure 5.1 depicts the X-ray diffraction analysis of iron antimony oxide catalyst of Sb/Fe=1.5:1, calcined at 900°C. The X-ray diffractogram contains three major peaks at 2θ =27.1, 35.1, 53.1 respectively and were compared with the data from known phases. It is evident from Table 5.1 that the bulk of the catalyst has a $FeSbO_4$ phase with rutile structure, [Bithell et al 1994]. Burriesci et al [1982] and Schnobel et al [1997] reported that the lines become more intense with an increase in temperature (400-1100°C) due to the mobility of Sb_2O_4 at high temperatures. This was expected since the catalyst was calcined at 900°C and Sb_2O_4 melts at 635°C. The peaks at 2θ = 34.0°, 37.0°, 40.1°, 44.5°, 49.0°, 60.0°, 63.2° were identified to be those of β-Fe_2O_3 as suggested by [Schnoebel et al 1997]. The peaks at 25.8°, 29.0°, 30.8°, 38.0°, 51.2°, 64.5° and 67.8 were identified to be those of α-Sb_2O_4 as suggested by [Allen et al 1996]. The small peaks next to the α-Sb_2O_4 peak have been suggested to be those of β-Sb_2O_4 phase. Miller indices and d-spacing for the rutile structure from [JCPDS, 1990] are tabulated in Table 5.1 and were used to determine the lattice parameters.

Table 5.1: Miller indices and d spacing [JCPDS, 1990].

Data for $FeSbO_4$		Data for the sample	
d[hkl]	(hkl)	d[hkl]	hkl
3.28	(110)	3.28	(110)
2.56	(101)	2.56	(101)
2.32	(200)	2.32	(200)
1.72	(211)	1.72	(211)
1.64	(220)	1.64	(220)
1.47	(310)	1.46	(310)

The formula below was used to calculate the unit cell parameters for the sample:

$$\frac{1}{d_{hkl}^{\ 2}} = \frac{h^2}{a^2} + \frac{k^2}{b^2} + \frac{l^2}{c^2} + \frac{2kl}{bc\cos\alpha} + \frac{2lh}{ca\cos\beta} + \frac{2hk}{ab\cos\gamma} \qquad (5.1)$$

because of a=b and $\alpha=\beta=\gamma=90^0$. Equation 5.1 simplifies to

$$\frac{1}{d_{hkl}^{\ 2}} = \frac{h^2}{a^2} + \frac{k^2}{b^2} + \frac{l^2}{c^2} \qquad (5.2)$$

for a tetragonal system of $FeSbO_4$ .Using equation 5.2 the cell parameters from the d-spacings obtained from the literature gave:

a=4.64Å

b=c=3.04Å

The results were compared with the d-spacings obtained from XRD analysis of the sample as shown in Table 5.2:

Table 5.2: Cell parameters

Unit cell Parameters	Literature values	Experimental values
A	4.64 Å	4.64
b=c	3.08 Å	3.07

The values in table 5.2 compare very well with each other as verified by [Aso et al 1979], [Allen et al [996] and [Schnobel et al 1997] and contradicts the cell parameter value of c=9.23Å obtained by [Berry et al 1987] for a trirutile structure using a neutron diffraction analysis.

5.1.2 Infra-red analysis.

Figure 5.2 shows an infrared spectrum of iron antimony oxide (Sb/Fe 1.5) calcined at T=900°C). The analysis was carried out at wavenumbers between 4000-400cm^{-1} with a ratio of sample to KBr of 1:20. The low infra red transmittance obtained was attributed to adsorption as well as the reflection of infra red light from the KBr wafer since it was dark brown. This was also the case with Bowker et al [1996] but they were able to identify the characteristic IR peaks for their sample.

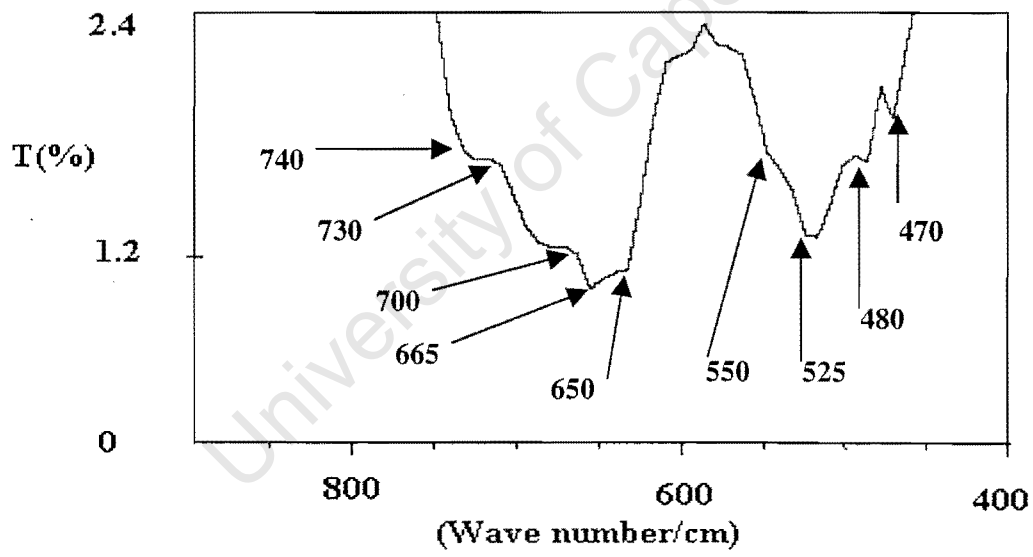

Figure 5.2: Infra-Red spectrum of $FeSbO_4$ (Sb/Fe = 1.5)

The wavenumbers at 730, 665 and 525 cm^{-1} were the characteristic peaks for a non-symmetrical antimonate rutile structure [Grasselli et al 1990],[Nyqiust et al 1971]. Other bands detected at 550,480,470 cm^{-1} were attributed to Sb_2O_4 by [Bowker et al 1996] and [Gadsden et al 1975]. The shoulder at 740 cm^{-1} was attributed to Sb_2O_3/Sb_2O_5.

5.1.3 Nitrogen BET analysis at 77 K

Figure 5.3 shows the adsorption isotherm of iron antimony oxide catalyst (Sb/Fe=1.5, calcined at 900°C). The plot shows that the sample has a type IV adsorption isotherm because of the hysteresis loop and a plateau between ($0.1<P/P_0<0.8$). This type of isotherm is found only on mesoporous materials such as silica gel, metal oxides and supports.

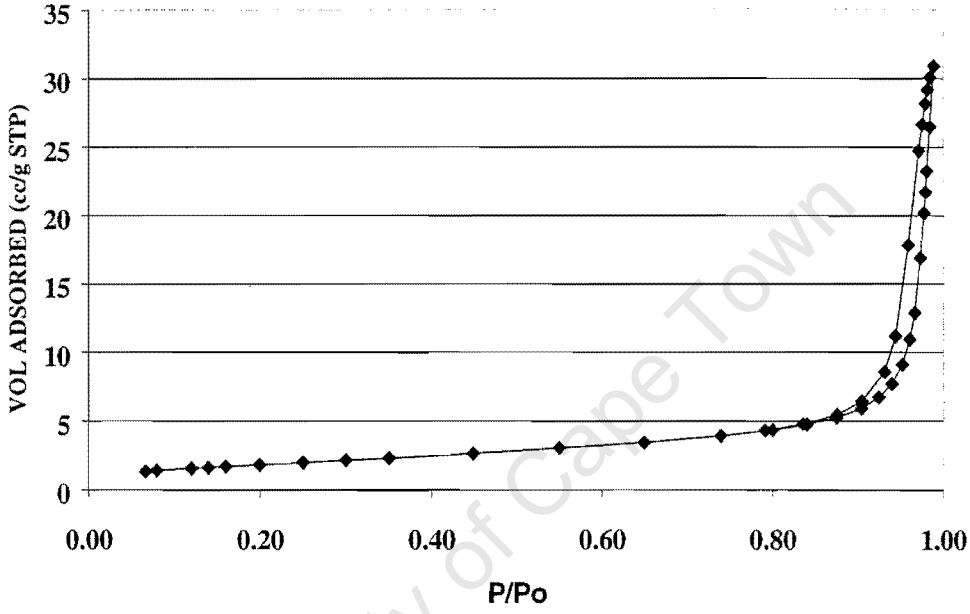

Figure 5.3: Nitrogen adsorption Isotherm for $FeSbO_4$ [Sb/Fe=1.5] at 77K

Three methods were used to estimate the surface area of the sample. The BJH method [Micromeritics ASPAP 2000] gave a value of 7.8 m^2/g. The t-plot method estimated a surface area of 6.4 m^2/g while the BET gave 6.8m^2/g. Schnobel et al [1997] reported that the maximum BET surface area is obtained when Sb/Fe=1:1 and decreases when the content of Sb_2O_4 increases or decreases. Figure 5.4 shows the differential pore volume distribution plotted against the pore diameter. The curve shows the maximum at d_{pore} =400Å signifying that the sample is mesoporous (20 Å $<d_{pore}<$ 500 Å). Table 5.3 shows the summary report obtained from Micromeritics ASPAP 200.

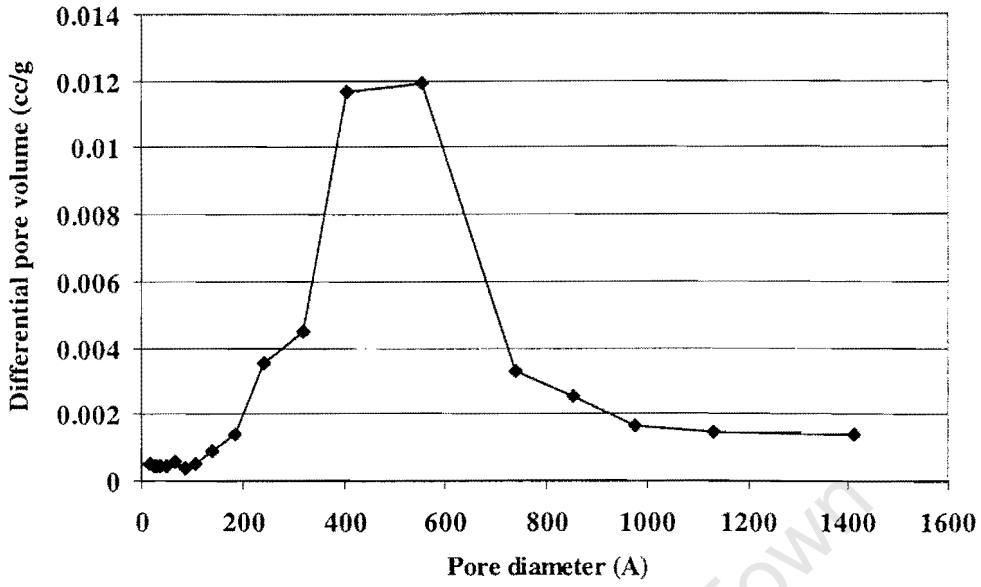

Figure 5.4 Pore distribution distribution of $FeSbO_4$ (Sb/Fe=1.5:1)

Table 5.3 Micropore summary report: Area, volume and pore size

Method of Analysis	Surface area M^2/g	Pore volume cm^3/g	Pore size Å
BET	6.8		197
Single point	6.4	0.034	
BJH (adsorption)	7.8	0.041	209.1
BJH(desorption)	8.2	0.048	233.7

5.2 Propene partial oxidation

5.2.1 Mass balance and Repeatability

In order to analyse and understand the effects of periodic operation imposed on the catalyst, it was essential to run steady-state experiments and thereafter carryout periodic cycling experiments. Figure 5.5 shows that a mass balance closure of 98.15±0.75% was attained for the steady state experiment. The accuracy of the experimental values were evaluated using a confidence limit of 95%.

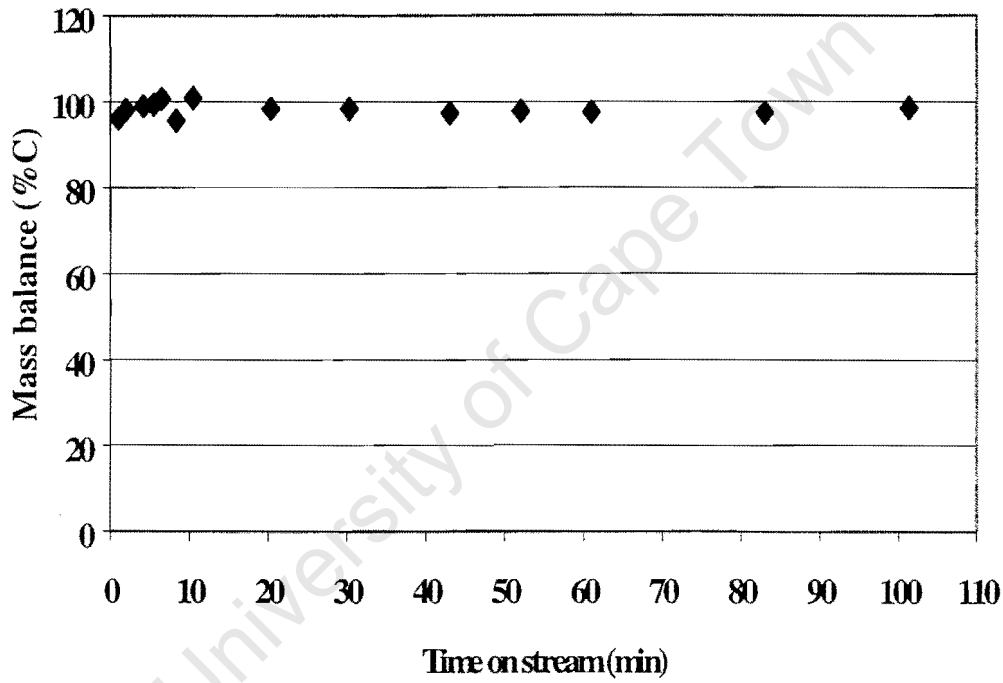

Figure 5.5: Mass balance (%C) plotted against time on stream for partial oxidation of propene to acrolein, CO_2 and CO: T_r=375°C; WHSV=1.2 hr^{-1}.

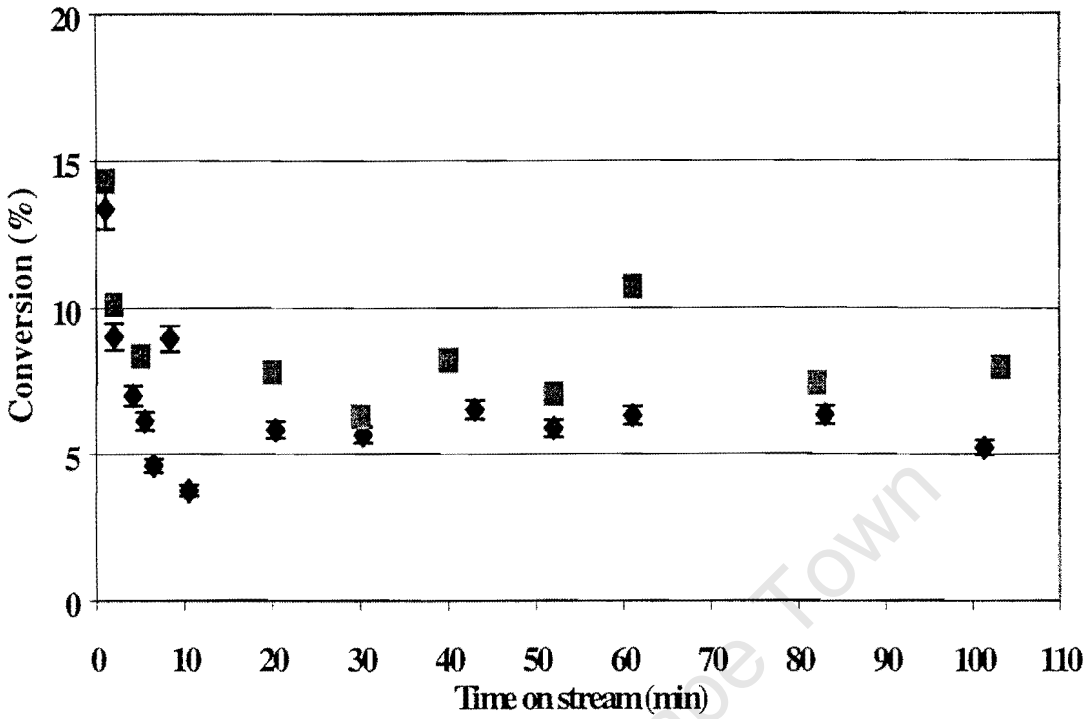

Figure 5.6 Repeatability analysis: Run A◆, Run B ■; T_r=375°C; WHSV=1.2 hr^{-1}.

Figure 5.6 shows the repeatability of the results. The error associated with the mass flow controllers [propene: 12.3±0.3ml/min (STP); He: 84.0±0.1ml/min (STP); O_2: 19.9±0.6ml/min (STP) and thermocouples (T_r=377.±1.°C)] was calculated. The error bars were plotted by assigning an error of 4% which is the sum of the errors obtained from the mass flow controller (3%) and the temperature controller (0.87%). The fluctuations observed in figure 5.6 may be due to non-uniformity of temperature in the reactor. Now since partial oxidation reactions are very sensitive to changes in temperature, the conversion may change significantly as the reaction rate is related to the temperature exponentially. During the experiments a temperature rise of 5°C was observed when propene was introduced. Magagula at al. [1997] reported temperature differences as high as 10°C.

The ampoule technique can also contribute to the observed fluctuations. During sealing with the flame, combustion due to hydrocarbons can occur and gas condensation if the sample is not properly heated in the ampoule breaker.

5.2.2 STEADY-STATE EXPERIMENT

5.2.2.(i) Yield

The yield of the products was evaluated using the formulae presented in section 4.7.5 and plotted against time on stream. Figure 5.7 shows the time on stream behaviour of acrolein, CO_2 and CO. Initially the yield of CO_x was higher than that of acrolein. With increasing time on stream both yields decreased, CO_x decreasing faster than acrolein. Steady state is reached at 20min time on stream at which the yield of acrolein is about 2%.

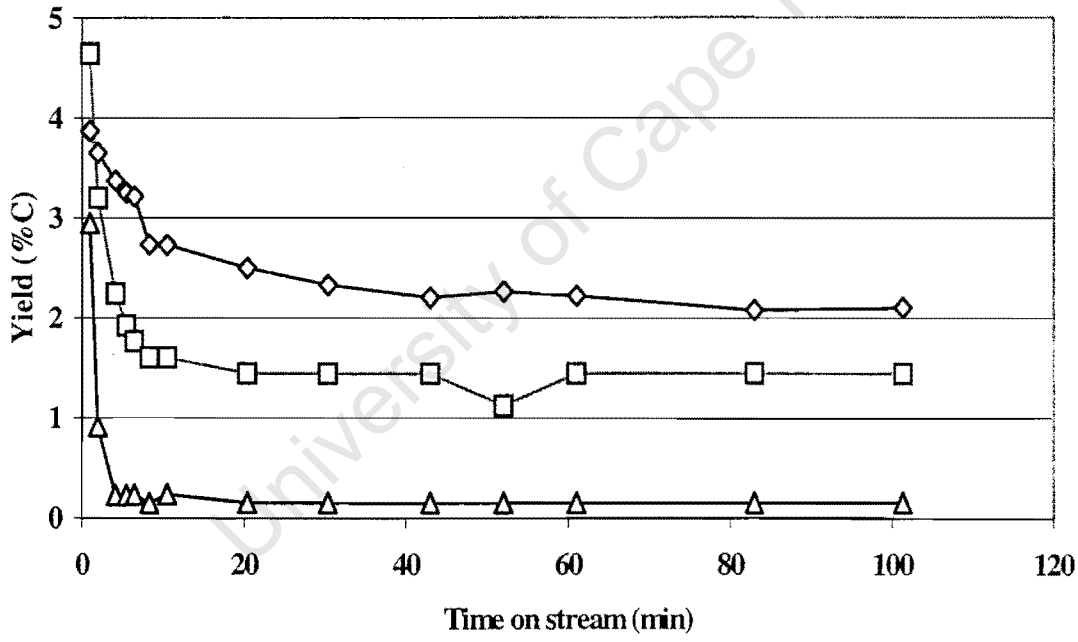

Figure 5.7: Yield plotted against time on stream for partial oxidation of propene to acrolein, ◇ CO_2 □ and CO △ T_r=375°C; WHSV=1.2 hr^{-1}.

5.2.2.(ii) Selectivity

The selectivity towards, acrolein and total oxidation products was plotted as a function of time on stream in Figure 5.8. The results show that the total oxidation selectivity is

high at short times on stream and declines slowly until 40% at steady state. Low initial selectivity to acrolein is attained but this increases to a 55% steady-state value with increasing time on stream.

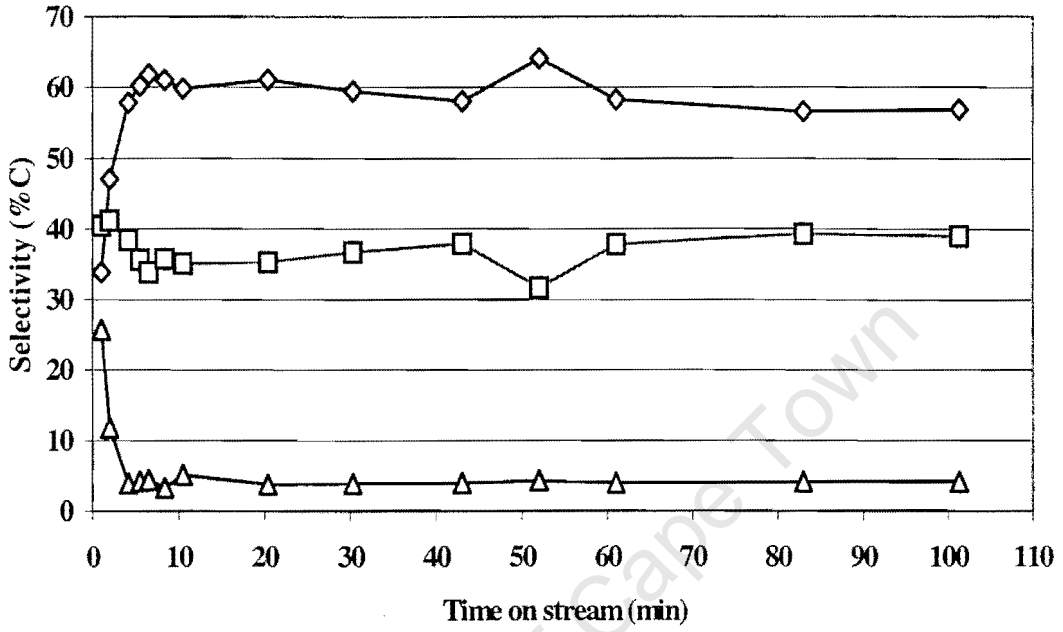

Figure 5.8: Selectivity plotted against time on stream for partial oxidation of propene to acrolein◇ CO_2 □ and CO △ T_r=375°C; WHSV=1.2 hr^{-1}.

5.2.3 Unsteady-state experiment

5.2.3.(i) Introduction

The effect of periodic switching was investigated on propene partial oxidation over iron antimony oxide catalyst (Sb/Fe=1.5:1). The time when the pneumatic valve was opened was defined as zero. Figure 5.9 shows an input propene step function used in the experiment. Occasionally in the data that follows, data points are missing due to poorly evacuated ampoules, which could not be analysed. High frequency sampling made it impossible to take two samples because of the short difference of time between one data point and the next.

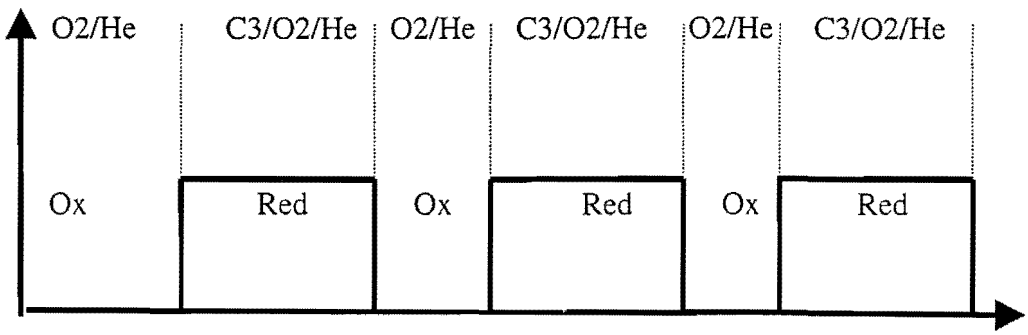

Ox = Oxidation phase Red = Reduction phase

Figure 5.9: Input step function for periodic switching

5.2.3.(ii) Repeatability

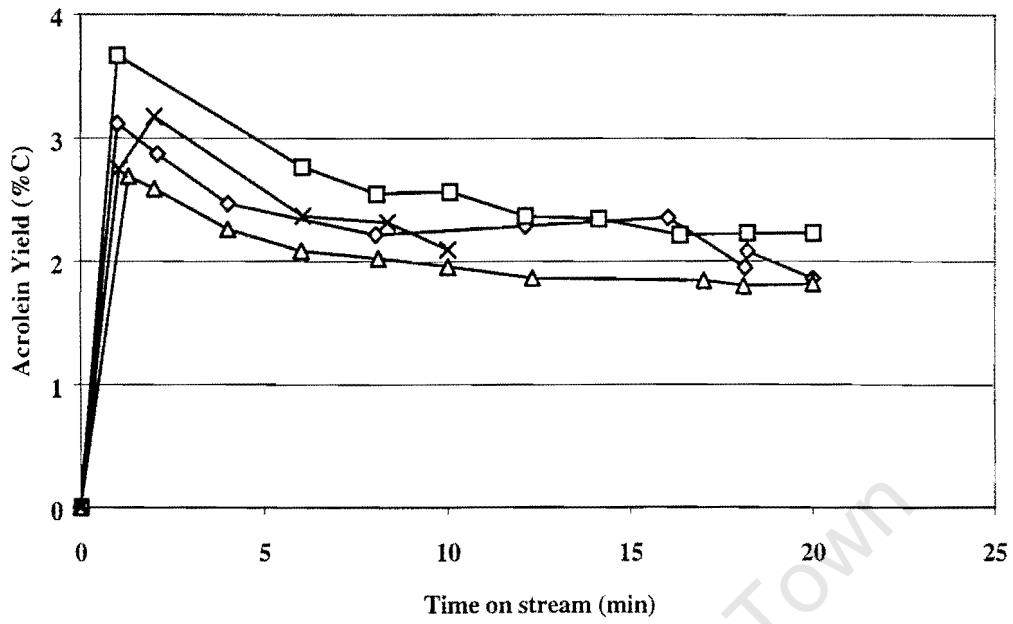

Figure 5.10 Yield of Acrolein for the first oxidation cycle compared with the initial Acrolein yield for the steady-state experiment: 5min△ , 10min□ , 20min◇, 30min × :T_r=375°C;WHSV=1.2 hr^{-1}
60min oxidation ; 20min reduction :

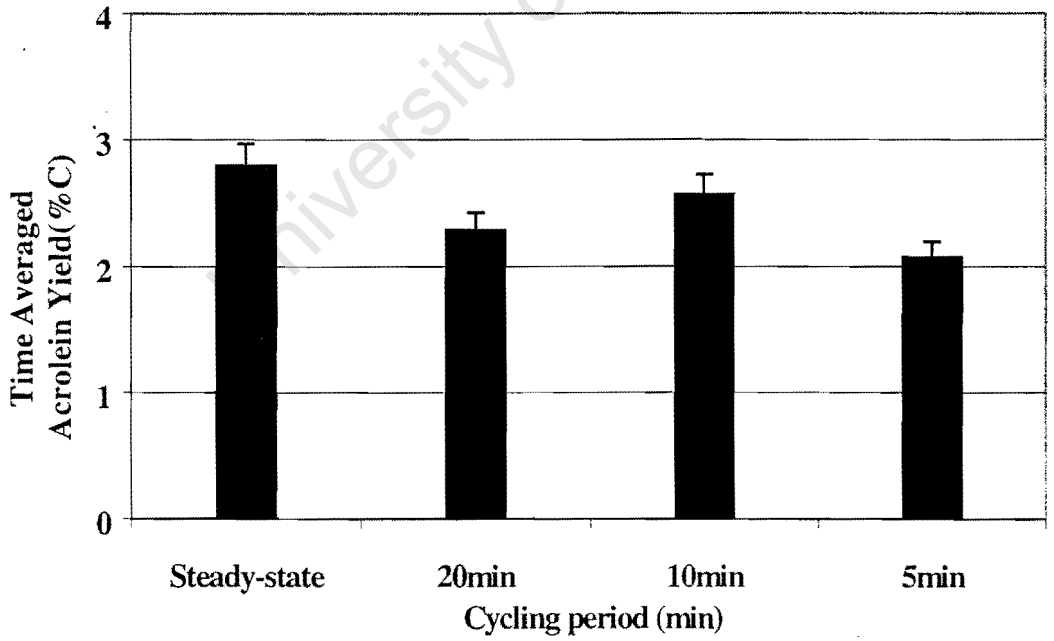

Figure 5.11 Time averaged acrolein yield for the first oxidation cycle compared with the initial Acrolein yield of the steady-state experiment

Figure 5.10 shows that all runs show deactivation in the first 20 min. There is no trend in these data, other than that all transient runs are below the steady state run. Ideally all

these responses should have been the same as each represents the first cycle of a freshly oxidised catalyst. The time average yield shown in figure 5.11 shows that there is no trend with the run number as the experiments were carried out in the following order: steady state, 30 min, 10 min, 20 min and 5 min cycling. The discrepancy of the results may be due to not carrying out the experiments on consecutive days as that introduces delays between the runs (i.e. oxidation) and thus leading to different states of the catalyst. It is also possible that the catalyst undergoes a permanent change and that high oxidation temperatures are needed to fully regain its initial activity. It is also possible that small conversions that have been attained have led to inaccuracies.

5.2.3.(iii) 5min oxidation time

Figure 5.12 shows that the catalyst has a high initial yield, which declines with time on stream. On the second cycle the high initial yield was not observed due to short re-oxidation times. The third cycle does not differ much from the second cycle and is approaching cyclic steady-state.

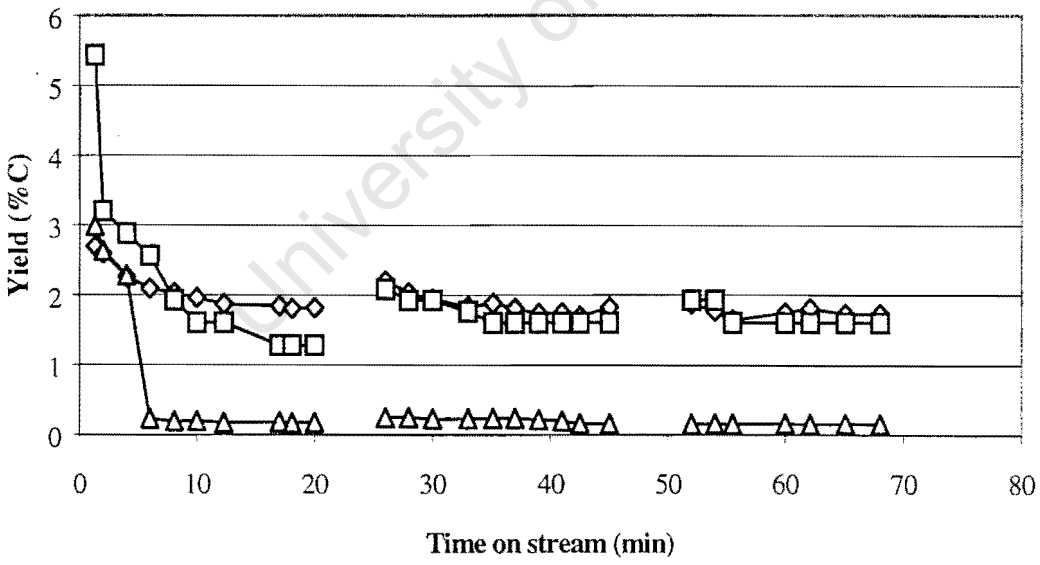

Figure 5.12 Yield plotted against time on stream for partial oxidation of propene to Acrolein ◇ , CO_2 □ , CO △ ; T_r=375°C; WHSV=1.2 hr^{-1}; 5 min oxidation; 20 min reaction.

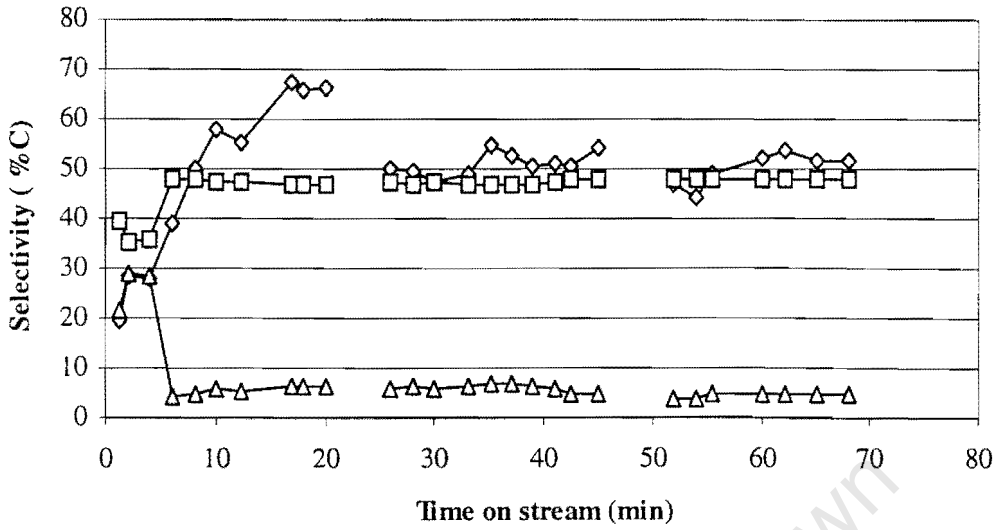

Figure 5.13: Selectivity plotted against time on stream for partial oxidation of propene to Acrolein ◇ CO_2□ and CO △: T_r=375°C;WHSV=1.2 hr^{-1}; 5min oxidation; 20min reaction:

Figure 5.13 depicts that for the first cycle the initial selectivity towards acrolein is less than that of carbon dioxide but improves with time on stream to 48% C. The selectivity to carbon monoxide is observed to decline drastically in a short time to a value 5%. On the second and third cycle carbon monoxide selectivity was observed not to change with switching instead the reaction cycles were similar, while selectivity towards acrolein remained above that of carbon dioxide.

5.2.3.(iv) 10 min oxidation

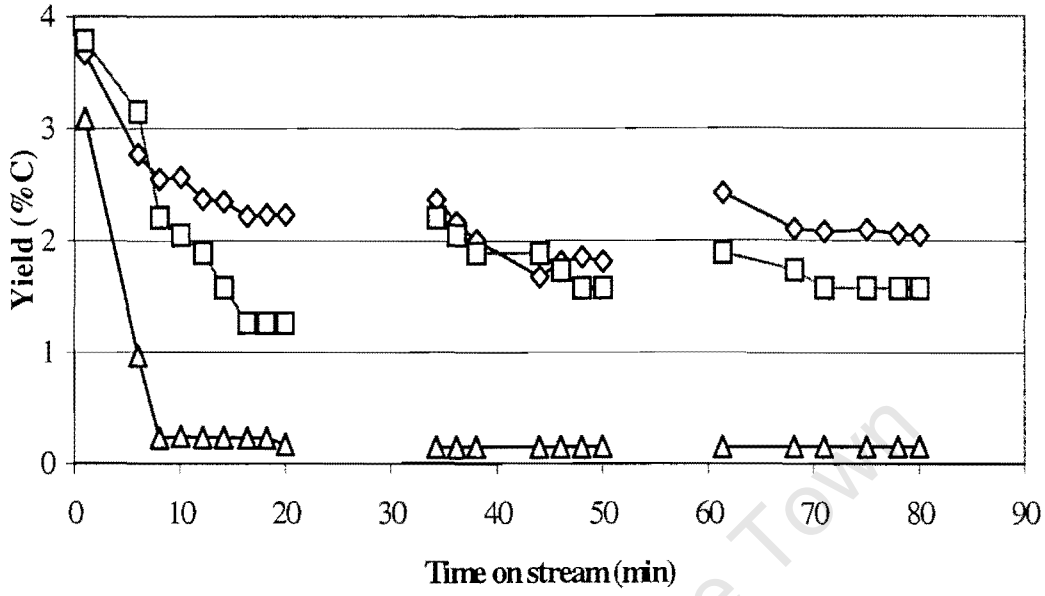

Figure 5.14: Yield plotted against time on stream for partial oxidation of propene to Acrolein ◇ CO_2 □ and CO △ : T_r=375°C; WHSV=1.2 hr^{-1}. 10min oxidation; 20min reaction.

Figure 5.14 shows that on the first cycle the yield of acrolein and that of carbon dioxide are approximately similar. But the yield of acrolein declines with time on stream to a value c.a. 2.1C% while that of carbon dioxide attains a value 1.3C%. The second cycle shows slight improvement in initial yield of acrolein as compared to the 2nd cycle in 5min re-oxidation. This effect is lost during the 3rd cycle, which approach steady state performance.

Figure 5.15 shows that the initial selectivity to acrolein and carbon dioxide are similar in the first cycle but improves with time on stream to 60%, while carbon dioxide attained a value c.a. 35% after 20 min time on stream. During cycles 2 and 3, selectivities are approximately constant with a final yield for acrolein/CO_2/CO of 55/42/3.

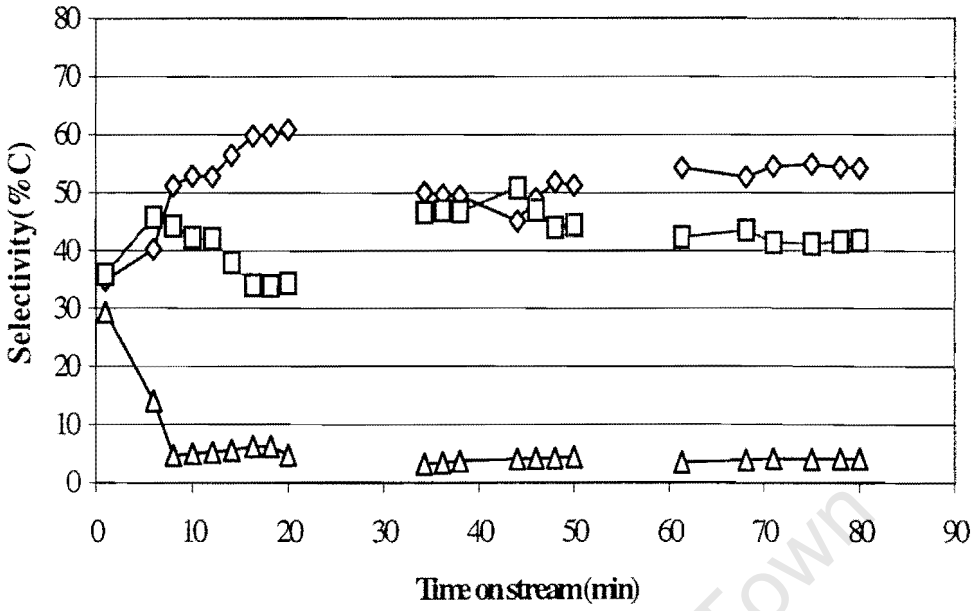

Figure 5.15: Selectivity plotted against time on stream for partial oxidation of propene to Acrolein ◇ CO_2 □ and CO △ T_r=375°C; WHSV=1.2 hr^{-1}. 10 min oxidation; 20 min reaction.

5.2.3. (v) 20 min re-oxidation

Figure 5.16 shows similar trend for the first cycle as the previous runs. However cycle 2 shows a similar high initial yield of CO_2 and acrolein in contrast to the previous runs at 5 min and 10 min re-oxidation. The CO yield on the first cycle did not show any high initial yield as in the previous runs. However by the third cycle cycling was not able to provide high initial selectivity observed in the second cycle. The yield of CO_x is higher than acrolein at short time on stream. On all the cycles the CO_x yield decreases faster than that of acrolein to achieve a final yield of 1.5%C for CO_x and 2 C% for acrolein. Selectivity as previously observed is higher for CO_x than for acrolein at short time on stream, but decreases to 40%C. The acrolein selectivity increases with time on stream to a value of 52% as shown in Figure 5.17.

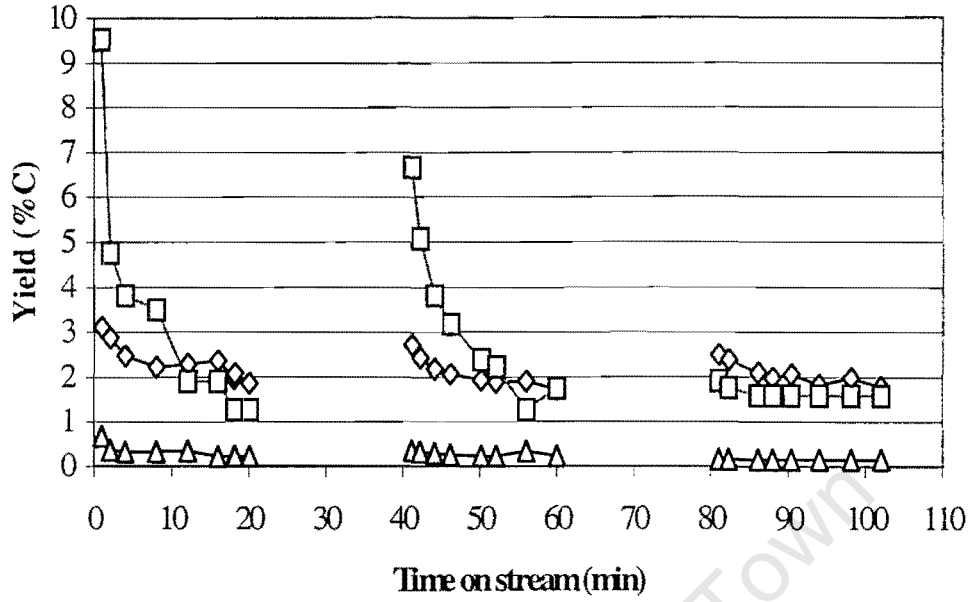

Figure 5.16: Yield plotted against time on stream for partial oxidation of propene to Acrolein◇ CO_2 □ and CO△ T_r=375°C;WHSV=1.2 hr^{-1}. 20min oxidation; 20min reaction.

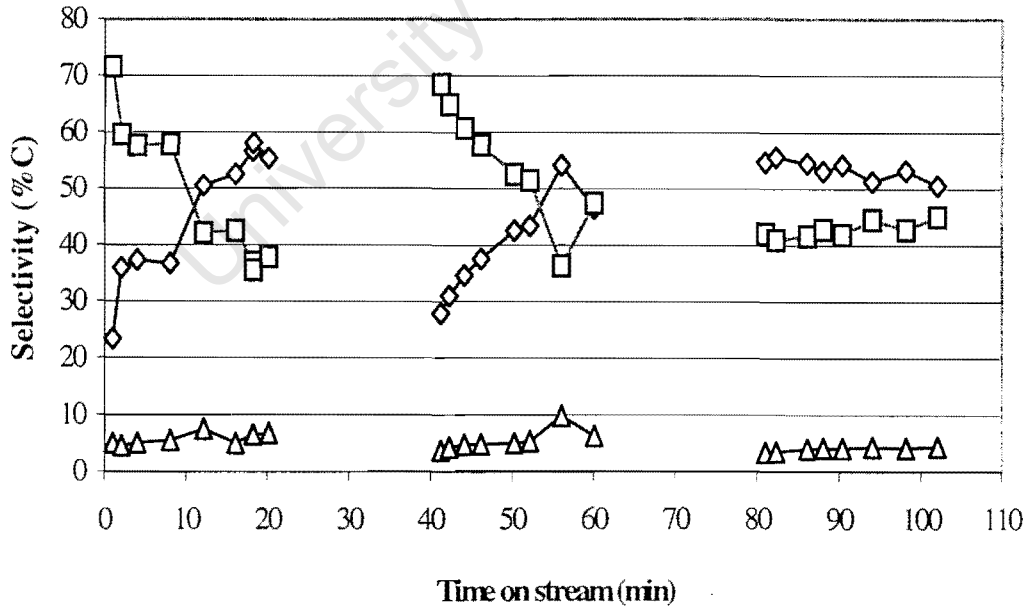

Figure 5.17 Selectivity plotted against time on stream for partial oxidation of propene to acrolein◇ CO_2 □ and CO△ T_r=375°C;WHSV=0.02; 20min oxidation phase: 20min reduction phase.

5.2.3.(vi) Time averaged acrolein yield

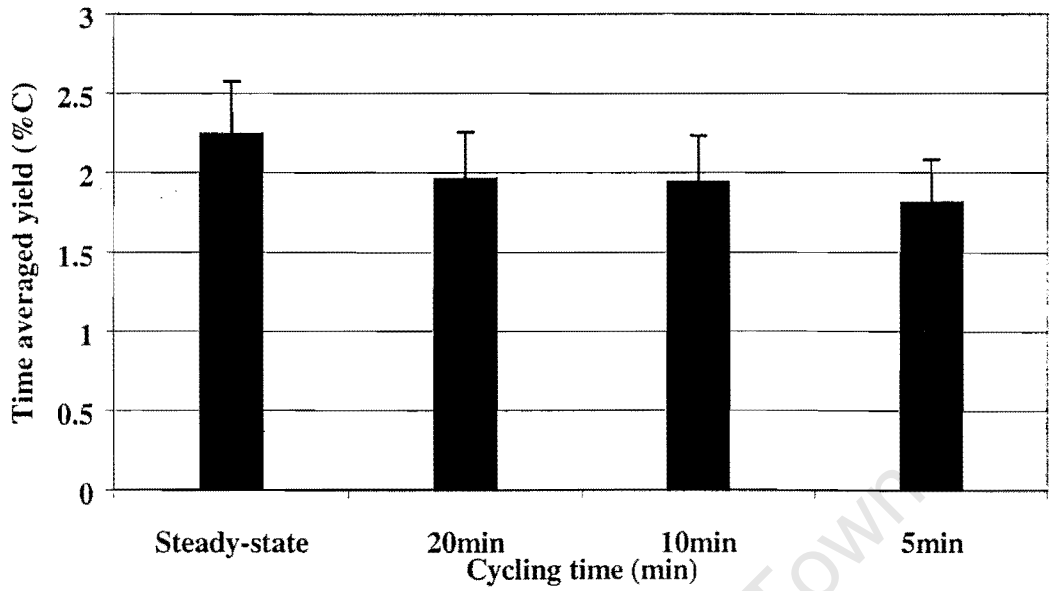

Figure 5.18 Time averaged Acrolein yield against Oxidation time for 2nd oxidation cycle.

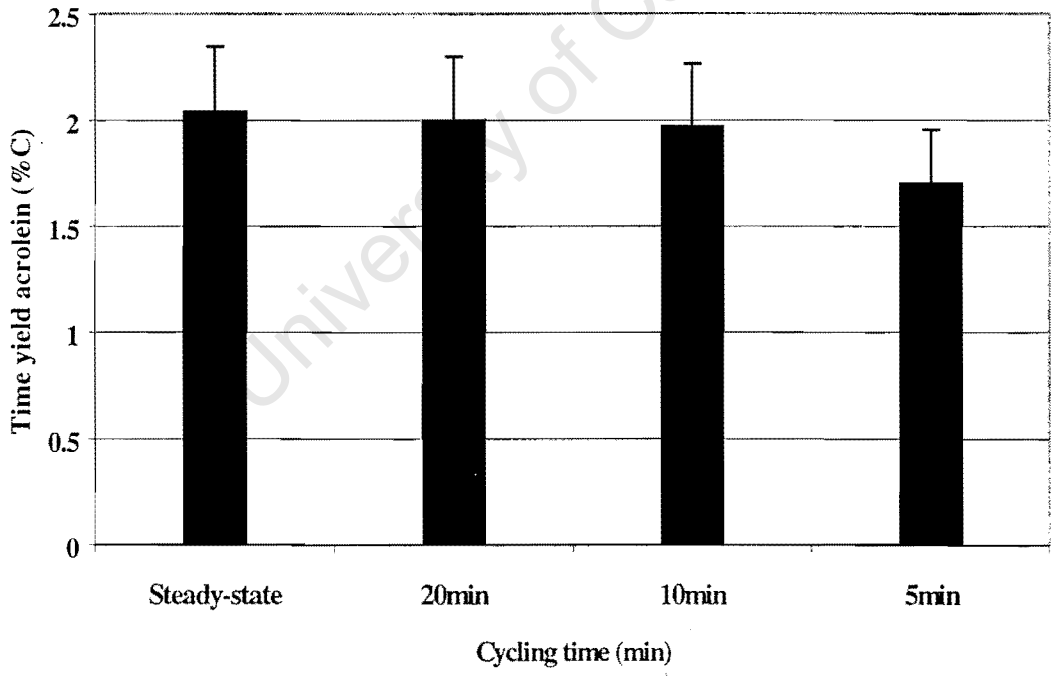

Figure 5.19 Time averaged Acrolein yield against Oxidation time for 3rd oxidation cycle.

The time averaged value for acrolein yield were evaluated for each cycle and compared to the time averaged steady-state acrolein yield evaluated by sectioning the graph into 20 min intervals corresponding to the sampling time used in the cycling experiments. The selectivity calculation depends on the yield of all the products. The time averaged selectivity plots were not plotted due to unreasonable selectivity trends observed in figures 5.8, 5.13 and 5.15. It was then necessary to show the effect of cycling time by using the yield of acrolein. The analysis was feasible since the yield of acrolein was calculated based on the data obtained from the G.C using an internal standard. The yields of carbon dioxide and carbon monoxide were calculated from the data obtained from NDIR CO/CO_2 analyser were unreasonable. This instrument is sensitive to water, it is believed that the water trap (magnesium perchlorate) was not sufficient enough in removing all the water, thus leading to a signal interference.

Long dead times existing in the CO/CO_2 are also believed be responsible for the abnormal responses in CO_x since it had to be properly purged and ran until steady state before carrying out other analysis. All the above are possible errors associated with the discrepancy observed in the CO_x data.

5.3 Simulation

5.3.1 Introduction

The cyclic behaviour of propene oxidation was simulated using the kinetic model proposed in section [3.1.1]. The reaction conditions are given in appendix 3B and reaction parameters are given in Table 5.4. The number of active sites were obtained by assuming that 2 lattice O per unit cell on the plane were exposed. Assuming that all the surface area measured by BET was the exposed 110 plane, the active site concentration was 7.2 kg_{cat}/mol O per exposed layer. The simulation was carried out in the following way. Initially the fraction oxidation sites was 0.2 and reduced sites 0.8. The system was then pre-treated in O_2 for 1 hour in order to fully oxidise the catalyst. After 1 hour the propene was fed through the reactor; no adjustment on the residence time was made to account for the effect of adding/removing propene, as this flow was only 10% of the total flow. The reactor was also treated as isothermal based on the external heat transport calculations in appendix 3.

Table 5.4 Rate constants used in the simulation

Rate constants	value	Units
k_1	0.1	m^3/kg.s
k_2	0.4	mol/kg.s
k_3	0.5	mol/kg.s
k_4	0.3	mol/kg.s
k_5	0.6	mol/kg.s
k_6	0.1	mol/kg.s
k_7	0.00001	m^3/kg.s

The aim of these results was to qualitatively predict the trend in the experimental data without having to resort to complex parameter estimation. Additionally, without time dependent analysis of all products (including H_2O), it is not possible to estimate all the modeling parameters. Thus for the data presented here only qualitative analysis is

possible. As it is qualitative, the time scales of experiment and simulated data are of no consequence, but rather the time dependent trends are what need to be considered.

5.3.2 Steady state simulation

Figure 5.20 shows the response of all the gaseous species and oxidation sites. The CO_x yield has a much greater maximum than acrolein, as observed in the experimental data. The same effect was observed in the other gaseous species, which cannot be measured. Figure 5.20(f) shows that 30 min is sufficient time to achieve complete oxidation of all active sites. Thus the 60min pre-treatment is sufficient to produce a fully oxidised catalyst.

The oxidation of propene causes the lattice oxygen site concentration to decrease. These sites are either occupied by adsorbed propene or water molecules or are in the reduced state [vacant]. From Figure 5.21 it can be seen that the dominant surface species during reaction appear to be OH, oxidised and reduced sites, the concentration of acrolein in the surface is minimal. The fact that OH concentration is high on the surface reflects the choice of rate constants. The results also show that only C_3H_5 and C_3H_5O sites are responsible for the formation of acrolein and CO_x. From the proposed mechanism it is noted that the reaction order with respect to C_3H_5 for the CO_x formation is much higher than acrolein formation. Thus low concentration of C_3H_5 favour the formation of acrolein as observed. This also explains the trend, that acrolein has a much lower initial yield than CO_x.

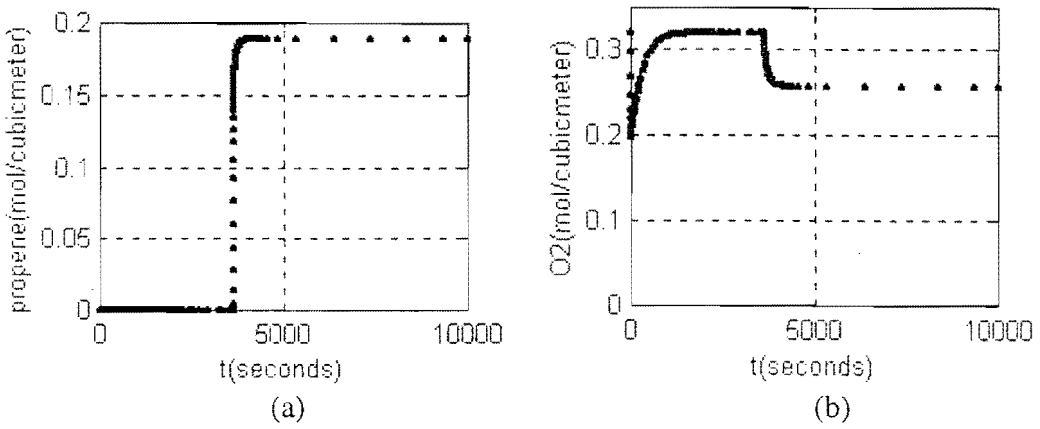

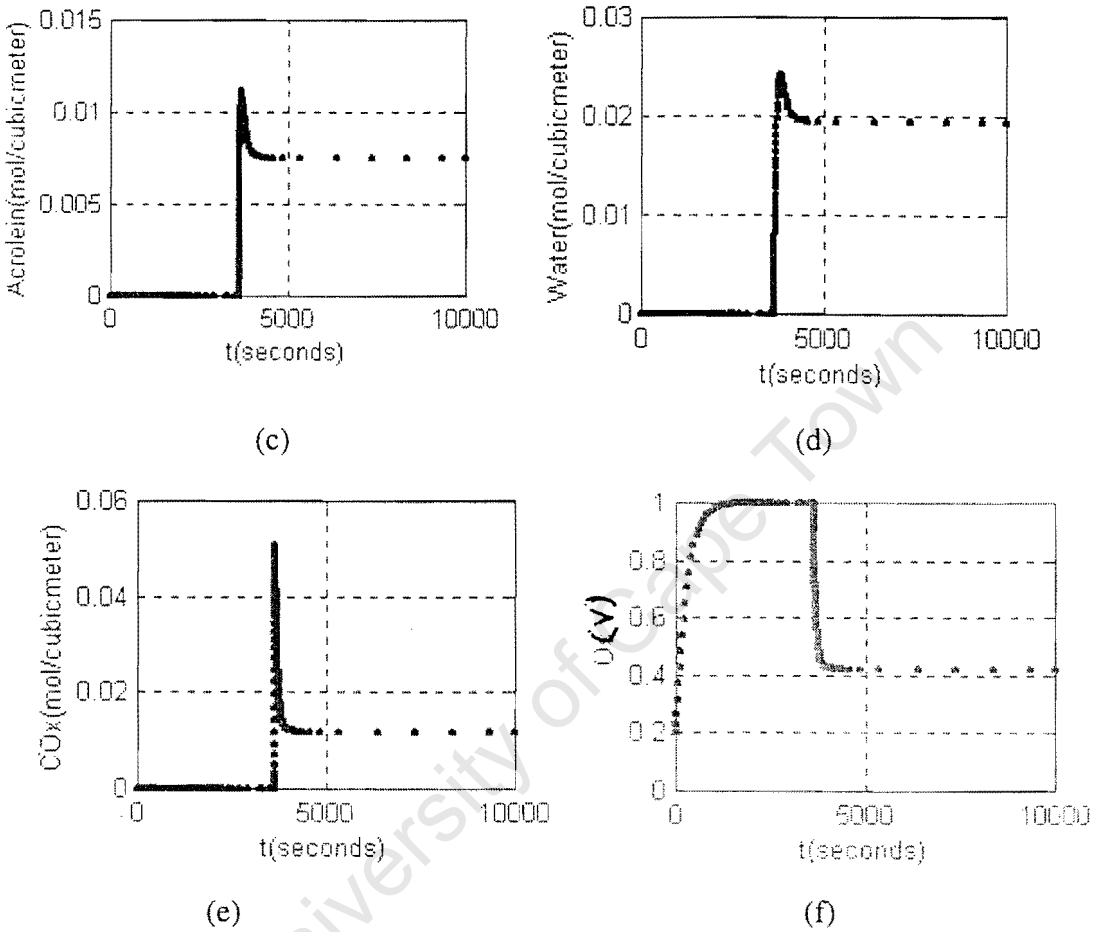

Figure 5.20 The response curves for the reactants (a) and (b) the products (c), (d), (e) and the behaviour of the reactive oxygen sites (f)

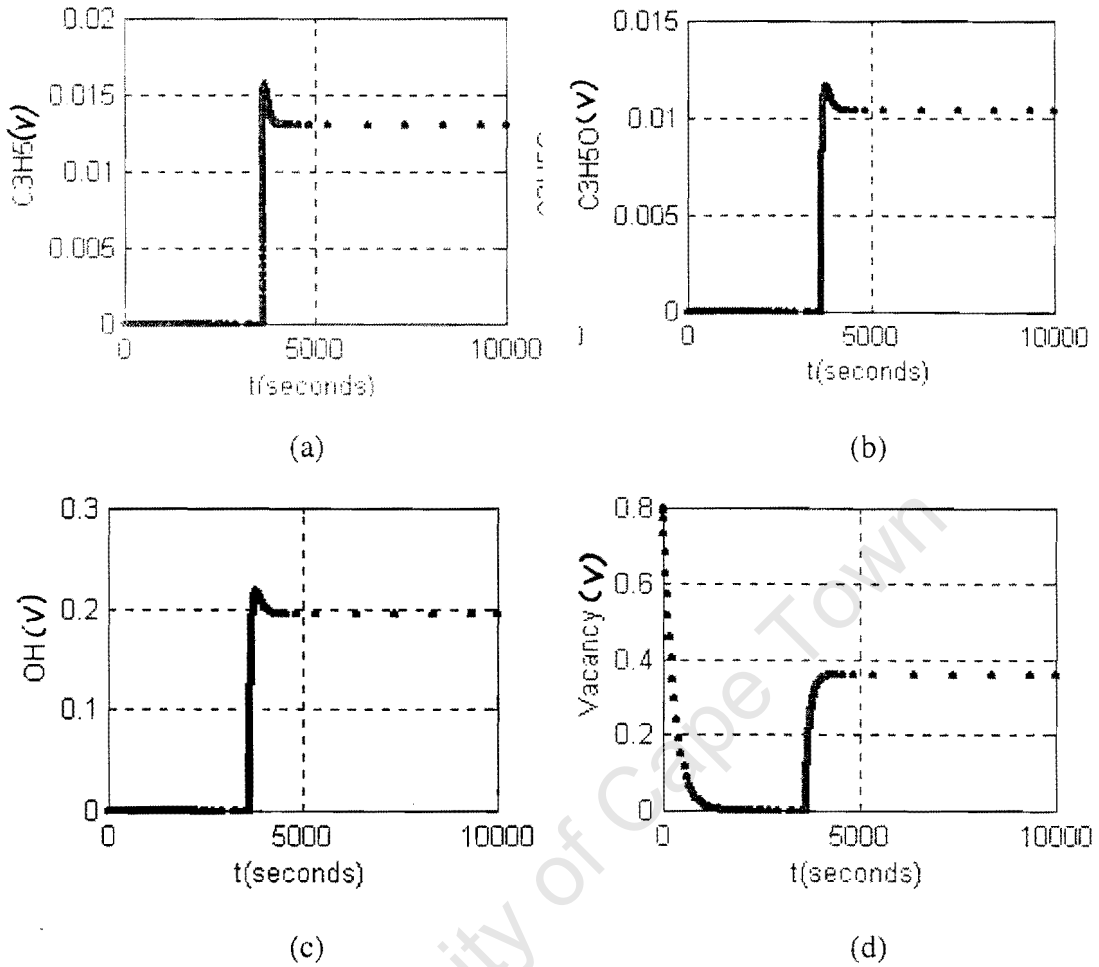

Figure 5.21 The behaviour of the surface species with time on stream.

The fraction of surface sites from figures 5.21 (a),(b),(c),(d) and 5.20(f) were added and were found to be unity verifying that the surface consistency imposed in equation 3.30 is obeyed.

5.3.3 Cyclic simulation

Figure 5.22 shows the cycling behaviour of acrolein yield when oxidation time was varied from 5 min to 30 min and the reaction cycle was kept constant at 20 min. Short cycle times of 5 min were not sufficient to re-oxidise the catalyst, thereafter the initial yield on the first cycle, subsequent cycles had much lower yields. As the oxidation time

was increased; the initial yield of acrolein increased. At 30 min re-oxidation time, the catalyst achieved its initial activity after reaction.

It is also clear that the cyclic behaviour of the species in the periodic environment has been described by using the proposed single site mechanism. Figure 5.23 shows that CO_x undergoes the same trend as acrolein. Figure 5.24 shows that the oxidation sites are not completely regenerated by short cycling times and that at least 30 min is required to achieve 99% oxidation sites. Thus the decrease in the initial yield can be attributed to the decrease in the number of oxidation sites available for reaction. It is also important to notice that in all cases the 2nd and 3rd cycle are identical (i.e. cyclic steady states). Thus the slow deactivation of the active sites observed in cycle number in the experimental data is not reproduced by this model.

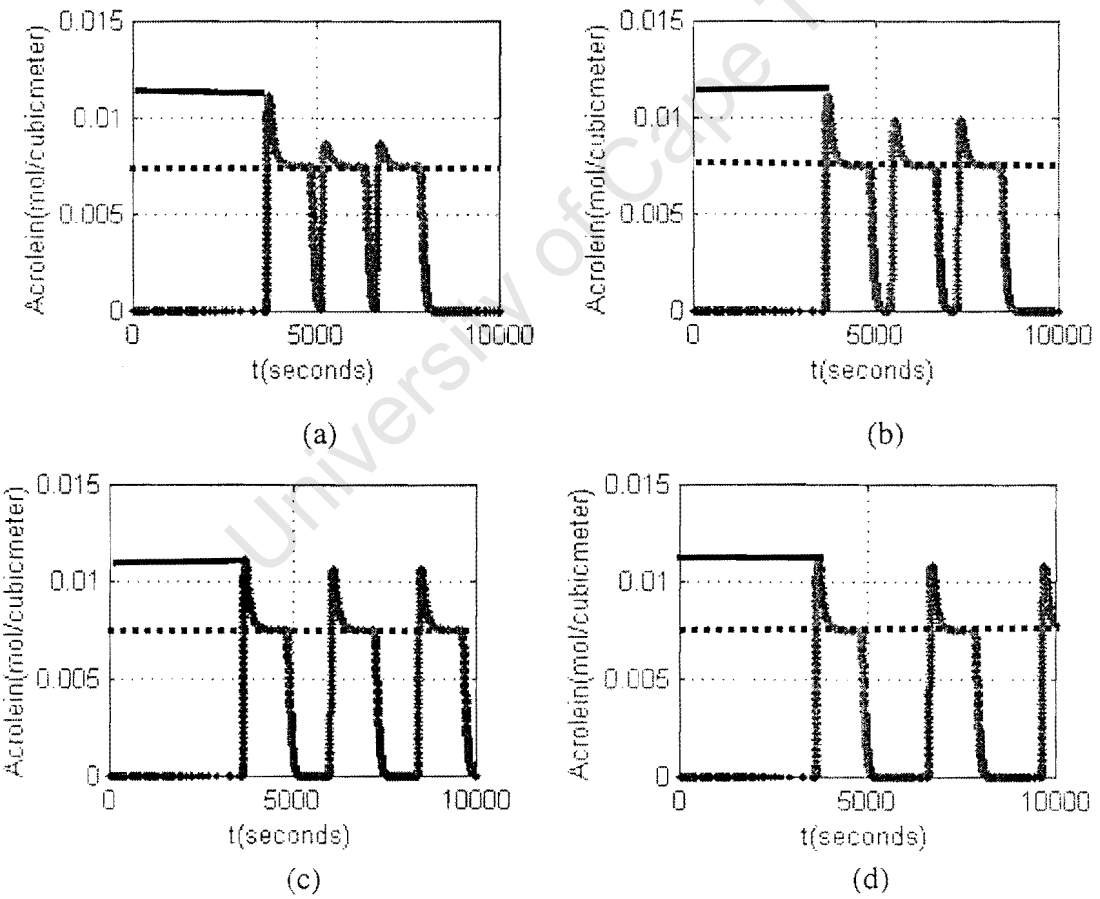

Figure 5.22 Transient simulation results for the acrolein concentration (a) 5min oxidation (b) 10min oxidation (c) 20 min oxidation (d) 30 min oxidation. Steady state concentration. ▪▪▪▪▪ Initial concentration. ▬▬

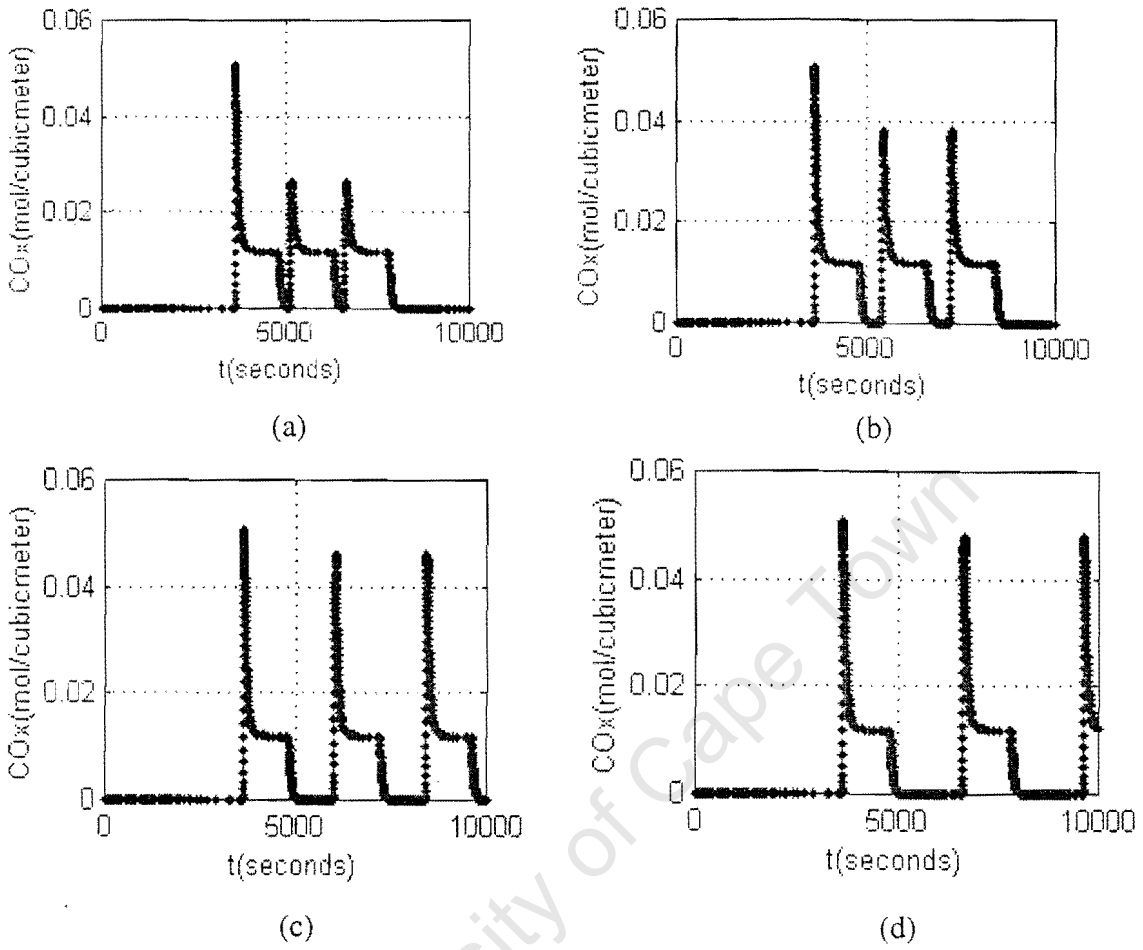

Figure 5.23 Transient simulation results for the COx concentration (a) 5min oxidation (b) 10min oxidation (c) 20 min oxidation (d) 30 min oxidation

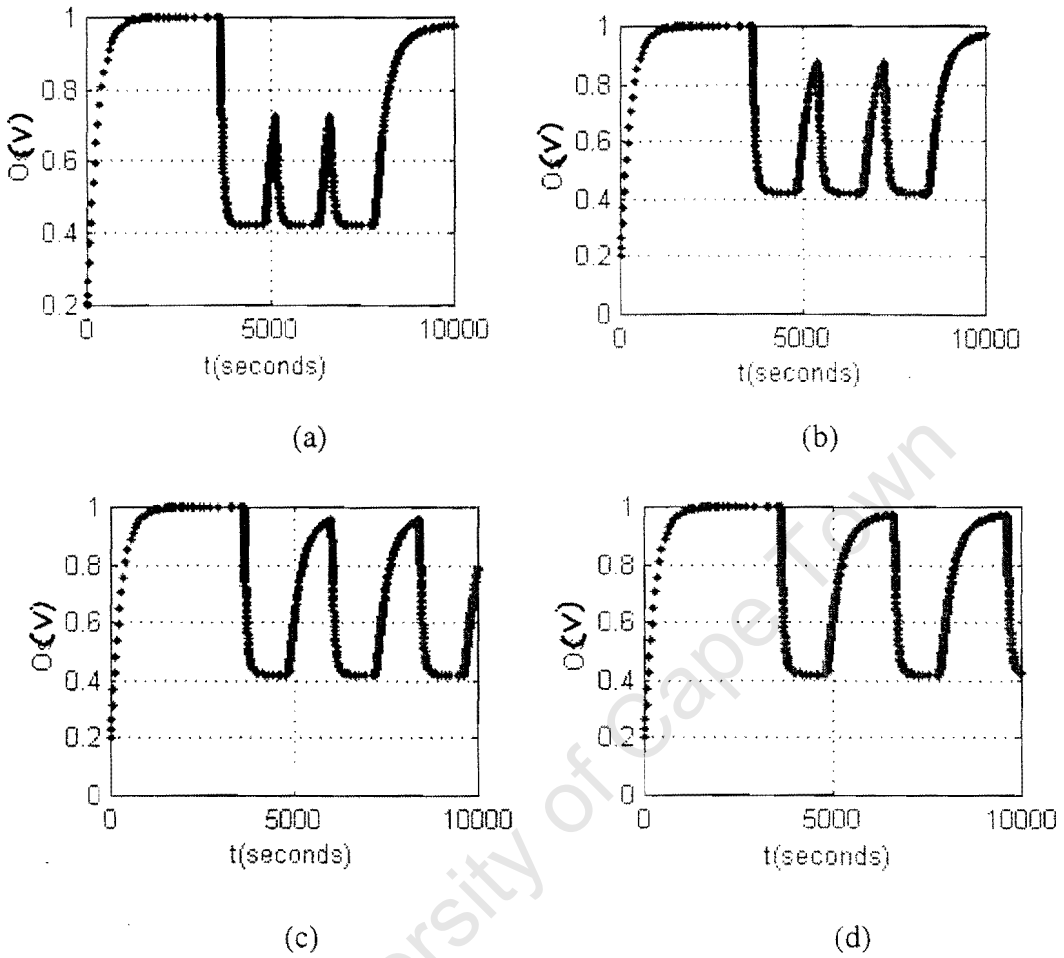

Figure 5.24 The effect of cycling time (t_c) on the behaviour of the lattice oxygen: (a) t_c=5min, (b) t_c=10min,(c) t_c=20min, (d)t_c=30min.

6 DISCUSSION

6.1 $FeSbO_4$ characterisation

The formation of $FeSb_2O_6$ bulk phase was not observed in the diffractogram of Figure 5.1. It has been suggested by Brystrom et al [1941] that excess Sb leads to the formation of $FeSb_2O_6$ bulk phase. The suggestion was ruled, out since the characteristic angle at $2\theta=21°$ was not observed. The non-existence of this peak favours the existence of $FeSbO_4$,a single rutile structure. This was also in agreement with Carbucicchio et al [1985]; Teller et al [1985] and Allen et al [1996].

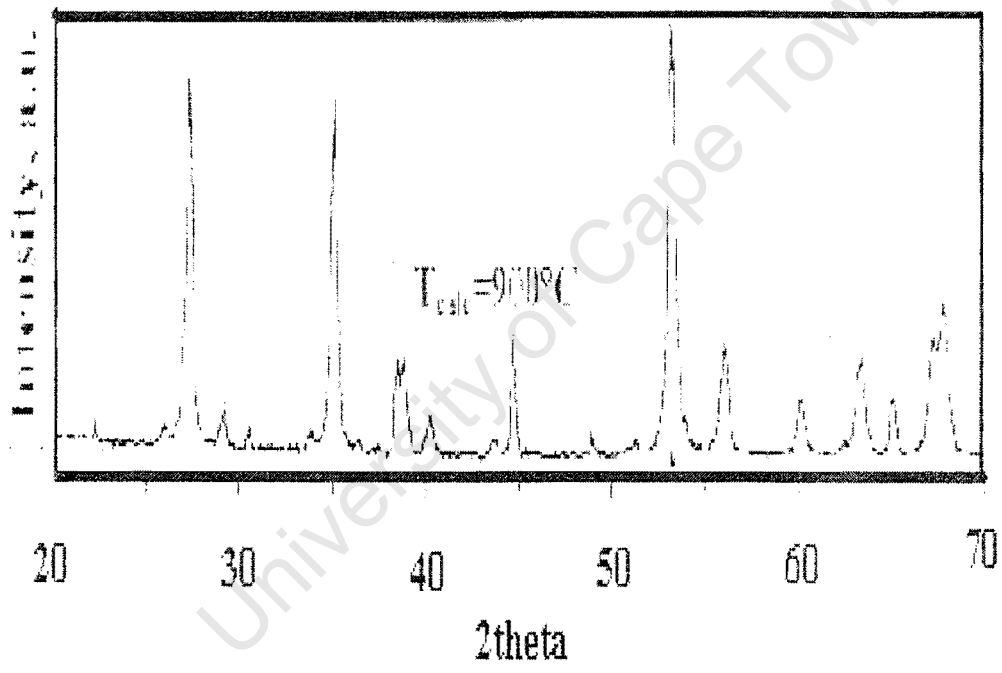

Figure 6.1 X-ray diffraction for Iron antimony oxide catalyst (Sb/Fe=1:1.5) [Schnobel et al. 1997]

Figure 5.1 shows the existence of intense peaks of Fe_2O_3 which were not visible in the diffractogram of the catalyst prepared by Schnobel et al [1997] which was calcined at 900°C for 7hours with Sb/Fe=1.5:1 as shown if figure 6.1. The existence of these peaks implies that the catalyst has excess iron oxide, which is known to favour the formation of total oxidation products [Schnobel et al. 1997]. Figure 5.1 shows that the catalyst has multiphases as compared to that prepared by Schnobel et al [1997].

The infrared spectroscopy spectrum shown in figure 6.2 shows the existence of the Sb $^{(V)}$=O groups which were believed to be responsible for activating propene [Carbucicchio et al 1985]. Although not well resolved due to low transmittance, a small peak at 850 cm^{-1} was observed and was attributed to the existence of Sb $^{(V)}$=O group as stated in the literature by Sala and Trifiro [1976]

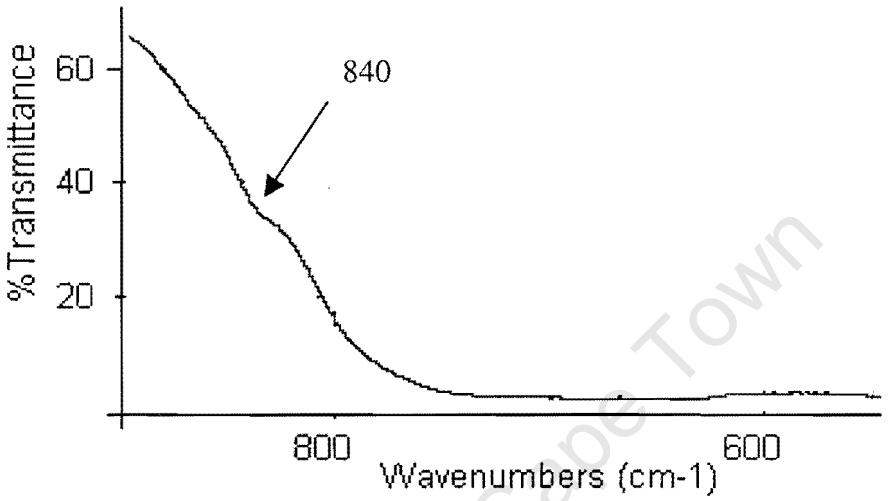

Figure 6.2 The Infrared spectrum of $FeSbO_4$

The BET surface area obtained for the catalyst was 6.8m^2/g compared to 20m^2/g obtained by Schnobel et al [1997] for the same catalyst having Sb/Fe=1.5 and calcined at 800°C as shown in Table 6.1. That was attributed to sintering of the catalyst at high temperatures as suggested by Allen et al [1996] and was later confirmed by Schnobel et al [1997]. The small surface areas of Sb_2O_4 and Fe_3O_4 are believed to contribute to the low surface area of $FeSbO_4$ [Schnobel et al 1997]. The difference in the surface areas of the catalysts can affect the reaction rate of conversion of the reactant feed.

Table 6.1 BET surface area for compounds of Fe_3O_4,Sb_2O_4,$FeSbO_4$

Literature	[Schnobel et al. 1997]	This work	
Compound	Surface area (m^2/g)	Surface area (m^2/g)	Calcination Temperature (°C)
Sb_2O_4	0.5	-	800
Fe_3O_4	2.5	-	800
$FeSbO_4$(Sb/Fe=1:1.5)	20	6.8	800

6.2 Steady-state experiment

The experimental results contradicted those obtained by Magagula et al [1999] and van Steen et al [1997] for an iron antimony oxide catalyst. They found that the iron antimony oxide catalyst was initially highly selective to acrolein. In this work the initial selectivity to CO_x was higher than that of acrolein. This was observed by Magagula et al [1999] for bismuth molybdate catalyst. The product sampling in this work was carried out at times greater than 1min as oppose to sampling times of less than 1min as carried out by Schnobel et al [1997] and Magagula et al [1999]. Thus the comparison of the data from this work to that of Schnobel et al [1997] and Magagula et al [1999] was not feasible.

The differences between the experimental results obtained and those reported in the literature may be attributed to the quality of the catalyst, reaction condition, the initial pretreatment of the catalyst, WHSV, calcination temperature and the antimony to iron ratio. These parameters have a significant effect on the response of the reactor system.

6.2.1 The effect of the quality of the catalyst

The quality of the catalyst used was compared on the basis of an X-ray diffraction experiment to that used by Schnobel et al [1997]. Figure 5.1 shows a presence of

many phases with F_2O_3 having high intensity, while the X-ray diffractogram in figure 6.1 shows the non existence of Fe_2O_3, known to favour the formation of total oxidation products. The diffractogram in Figure 5.1 also shows that the catalyst is enriched with antimony oxide. Allen et al [1991] suggested that excess antimony inhibits the reduction of the catalyst and thus increases the probability of the adsorbed propene to react with electrophilic oxygen forming total oxidation products. The electrophilic oxygen species are formed during the re-oxidation phase and they are used up until the nucleophilic oxygen begin to react. Aso et al [1980] reported that as the ratio of Sb/Fe decreases, the formation of total oxidation products is favoured and this was later confirmed by Schnobel et al [1997].

For a highly oxidised catalyst there is high probability of formation of COx gases due to the absence of the oxygen vacant sites. Grasselli and Suresh [1976] proposed a model for the selective oxidation of propene, which requires an oxygen vacancy adjacent to the Sb ion in order to facilitate the formation of an allyl intermediate thought to be responsible for selective oxidation i.e. the catalyst must be in a partially reduced state. The model was later validated by Allen et al [1996] and Bowker et al [1991] based on temperature programmed desorption experiments.

6.2.2 Reaction conditions and re-oxidation.

Partial oxidation reaction is very sensitive to changes in temperature. At high temperature total oxidation products are favoured more than acrolein. Magagula et al [1999] carried out partial oxidation of propene at 375°C while Schnobel et al [1997] and Aso et al [1980] carried out the reaction at 350°C and 400°C. van Steen et al [1997] showed that the rate of re-oxidation increases as the temperature increases. In this work the catalyst was re-oxidised at 375°C and is clear from Table 2.4 that re-oxidation is slow as compared to rate of reduction.

6.2.3 WHSV

Schnobel et al [1997] have shown that the selectivity to acrolein increases as the WHSV increases while that of total oxidation products remains unaffected. The investigation

was carried out at 345°C, 375°C ad 400°C and it was found that at low WHSV there is consecutive formation of total oxidation products from acrolein. In this work the WHSV used was 1.2 hr^{-1} while Magagula et al [1999] and Schnobel et al [1997] used $2hr^{-1}$.

6.2.4 Calcination temperature.

Schnobel et al [1997] showed that a catalyst calcined at 800°C and having a Sb/Fe =1.5 was active for the formation of acrolein and beyond that the catalyst sinters and the selectivity to acrolein drops. While the catalyst calcined at 700°C was selective to the formation of total oxidation products. In this work the catalyst was calcined at 900°C and the catalyst was observed to be initially selective to total oxidation product formation and selective to partial oxidation products at steady state. Schnobel et al [1997] observed that the initial selectivity to total oxidation and acrolein were similar for the catalyst calcined at 900°C.

6.3 Unsteady state experiment

6.3.1 Effect of oxidation time

The acrolein yield of the first cycle of all the experiments should have been the same, but that was not observed. The average value of time average acrolein yield in Figure 5.11 was evaluated to be 2.4±0.4%C. There was no trend with re-oxidation time as shown also in figure 5.18 and 5.19, but there was a trend with experimental sequence. This deviation could not be attributed to some permanent deactivation occurring due to reaction, which was not reversible, by the oxidation step. Figure 6.3 shows the normalised average yield of acrolein at different cycles and re-oxidation time. These yields were obtained by first evaluating the time averaged yield for each cycle, which is the defined as the area underneath the curve divided by the reaction time. The time average yields for the steady state curve (Figure 5.7) were then obtained by dividing the graph into three sections, each having a reaction time of 20min.

It can be inferred from Figure 6.3 that cyclic yields exceed the steady state yields that would be obtained after long time on stream. Thus cyclic operation is beneficial, however, at the expense of using more oxygen. Increasing oxygen in the feed gas of the steady state run should also increase the yield, although this was not tested on this

particular sample. Nevertheless oxygen is already in large excess and increasing it even more is not expected to have a significant effect.

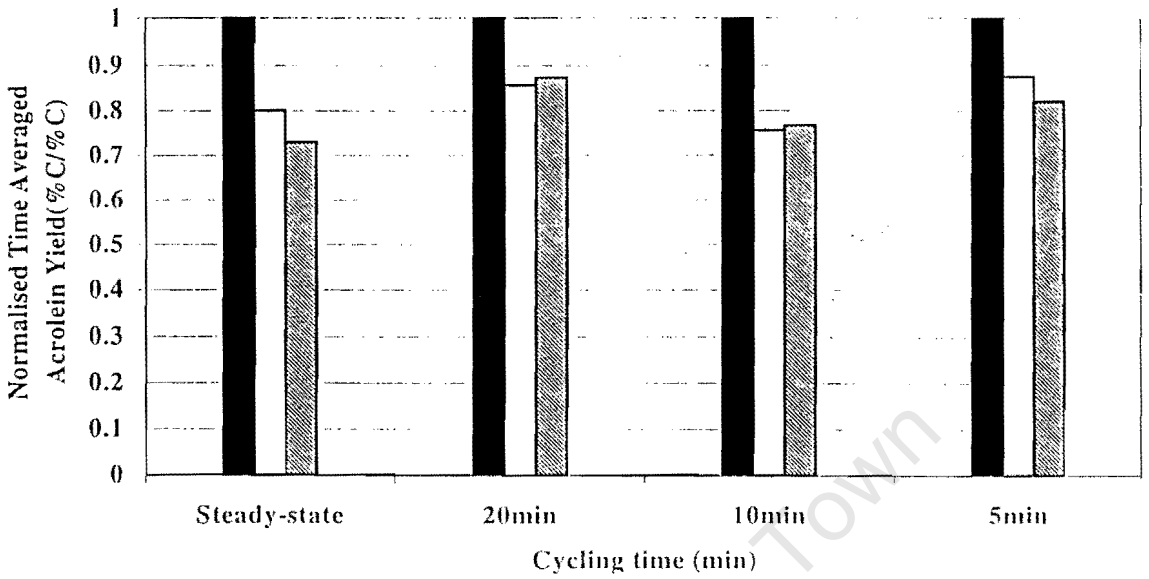

Figure 6.3 Normalised time averaged acrolein yield at different cycling times
Cycle 1 ■ Cycle 2 □ Cycle 3 ▨

Although the reaction conditions of Magagula et al [1999] were different, similar increased yields of acrolein were observed in cyclic experiments in which the oxidation time was 30min followed by 20min reaction. In this work the catalyst was oxidised for 30min and reduced for 10min as shown in Figures 6.4 and 6.5. Figure 6.4 shows that for the first cycle, the initial yield of acrolein is less than that of carbon dioxide but increases with time on stream to a steady-state value c.a. 2%. After the re-oxidation phase the original activity of the catalyst was nearly regained. Figures 6.5 shows that for the first cycle the selectivity of acrolein was initially 20% but improved with time on stream to 65% while carbon dioxide reached a value of 32%.

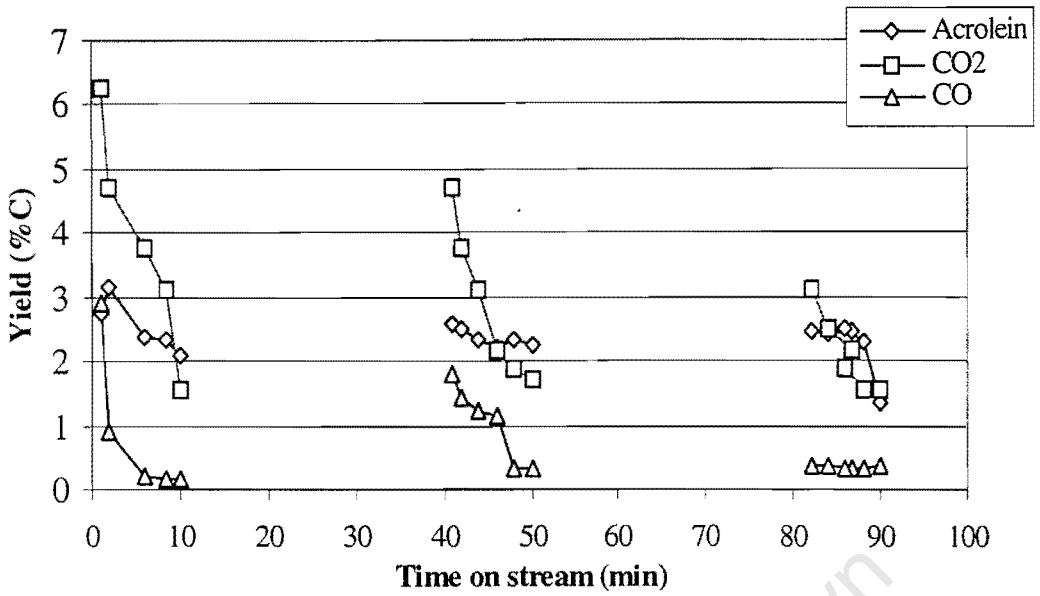

Figure 6.4 Yield plotted against time on stream for partial oxidation of propene to acrolein and CO_2 and CO: T_r=375°C; WHSV=0.02; 30min oxidation phase: 10min reduction phase.

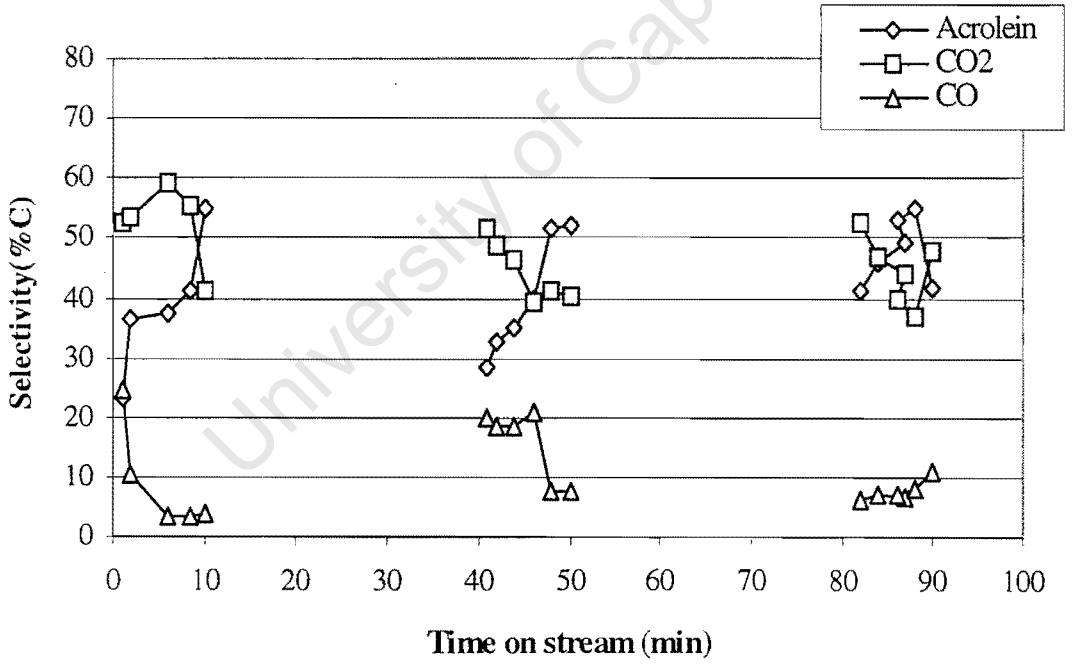

Figure 6.5 Selectivity plotted against time on stream for partial oxidation of propene to acrolein and CO_2 and CO: T_r=375°C; WHSV=0.02; 30min oxidation phase: 10min reduction phase.

Aso et al [1980] showed that the re-oxidation rate constant was significantly smaller than the reduction rate constant for Sb/Fe=1:1 and Sb/Fe=2:1,which implies that longer oxidation times and higher temperatures are needed to bring the catalyst back to its high oxidation state.

The extensive reduction of the catalyst in short times was reported by Sala and Trifiro [1976] to be associated with difficulty in oxidising $Sb^{3+}$and Sb^{5+}. Sb_2O_5 can be easily reduced while Sb_2O_4 re-oxidation is difficult as reported by Sala and Trifiro [1976]. The reduction was assumed to occur via reaction 6.1

$$\mathbf{Sb_2O_5 \leftrightarrow Sb_2O_4 + 1/5O_2} \qquad 6.1$$

The rate of oxidation of the catalyst was also reported to be slow by van Steen et al [1997] as compared to the rate of reduction using a catalyst with Sb/Fe=1.5:1 at 375°C. From Table 2.4 it can be seen that the rate of oxidation increases with an increase in temperature suggesting that higher temperatures are required to bring the catalyst to a higher oxidation state more rapidly.

For the steady-state experiment the productivity is yield × time on stream, for the cyclic experiments of equal oxidation and reaction cycles the productivity is yield × 1/2 time on stream and the cost of operation is high. If the yield obtained from cyclic experiments is not more than the steady state yield, thus it makes no sense to opt for cyclic operation. There are, of course other factors to consider such as ease of separation and selectivity. If in the cyclic experiment the selectivity exceeds 99% no separation would be needed. This is not the case here, so it looks like the commercial value of cyclic experiment is very poor. However, they represent a useful tool to analyse kinetics, provided that all products can be analysed under transient conditions. Hence one can find an improved catalyst.

6.3.2 Reaction simulation

The simulation results show that the proposed single site mechanism was adequate to simulate the trends observed during the steady state and periodic propene partial oxidation to acrolein and COx. The simulation results also provide the qualitative information about the dynamics of the surface species as the catalyst is exposed in periodic reaction environment, as these cannot be measured. In order to simulate the observed trends correctly, adjustments to the number of active sites was necessary. The experimental curves have a relatively slow deactivation over time i.e. many residence times to reach steady state. Such data may be attributed to a number of factors viz. the oxidation-reduction steps are slow, there is a slow adsorption or capacity in the system, or a slow side reaction which is eliminating active sites irreversibly (i.e. propene adsorption).

Considering the reduction step to be slow, it was found that steady state was still achieved in about 1 residence time and the only influence this had was to reduce the yield. Due to low surface area of this catalyst no large adsorption capacity was expected and hence this could not be the cause of the slow approach to steady state. Recalling that multiple layers are responsible for reduction by reaction as shown in figure 6.7 and if the lattice diffusion could be lumped in the rate constant, a way to increase oxidation capacity would be simply to increase the number of active sites. In figure 6.7 (a) the catalyst has limited amounts of oxygen available, hence the catalyst is rapidly reduced resulting in the formation of vacancies. In figure 6.7(b) the oxygen capacity is high, because the oxygen in the deeper layers of the catalyst diffuse through to the surface monolayer filling the vacant sites created by propene reduction.

Figure 6.6 shows that when the number of active sites (n represents the number of equivalent monolayers) are increased the system approaches steady state over many residence times as observed experimentally. This means that at large n there is not sufficient O_2 in the gas stream to rapidly oxidise the surface. Although n=100 or 200 may seem rather unrealistically large numbers of monolayers, these data do support the idea that multiple layers of lattice oxygen participate in the reaction mechanism.

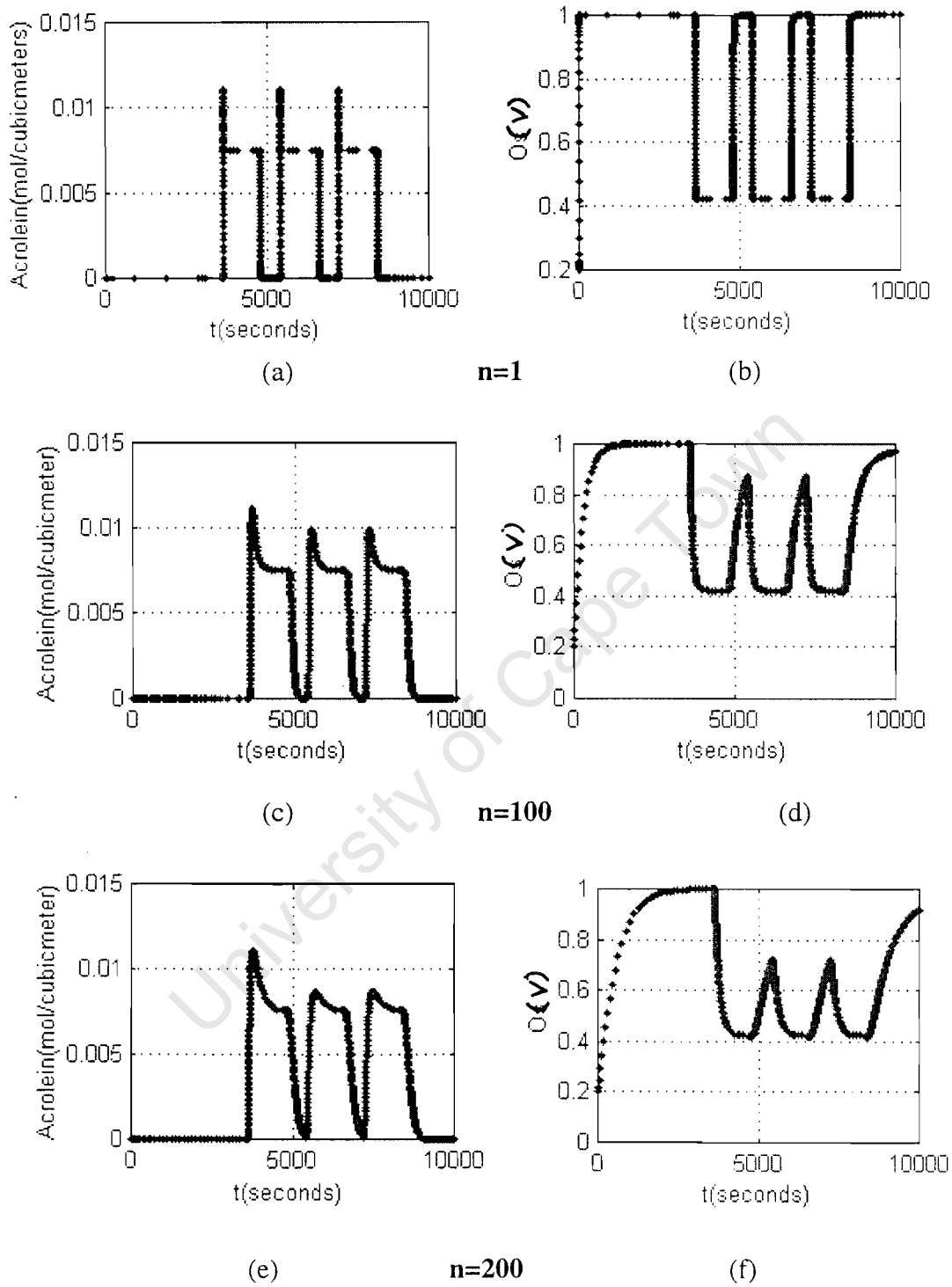

Figure 6.6 The behaviour of acrolein and the lattice oxygen ion with an increase in **n** the number of monolayers.

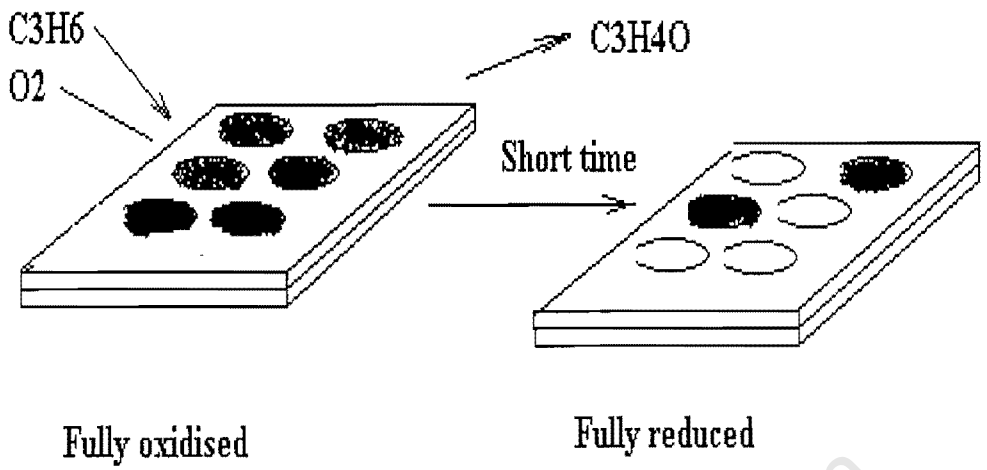

(a)

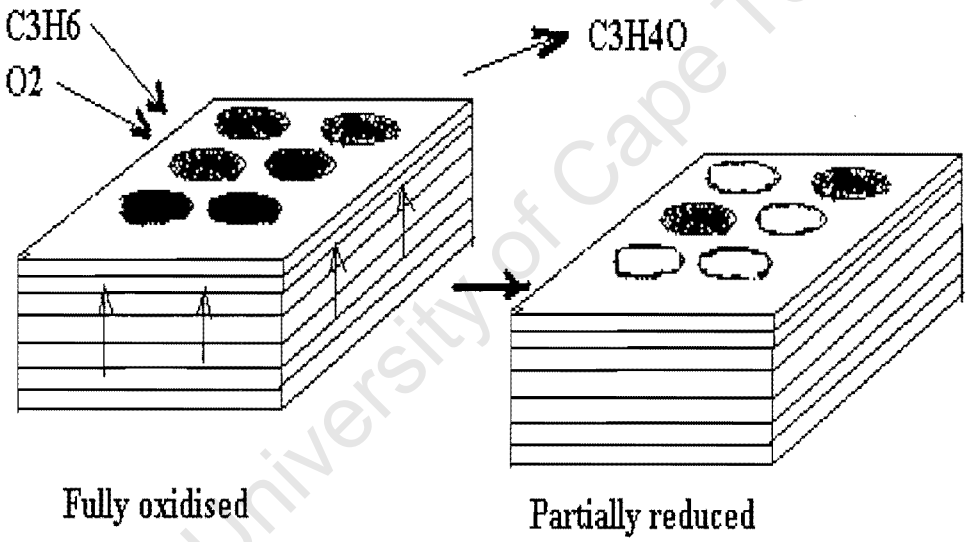

(b)

Figure 6.7 Dependency of degree of reduction of the catalyst on the number of oxygen monolayers.

Notice that the oxidation reaction proceeds via a semi-batch mode in which the catalyst takes up O_2 as if adsorption were taking place, and thus oxidation is linked to the number of active sites. The slow reaction of propene eliminating active sites was not investigated as the previous mechanism worked. Furthermore this concept would require the introduction of additional reaction steps for both reduction and oxidation. More than likely both propene deactivation and multiple oxidation layers occur, providing the expected response.

Table 6.2 Number of lattice oxide ion layers involved in the partial oxidation of propene to acrolein and carbon dioxide.

Catalyst	Temperature(°C)	No of oxygen layers	References:
Sb/Fe=2:1	450	5 #	Haber et al [1991]
Sb/Fe=4:1	45O	6-7*	Haber et al [1991]
Sb/Fe=4.1	350	1.5*	Keulks et al [1986]
Sb/Fe=4.1	400	3.2*	Keulks et al [1986]
Sb/Fe=4.1	450	4.6*	Keulks et al [1986]
Bi/Mo=2:3	430	75*	Haber et al [1991]
Bi/Mo=2:6	430	286*	Haber et al [1991]

the formation of acrolein.

* the formation of both acrolein and total oxidation .

Table 6.2 shows that for $FeSbO_4$ the number of monolayers active in the reaction are between 2 and 7. Considerably less than the 100 proposed here. These results are also supported by Moroka et al [1981], Allen et al [1996] and Fattore et al [1975b]. However, for $BiMoO_x$ catalyst, 100 to 300 layers have been reported to be active in the oxidation reaction (Table 6.1). Thus it appears that this $FeSbO_4$ catalyst behaves similarly to the $BiMoO_x$ catalyst. The observed trends, in the CO_x and propene yield also follow the similar time dependent behaviour.

These results seem to suggest that in the $FeSbO_4$ prepared in this work a large number of monolayers participate in the reaction and that the reactive oxygen is relatively mobile in the lattice.

7 CONCLUSION

The transient experiments revealed that the yield of acrolein could be improved by operating the reactor in a periodic mode. The cycling time was observed to be a crucial parameter in these experiments. Longer cycling times were needed to oxidise the catalyst back to its initial oxidation state, while shorter cycling time were not sufficient to replenish the lost sites instead the characteristics of steady state behaviour were observed.

The proposed single site mechanism along with the assumption of a CSTR gave results, which qualitatively described the trends and the behaviour of the products, reactants and the surface species of the catalyst. The simulation results showed that the partial oxidation of propene occurs not on the few monolayers of an oxide ion as reported by Keulks et al. [1986], Haber et al. [1991] and Schnobel et al. [1997] but on the deeper layers.

APPENDICES

APPENDIX 1 Catalyst preparation and gas flow calculations

Appendix1 (a) Preparation of Iron Antimony Oxide (Sb/Fe=1.5:1)

mass of $Fe_2(NO_3)_3$ = 20g

mol of $Fe_2(NO_3)_3$ = 0.03714 mol

mol of Fe/ mol of $Fe_2(NO_3)_3$ = 2/1

then mol of Fe = 0.03714 mol

also Sb/Fe = 1:1.5

therefore mol Sb =0.0557 mol.

but mol Sb/mol Sb_2O_4 = 2/1

therefore mol Sb_2O_4 = 0.02785 mol

and the mass of Sb_2O_4 = 8.121g is required to prepare Sb/Fe = 1.5:1

Appendix 1(b) Sample calculations of gas flow rates from the WHSV.

The WHSV of $0.02g_{propene}/g_{cat}$.and a catalyst was of 1g were used in the experiment, thus obtaining the amount of propene and hence the flowrate of the gases:

Mass propene = 0.02g

M_r of propene = 42g/mol

Mols of propene = 4.76×10^{-4} mols/min

Volume of propene = nRT/P

= $(4.76\times10^{-4}\times8.314\times298)/101325$

= $1.19\times10^{-5}m^3$/min

=12ml/min (NTP).

Volume of O_2 =1.6×12ml/min

=19.2ml/min (NTP).

Volume of Helium = 7×12ml/min

=84ml/min (NTP).

APPENDIX 2 Mass balance calculations

Appendix 2(a) Determination of conversions, yields selectivity and carbon balances

2(a).1 Conversion calculation

The area obtained in the gas chromatogram is an indication of the amount of acrolein in the sample. The amount of carbon dioxide coming out of the reaction was analysed using the Braun CO/CO_2 analyser.

$$Conversion = 1 - \frac{molesout}{mole\,\text{sin}}$$

$$= 1 - \frac{noC_3(reactor)/noC_1(methane)}{noC_3(bypass)/noC_1(methane)}$$

Now in terms of the peak areas:

$$\frac{AreaC_3}{AreaC_1} = \frac{noC_2}{noC_1} \times \frac{1}{3}$$

hence the conversion of propene was evaluated using the equation below:

$$Conversion = 1 - \frac{(AreaC_3/AreaC_1)_{reactor}}{(AreaC_3/AreaC_1)_{bypass}}$$

2(a).2 Yield calculation for acrolein , carbon dioxide and carbon monoxide

$$Yield_{acrolein} = \frac{molsAcrolein,out}{mols\,\text{Pr}opene,in}$$

$$Yield_{acrolein} = \frac{(\frac{Area_{acrolein}}{Area_{methae}})_{reactor}}{(\frac{Area_{acrolein}}{Area_{methae}})_{bypass}}$$

$$Y_{CO2} = \frac{molsCO_2, out}{mols\,\mathrm{Pr}opene, in}$$

but $$n(molsCO_2) = \frac{PV}{RT}$$

then $$Y_{CO2} = \frac{\frac{y_{CO2} \times PV}{n(methane) \times RT}}{(\frac{Area_{acrolein}}{Area_{methae}})_{bypass}}$$

The analysis is the sample for carbon monoxide, in the place of CO_2 put CO.

2(a).3 Selectivity of acrolein , carbon dioxide and carbon monoxide:

$$S_{acrolein} = \frac{Y_{acrolein}}{Y_{acrolein} + Y_{CO_2} + Y_{CO}}$$

$$S_{acrolein} = \frac{Y_{CO_2}}{Y_{acrolein} + Y_{CO_2} + Y_{CO}}$$

$$S_{acrolein} = \frac{Y_{CO}}{Y_{acrolein} + Y_{CO_2} + Y_{CO}}$$

2(a).4 Overall mass balance:

$$\%Carbon, balance = (1 - X_{propene} + Y_{acrolein} + Y_{CO} + Y_{CO_2})$$

Appendix 2(b) Sample calculation of yields, selectivity, conversion and carbon balance.

Reaction temperature: 375°C.
Catalyst : Iron antimonate (Sb/Fe=1.5:1)

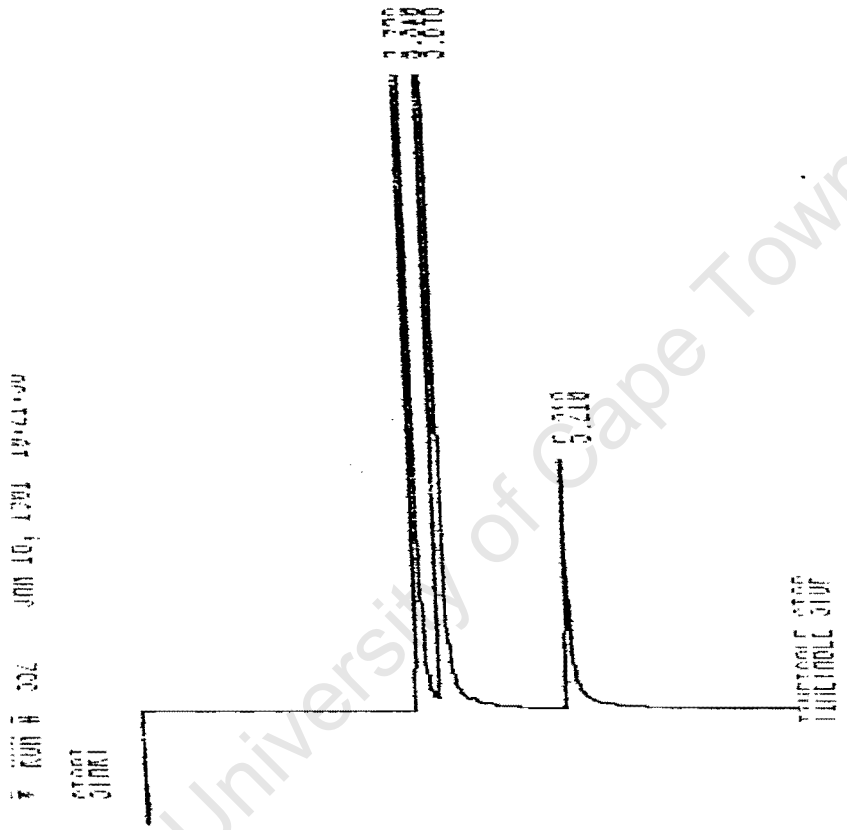

Figure 2(b) Typical gas chromatogram.

Compound	Retention Time(min)	Reactor Area	Bypass Area
Methane	3.3	2350622	2394144
Propene	3.8	2762422	3060958
Acrolein	5.21	87956	-

The areas are for t= 40min time on stream.
Data for CO/CO_2 analyser : CO_2 = 0.8 volume% and CO =0.06 volume%
Flow rate of methane = 29ml/min
Total flowrate less methane = 116ml/min
Total flow rate with methane = 145ml/min
The flows were measured at T=298K

Conversion calculation

$$Conversion = 1 - \frac{\frac{3060958}{2394144}}{\frac{2762422}{2350622}}$$

$$= 8.19\%$$

Yield calculation:

Yield of Acrolein

$$Yield_{acrolein} = \frac{\frac{87956}{2394144}}{\frac{2762422}{2350622}}$$

$$=2.92\%$$

Yield of CO_2

$$Y_{CO2} = \frac{y_{CO2} \times \frac{Totalflowrate}{flowrate(Methane)}}{(\frac{2762422}{2350622})_{bypass}}$$

$$= 3.13\%$$

Yield of CO

$$Y_{CO} = \frac{y_{CO} \times \frac{Totalflowrate}{flowrate(Methane)}}{(\frac{2762422}{2350622})_{bypass}}$$

$$=0.27\%$$

Selectivity of Acrolein:

$$S_{acrolein} = \frac{Y_{acrolein}}{Y_{acrolein} + Y_{CO_2} + Y_{CO}}$$

$$S_{acrolein} = \frac{2.92}{2.92 + 3.13 + 0.2}$$

$$= 46\%$$

For CO_2 annd CO was calculated to be 49 and 4% respectively

Total carbon balance:

$$\%C = (1 - 0.819 + 0.029 + 0.0314 + 0.004) \times 100$$

$$=98.3\%$$

The standard deviation and the mean of the flows were calculated from EXCEL using STDEV(x) and AVERAGE(x) functions assuming a confidence limit of 95%

APPENDIX 3 Heat and mass transfer limitations.

Appendix 3(b) External and Internal heat and mass transport limitation

The effective diffusivity of propene in the catalyst was estimated using equation (1):

$$D_{eff} = D_{avg}\varepsilon_p / \tau \quad (1)$$

The average diffusivity of propene in the pores of the catalyst was estimated using equation (2):

$$\frac{1}{D_{avg}} = \frac{1}{D_k} + \frac{1}{D_m} \quad (2)$$

and

$$D_k = 97 \times r_{pore}\sqrt{\frac{T}{M}} \quad (3)$$

where r_{pore} is the pore radius.

The final value of D_{avg}, voidage and totorsity value estimated by using the parallel pore model stating that $\tau = 1/\sqrt{\varepsilon} = 2.5$.

The dimensionless groups were evaluated from the expressions below

Reynolds number:

$$\mathrm{Re}_p = \frac{d_p u \rho_{air}}{\mu_{gas}} \quad (4)$$

Schmidt number:

$$Sc = \frac{\mu_{N2}}{\rho_{gas} D_{i,m}} \quad (5)$$

Prantl number:

$$\mathrm{Pr} = \frac{\mu C_p}{k_f} \quad (6)$$

Sherwood number: $$\frac{k_m L}{D_{AB}} \quad (6)$$

The mass transfer coefficient kc was determined by the correlation recommended by Kakteijn et al [1993]

$$J_D = \frac{Sh}{\mathrm{Re}_p Sc^{1/3}} = 1.66\,\mathrm{Re}_p^{-0.51} \quad (7)$$

The Chilton-Colburn analogy of the form shown in equation (8) was used so to estimate the heat transfer coefficient, h, because of the low Reynolds number.

$$J_D = \frac{Sh}{\mathrm{Re}_p Sc^{1/3}} = \frac{Nu}{\mathrm{Re}_p \mathrm{Pr}^{1/3}} = J_H \quad (8)$$

$$h = \mathrm{Re}_p \mathrm{Pr}^{1/3}(\lambda / D)k_c \quad (9)$$

The r_{obs}(reaction rate observed) was evaluated from the experimental data corresponding to the conversion of 11% in a catalyst bed of 1g and was found to be=0.78 mol/(s.m^3(cat)).

Appendix 3(a). 1 External mass transfer limitations

Table3(a).1.1 shows the criteria, which needs to be satisfied for negligible transport effects in steady-state kinetic research.

Transport process	Expression	Criteria
Extraparticle mass transport	$Ca = \frac{r_{Obs}}{k_g a' C_b}$	< 0.05
Intraparticle mass trasport Wheeler-Weisz criterion	$\eta_{in}\varphi_{in}^{\ 2} = \frac{r_{obs} L^2 (n+1)}{2 \times D_{eff} C_s}$	< 0.1
Extraparticle heat transport	$\frac{k_g(-\Delta H)C_b}{hT_b} \times \frac{E_a}{RT} \times Ca$	< 0.05
Intraparticle heat transport	$\frac{k_g(-\Delta H)C_s}{hT_s} \times \frac{E_a}{RT_s} \times \eta_{in}\varphi_{in}^{\ 2}$	< 0.05

Table 3(a).1.2 shows the criteria, which needs to be satisfied for negligible transport effects in transient kinetic research.

Transport process	Expression	Criterion
Extra/intraparticle mass transport ($Bi \geq 20$)*	$\tau_{in} = \frac{D_{eff}}{\varepsilon_p R^2} t$	>0.25

* denotes the expression for the mass Biot number.

Dekker et al [1995] introduced a critical time defined in equation (10):

$$t_{ex} = \tau_{ex}\varepsilon_b / [k_c a'(1-\varepsilon_b)] \qquad (10)$$

after which the reactant concentration on the surface of a catalyst ,C_s , reaches a predetermined fraction of the steady state concentration. This time depends on the Carberry number Ca shown below

$$Ca = \frac{C_b - C_s}{C_b} = \frac{-r_{i,\max,pellet}}{C_b k_f a_m} \qquad (11)$$

Using equation (11) above the Carberry number was found to be Ca = 2.59 $\times 10^{-5}$ less than the imposed steady-state criteria of Ca<0.05 [Moulijn et al 1991] and [Kapteijn et al 1997.]This value was then used to find τ_{ex}, the time taken for the bulk concentration to reach 95% of the surface concentration after a step input of the feed. It was found to be $\tau_{ex} \cong$ 3ms from figure 3.(a).3.

Appendix 3(a). 2 Internal mass transfer limitations.

Dekker et al [1995] define the time:

$$t_{in} = \tau_{in} \varepsilon R^2 / D_{eff} \qquad (12)$$

after which the average reactant concentration in the pores reaches a predetermined fraction of the steady-state concentration. τ_{in} depending on the mass Biot number , Wheeler –Weisz modulus $\eta\varphi^2$ and the reaction order. In our case the Biot number was calculated to be, Bi_m=2.54×10^2 giving a value of $\eta\varphi^2$ =0.07 from Figure 3.(a).2 . Hence then using the graph in figure 3.(a).3 the value of τ_{in} was obtained, and was found to be higher than the stated criterion in table 3A.2.

Appendix 3(a).3 Heat transfer limitations.

The values of activation energy were extracted from the values obtained by Schnobel et al [1997] and van Steen et al [1997]: E_a =55 kJ/mol .The value of the enthalpy of reaction was obtained from thermodynamic analysis of the reaction: (-ΔH) =1924 kJ/mol.

According to Dekker et al [1995], heat transfer effects in the transient (concentration steps) are neglected, if the following criteria in equations (13) and (14) are satisfied:

$$\left(\frac{E_a}{RT}\right)\times\beta_e Ca < 0.05 \quad \text{External} \tag{13}$$

$$\left(\frac{E_a}{RT}\right)\times\beta_i\times\eta\times\varphi^2 < 0.1 \,\text{Internal} \tag{14}$$

are satisfied (Moulijn et.al 1991:Kapteijn et.al..1997) with $\left(\frac{E_a}{RT}\right)=10.51$ and for the maximum values of the external and internal **Prater numbers $\beta_e = 1.39\times10^3$ and $\beta_i = 0.0024$.**

$$\left(\frac{E_a}{RT}\right)\times\beta_e Ca = 0.37 > 0.05$$

Indicates that external heat transports are occurring.

$$\left(\frac{E_a}{RT}\right)\times\beta_i\times\eta\times\varphi^2 < 0.00043 < 0.1,$$

Indicating that internal heat transfer limitations are not occurring.

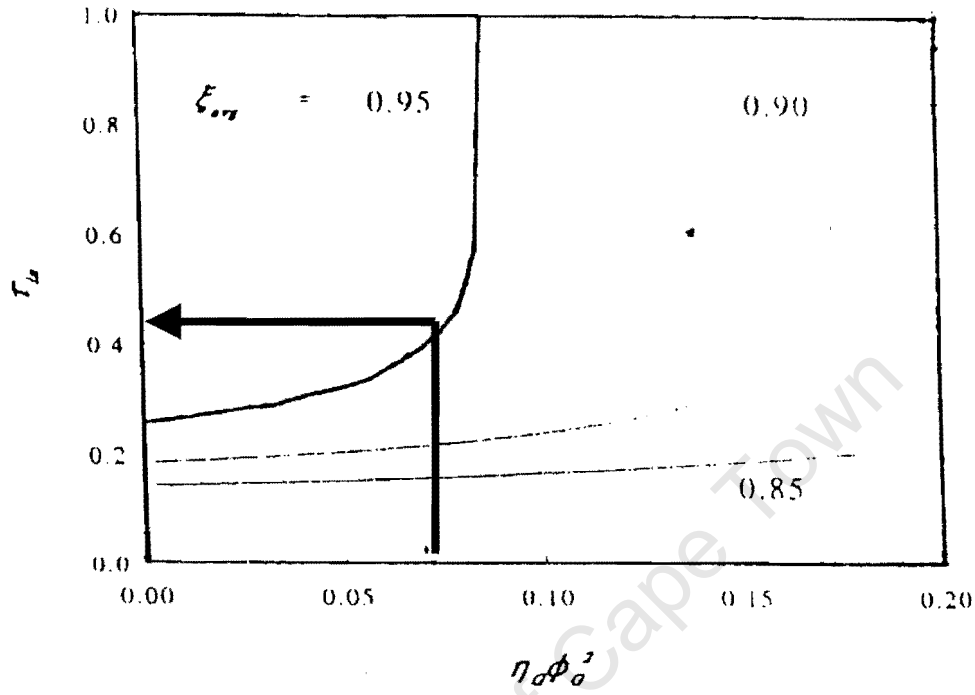

Figure 3.(a).1 Dimensionless time τ_{in} needed to reach a certain average dimensionless concentration $\xi_{avg}= C_{surface}/C_{bulk}$ after the step input of the reactive gas.

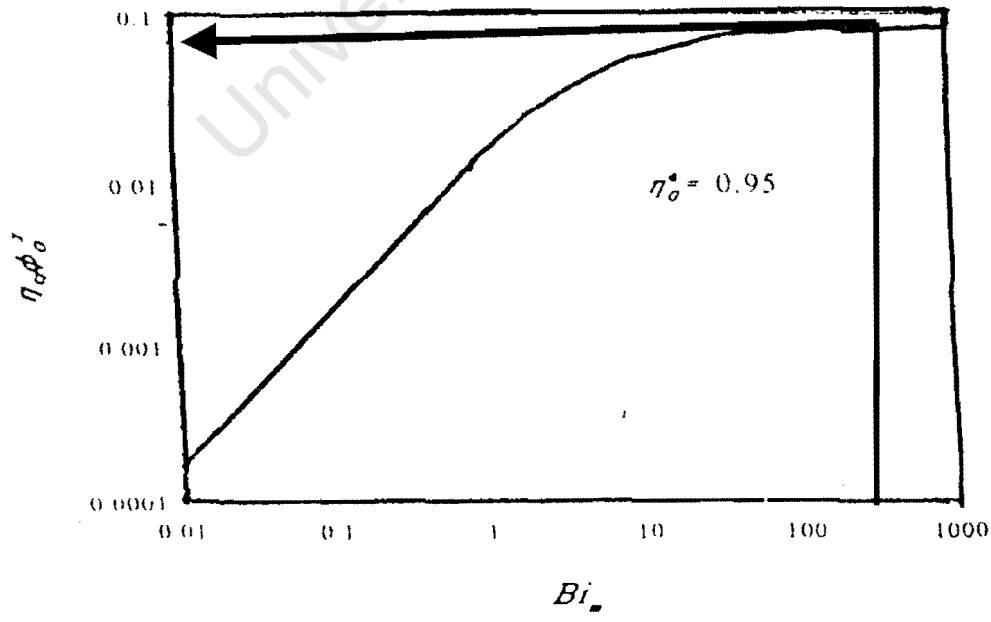

Figure 3.(a).2 Relation between $\eta\varphi^2$ and Biot number.

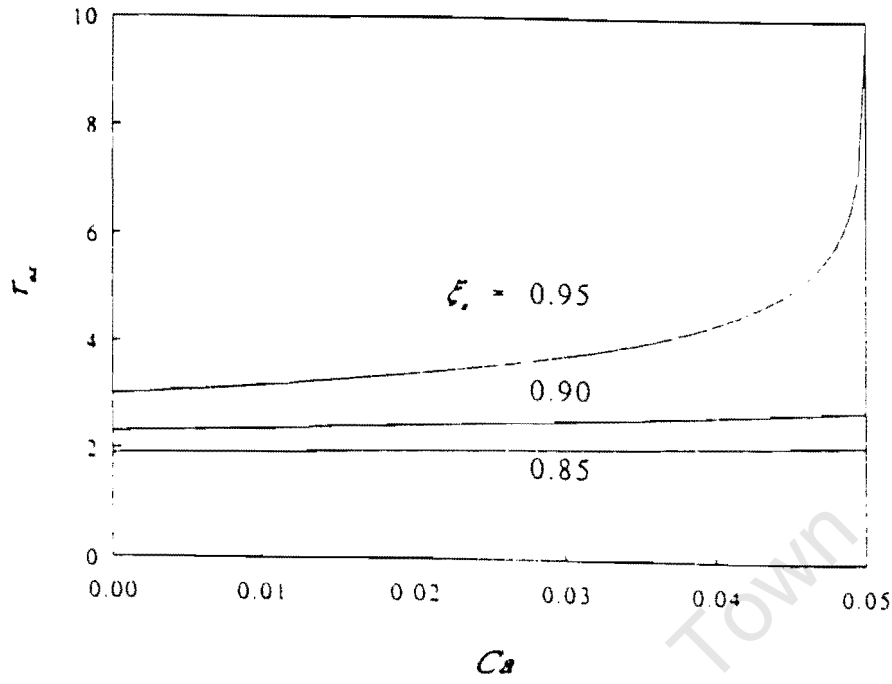

Figure 3.(a).3 Dimensionless time, τ_{ex} needed to reach a certain dimensionless surface concentration ξ_{avg} as function of Carberry number for a step change of reactive gas.

Appendix 3(b) Data for the evaluation of mass and Heat transport limitation

Table 3(b).1 Data for evaluating heat and mass transfer limitations

Components	Value	Units
C3H6	4.54	
He	2.88	
O2	5.50	
Molarmass mix.	12.92	
Property	**Value**	**Units**
T	643.15	K
P	1	atm
Av Cpmix	1.09E+01	J/mol.K
Viscosity mix	3.15587E-05	kg/m.s
Thermal cond. Mix	0.003163676	
DC3H6-mixture	6.33514E-05	m^2/s
Density.mixture	0.244880556	kg/m^3
Molmass mixture	1.29E-02	kg/mol
Totalflowrate mixture	1.9475E-06	m^3/s
Dtube(m)	0.004	m
L(tube)	0.36	m
dp(m)	2.70E-04	m
Dk	2.97E-05	m^2/s
a	0.00000004	m
Tortosity	2.5	
Davg	2.01973E-05	m^2/s
voidage	0.4	
Heat of reaction	-1924000	J/mol
Activation energy	95000	J/mol
Activation energy	55000	J/mol
R(gas constant)	8.13	J/mol.K
mol(in)	7.45E-06	mml/min
mol(out)	6.67E-06	mml/min
mass cat	1	g
Rate	0.783333333	$mol/m^3.s$
P(head)	40000	Pa
Cb	1.70498502	mol/m^3
a(particle)	2.22E+04	1/m

Table 3(b).1(Cont.) Data for evaluating heat and mass transfer limitations

Property	Value	Units
Deff	3.23e-06	m^2/s
Pr	1.08e-01	
Sc	2.03e+00	
Area	1.26e-05	m^2
U	1.55e-01	m/s
Re	3.25e-01	
Jd	2.95e+00	
Sh	6.49e-01	
kc	1.52e-01	m/s
h	5.58e-01	$J/(m^2.s.K)$
Ea/RT	1.05e+01	
Ca	1.36e-04	
Tauex		
Tex		
Bim	6.36e+00	
Na^2	1.70e-02	
Cs	1.70e+00	mol/m^3
Be	1.39e+03	
Bi	1.65e-01	
(Ea/RT)Be*Ca	1.99e+00	
(Ea/RT)Bi*na^2	2.95e-02	
UL/D	2.76e+03	
1/Pe	3.62e-04	
L/u	2.32e+00	s
DC3H6-mixture	6.34e-05	m^2/s
Dk	2.97e-05	m^2/s
Avg Cpmix	1.09e+01	J/mol.K
Viscosity of the mixture	3.16e-05	Kg/m.s
Thermal cond.of mixture	1.09e+01	J/s.m.K
Density	2.45e-01	kg/m^3
Total flowrate	1.17e+02	ml/min

Appendix 3(c) Thermodynamic properties for the reaction compounds.

Table 3(c).1 Thermodynamic data

Compound	He	O2	C3=	C3O=	CO2	CO	H_2O
Molwt	4	31.999	42.081	56.064	44.01	28.01	18.015
Tfp	0	-218.8	-185.3	-87.2	-56.6	205.1	0
Tbp	-269	-183	-47.8	52.8	-78.5	191.5	100
Tc	5.2	154	365	506	304.2	132.9	647.3
Pc	2.3	50.5	46.2	51.7	73.8	35	220.5
Vc	0.057	0.073	0.181	0	0.094	0.093	0.056
Lden	123	1149	612	839	777	803	998
Tden	-269	-183	-50	20	20	-192	20
Hvap	92	6824	18422	28345	17166	6046	40683
Visa	0	85.68	273.84	388.17	578.08	94.06	658.25
Visb	0	51.5	131.63	217.14	185.24	48.9	283.16
Delhf	0	0	20.43	-70.92	-393.77	110.62	-242
Delgf	0	0	62.7	-65.19	-394.65	137.37	228.77
Cpa	0	28.106	3.71	11.97	19.795	30.869	32.243
Cpb	0	-3.68×10^{-6}	2.35×10^{-01}	2.11×10^{-01}	7.34×10^{-02}	1.29×10^{-02}	1.92×10^{-03}
Cpc	0	1.75×10^{-05}	-1.16×10^{-4}	-1.07×10^{-04}	-5.60×10^{-05}	2.79×10^{-05}	1.06×10^{-5}
Cpd	0	-1.07×10^{-8}	2.20×10^{-08}	1.91×10^{-08}	1.72×10^{-08}	1.27×10^{-08}	-3.90×10^{-9}
Anta	12.25	15.075	15.9087	15.9087	22.58	14.3686	18.3
Antb	33.73	734.55	2606.53	2606.53	3103.39	530.22	3816.44
Antc	1.79	-6.45	-26.15	-45.15	-0.16	-13.15	-46.13
Tmn	-269	-210	-113	-38	-119	-210	11
Tmix	-269	-173	-33	87	-69	-165	168

APPENDIX 4 Data for steady-state and unsteady-state experiment.

Appendix 4.(a).1 Steady-state propene partial oxidation experiment.

	Area Methane	Area Propene
BP1	2574544	3201781
BP2	2654144	3321958
BP3	2391878	3001621
Average	2540189	3175120

BP denotes bypass data and this notation is used throughout.

Time (min)	Area Methane	Area Propene	Area Acrolein	%CO_2	%CO	Area CO_2	Area CO
1	296896	321600	14372	1.45	0.85	17220	10934
2	317549	361171	14501	1	0.25	12702	3612
4.15	174668	203092	7370	0.7	0.06	4890.7	487.4
5.5	446759	524341	18160	0.6	0.06	10722	1258
6.5	255396	304621	10268	0.55	0.06	5618.7	731.1
8.35	1569995	1787107	53603	0.5	0.04	31400	2859
10.5	1805858	2172870	61611	0.5	0.06	36117	5215
20.35	2545912	2997461	79369	0.45	0.04	45826	4796
30.3	2128818	2510862	62005	0.45	0.04	38319	4017
43	1781049	2081507	49078	0.45	0.04	32059	3330
52	1990636	2342406	56309	0.35	0.04	27869	3748
61	1935825	2267325	53650	0.45	0.04	34845	3628
83	2021223	2366824	52398	0.45	0.04	36382	3787
101.3	2214178	2623408	58081	0.45	0.04	39855	4197

Conversion	Yield Acrolein	Yield CO_2	Yield CO	Selectivity Acrolein	Selectivity CO_2	Selectivity CO	%C
13.343	3.873	4.64	2.95	33.80	40.49	25.71	96.08
9.010	3.653	3.20	0.91	47.06	41.22	11.72	98.07
6.981	3.376	2.24	0.22	57.81	38.36	3.82	98.86
6.108	3.252	1.92	0.23	60.25	35.57	4.18	99.29
4.581	3.216	1.76	0.23	61.79	33.81	4.40	100.54
8.937	2.731	1.60	0.15	61.01	35.74	3.25	95.63
3.741	2.729	1.60	0.23	59.85	35.08	5.07	100.74
5.811	2.494	1.44	0.15	61.06	35.25	3.69	98.27
5.643	2.330	1.44	0.15	59.43	36.72	3.85	98.28
6.504	2.204	1.44	0.15	58.10	37.95	3.94	97.29
5.863	2.263	1.12	0.15	64.04	31.70	4.26	97.67
6.300	2.217	1.44	0.15	58.24	37.82	3.94	97.51
6.321	2.074	1.44	0.15	56.61	39.30	4.09	97.34
5.214	2.099	1.44	0.15	56.87	39.02	4.11	98.48

Appendix 4.(a).2 Steady-state propene partial oxidation experiment: Repeatability

	Area Methane	Area Propene
BP1	2499544	3211781
BP2	2394144	3060958
BP3	2641878	3371621
Average	2511855	3214787

Time(min)	Area Methane	Area Propene	Area Acrolein	%CO2	%CO	Area CO_2	Area CO
1	2203970	2417320	154034	1.45	0.75	127830	72520
2	2177338	2505272	131229	1.3	0.25	113222	25053
5	2154554	2527825	132732	1	0.06	86182	6067
20	2264632	2672838	94640	0.95	0.06	86056	6415
30	2522846	3026752	97014	0.8	0.06	80731	7264
40	2350622	2762422	87956	0.8	0.06	75220	6630
52	2660974	3166150	97230	0.75	0.04	79829	5066
61	2621325	2995470	92645	0.7	0.04	73397	4793
82.1	2698122	3197728	96159	0.6	0.04	64755	5116
103.2	2765734	3257480	94923	0.65	0.04	71909	5212
123	2941008	3422592	101153	0.65	0.04	76466	5476

Yield Acrolein	Yield CO_2	Yield CO	Selectivity Acrolein	Selectivity CO_2	Selectivity CO	Conversion	%C
5.46	4.5313	2.5706	0.43	0.36	0.20	14.31	98.25
4.71	4.0625	0.8989	0.49	0.42	0.09	10.11	99.56
4.81	3.1250	0.2200	0.59	0.38	0.03	8.34	99.82
3.26	2.9688	0.2213	0.51	0.46	0.03	7.79	98.66
3.00	2.5000	0.2250	0.52	0.44	0.04	6.27	99.46
2.92	2.5000	0.2203	0.52	0.44	0.04	8.19	97.46
2.85	2.3438	0.1487	0.53	0.44	0.03	7.04	98.30
2.76	2.1875	0.1428	0.54	0.43	0.03	10.72	94.37
2.78	1.8750	0.1481	0.58	0.39	0.03	7.41	97.40
2.68	2.0313	0.1472	0.55	0.42	0.03	7.98	96.88
2.69	2.0313	0.1455	0.55	0.42	0.03	9.08	95.78

Appendix 4.(b).1 5min cycling time on propene partial oxidation.

	Area Methane	Area Propene
BP1	2199861	2751854
BP2	2411061	3001254
Average	2305461	2876554

Time(min)	Area Methane	Area Propene	Area Acrolein	%CO_2	%CO	Area CO_2	Area CO
1.3	2275168	2499214	76537	1.7	0.85	154711	84973
2	2134326	2505222	69038	1	0.7	85373	70146
4	2081081	2468925	58736	0.9	0.6	74919	59254
6	2195459	2600632	57241	0.8	0.06	70255	6242
8.1	2321296	2756986	58666	0.6	0.05	55711	5514
10	2525150	3059762	61758	0.5	0.05	50503	6120
12.3	2761350	3300253	64359	0.5	0.045	55227	5940
17	3110861	3884504	71605	0.4	0.045	49774	6992
18.1	2689264	3231846	60516	0.4	0.045	43028	5817
20	2875246	3484101	65317	0.4	0.045	46004	6271
21							
22							
23							
24							
25							
26	3872085	4617939	106313	0.65	0.065	100674	12007
28	3714626	4437962	94227	0.6	0.065	89151	11539
30	2982037	3550301	72032	0.6	0.06	71569	8521
33	1313726	1566388	30027	0.55	0.06	28902	3759
35.12	3009446	3650538	70638	0.5	0.06	60189	8761
37	2961845	3603766	66769	0.5	0.06	59237	8649
39.01	2829552	3476488	61350	0.5	0.055	56591	7648
41	2854562	3463034	62048	0.5	0.05	57091	6926
42.5	2719294	3294134	57703	0.5	0.04	54386	5271
45	2980446	3653106	67905	0.5	0.04	59609	5845
46							
47							
48							
49							
50							
51							
52	2569328	3042850	60204	0.6	0.04	61664	4869
54	2151293	2600200	47392	0.6	0.04	51631	4160
55.5	2195077	2620376	45033	0.5	0.04	43902	4193
60	2613178	3164206	56926	0.5	0.04	52264	5063
62.1	2464797	2957766	55563	0.5	0.04	49296	4732
65.08	2493141	3021126	53765	0.5	0.04	49863	4834
68	2356653	2810258	50923	0.5	0.04	47133	4496

Appendix 4.(b).1(Cont) 5min cycling time on propene partial oxidation.

Yield Acrolein	Yield CO_2	Yield CO	Conversion	Selectivity Acrolein	Selectivity CO_2	Selectivity CO	%C
2.69	5.44	2.99	12.12	19.41	39.23	21.55	87.9
2.59	3.20	2.63	6.10	28.66	35.44	29.12	93.9
2.26	2.88	2.28	5.09	28.09	35.83	28.34	94.9
2.09	2.56	0.23	5.24	39.01	47.87	4.25	94.8
2.02	1.92	0.19	4.98	50.17	47.64	4.72	95.0
1.96	1.60	0.19	3.06	57.65	47.14	5.71	96.9
1.86	1.60	0.17	4.39	55.29	47.45	5.10	95.6
1.84	1.28	0.18	0.10	67.21	46.72	6.56	99.9
1.80	1.28	0.17	3.86	65.87	46.83	6.33	96.1
1.82	1.28	0.17	3.06	66.46	46.81	6.38	96.9
2.20	2.08	0.25	4.59	49.83	47.19	5.63	95.4
2.03	1.92	0.25	4.42	49.63	46.96	6.08	95.6
1.93	1.92	0.23	4.76	47.50	47.19	5.62	95.2
1.83	1.76	0.23	4.61	48.77	46.95	6.11	95.4
1.88	1.60	0.23	2.96	54.70	46.61	6.78	97.0
1.80	1.60	0.23	2.66	52.52	46.60	6.80	97.3
1.73	1.60	0.22	1.71	50.77	46.84	6.33	98.3
1.74	1.60	0.19	2.95	51.23	47.14	5.72	97.1
1.70	1.60	0.16	3.09	50.60	47.69	4.62	96.9
1.82	1.60	0.16	1.94	54.30	47.66	4.67	98.1
1.87	1.92	0.15	5.26	46.96	48.10	3.80	94.7
1.76	1.92	0.15	3.31	44.12	48.06	3.87	96.7
1.64	1.60	0.15	4.50	48.95	47.72	4.56	95.5
1.74	1.60	0.15	3.13	51.94	47.69	4.62	96.9
1.80	1.60	0.15	4.00	53.78	47.71	4.58	96.0
1.73	1.60	0.16	3.06	51.42	47.69	4.62	96.9
1.73	1.60	0.15	4.60	51.56	47.72	4.55	95.4

Appendix 4.(b).2 10min cycling time on propene partial oxidation.

	Area Methane	Area Propene
BP1	4742378	6025629
BP2	5052378	6410962
Average	4897378	6218296

Time (min)	Area Methane	Area propene	Area Acrolein	%CO_2	%CO	Area CO_2	Area CO
1	4224794	4872845	196662	1.2	0.85	202790	2E+05
6.02	4734579	5810637	166525	1	0.25	189383	58106
8.05	4131784	5034544	133678	0.7	0.06	115690	12083
10.05	4285434	5439837	139588	0.65	0.06	111421	13056
12.11	4787146	5894714	143869	0.6	0.06	114892	14147
14.12	4582805	5603805	136400	0.5	0.06	91656	13449
16.35	4363542	5285869	122544	0.4	0.06	69817	12686
18.2	4762864	5808250	134709	0.4	0.06	76206	13940
20	4762864	5808250	134709	0.4	0.045	76206	10455
22							
24							
26							
28							
34.28	5242493	6347363	157359	0.7	0.04	146790	10156
36.2	3872085	4617939	106313	0.65	0.04	100674	7389
38.01	3714626	4437962	94227	0.6	0.04	89151	7101
44	3382037	4050301	72032	0.6	0.04	81169	6480
46	3138754	3768144	72025	0.55	0.04	69053	6029
48	3363442	4049854	79190	0.5	0.04	67269	6480
50	3309846	4038181	76299	0.5	0.04	66197	6461
52							
54							
56							
58							
61.35	4220237	5102419	129705	0.6	0.04	101286	8164
68.16	4666205	5754867	124327	0.55	0.04	102657	9208
71	4263446	5280544	112381	0.5	0.04	85269	8449
75	4223733	5165130	112462	0.5	0.04	84475	8264
78	4442934	5501274	116117	0.5	0.04	88859	8802
80	4806666	5943357	124971	0.5	0.04	96133	9509

Appendix 4.(b).2(Cont.) 10min cycling time on propene partial oxidation.

Yield Acrolein	Yield CO_2	Yield CO	Conversion	Selectivity Acrolein	Selectivity CO_2	Selectivity CO	%C
3.67	3.78	3.088	9.18	34.80	35.88	29.32	101.4
2.77	3.15	0.966	3.36	40.22	45.74	14.03	103.5
2.55	2.20	0.230	4.06	51.13	44.25	4.62	100.9
2.56	2.05	0.240	0.05	52.86	42.19	4.94	104.8
2.37	1.89	0.233	3.04	52.72	42.10	5.18	101.4
2.34	1.57	0.231	3.72	56.48	37.95	5.57	100.4
2.21	1.26	0.229	4.62	59.76	34.05	6.19	99.1
2.23	1.26	0.230	3.98	59.91	33.89	6.20	99.7
2.23	1.26	0.173	3.98	60.85	34.42	4.72	99.7
2.36	2.20	0.153	4.67	50.07	46.70	3.23	100.1
2.16	2.05	0.150	6.09	49.59	46.96	3.45	98.3
2.00	1.89	0.151	5.93	49.47	46.80	3.73	98.1
1.68	1.89	0.151	5.70	45.11	50.83	4.06	98.0
1.81	1.73	0.151	5.47	48.96	46.94	4.10	98.2
1.85	1.57	0.152	5.19	51.78	43.98	4.24	98.4
1.82	1.57	0.154	3.93	51.22	44.44	4.34	99.6
2.42	1.89	0.152	4.80	54.23	42.35	3.41	99.7
2.10	1.73	0.155	2.89	52.64	43.46	3.90	101.1
2.08	1.57	0.156	2.48	54.53	41.37	4.10	101.3
2.10	1.57	0.154	3.71	54.81	41.17	4.03	100.1
2.06	1.57	0.156	2.50	54.32	41.57	4.12	101.3
2.05	1.57	0.156	2.64	54.19	41.69	4.12	101.1

Appendix 4.(b).3 20min cycling time on propene partial oxidation.

	Area Methane	Area Propene
BP1	2812378	3530629
BP2	3121378	3931629
Average	2966878	3731129

Time (min)	Area Methane	Area Propene	Area Acrolein	%CO_2	%CO	Area CO_2	Area CO
1	2313654	2449870	90774	3	0.2	277638	19599
2.09	2422654	2773205	87597	1.5	0.1	145359	11093
4	2381174	2771672	73945	1.2	0.09	114296	9978
8.03	2244146	2609250	62618	1.1	0.09	98742	9393
12.11	2500325	2959008	72027	0.6	0.09	60008	10652
16.02	2110779	2475712	62593	0.6	0.06	50659	5942
18.14	1848357	2173878	45389	0.4	0.06	29574	5217
18.2	4762864	5808250	124709	0.4	0.06	76206	13940
20.1	1716577	2042913	40142	0.4	0.06	27465	4903
22							
24							
26							
28							
30							
34.28							
36.2							
38.01							
41.2	2025053	2256957	69182	2.1	0.1	170104	9028
42.2	1831975	2111261	55884	1.6	0.09	117246	7601
44.07	2252606	2622837	61688	1.2	0.08	108125	8393
46.15	2144658	2539290	55779	1	0.07	85786	7110
50.18	2347634	2772846	57002	0.75	0.06	70429	6655
52.1	2345032	2806254	55331	0.7	0.06	65661	6735
56	2433366	2904533	58099	0.4	0.09	38934	10456
60	2375550	2870264	51151	0.55	0.06	52262	6889
62							
64							
66							
68							
70							
72							
74							
76							
78							
81	1925060	2306957	60182	0.6	0.04	46201	3691
82.3	1901975	2223661	56884	0.55	0.04	41843	3558
86.1	2352606	2822937	61688	0.5	0.04	47052	4517
88	2244658	2710290	55779	0.5	0.04	44893	4336
90.4	2199634	2672846	57002	0.5	0.04	43993	4277
94	2405032	2890254	55331	0.5	0.04	48101	4624
98.1	2333455	2804634	58099	0.5	0.04	46669	4487
102	2275550	2770300	51151	0.5	0.04	45511	4432

Appendix 4.(b).3(Cont.) 20min cycling time on propene partial oxidation.

Yield Acrolein	Yield CO_2	Yield CO	Selectivity Acrolein	Selectivity CO_2	Selectivity CO	Conversion	%C
3.11	9.52	0.67	23.39	71.55	5.05	15.96	97.35
2.87	4.76	0.36	35.89	59.56	4.55	9.15	98.84
2.46	3.81	0.33	37.30	57.66	5.03	7.62	98.99
2.21	3.49	0.33	36.67	57.83	5.50	7.72	98.32
2.29	1.90	0.34	50.48	42.06	7.47	6.08	98.45
2.35	1.90	0.22	52.51	42.50	4.98	6.91	97.57
1.95	1.27	0.22	56.61	36.88	6.51	6.66	96.79
2.08	1.27	0.23	58.04	35.47	6.49	3.22	100.36
1.86	1.27	0.23	55.36	37.88	6.76	5.55	97.81
2.71	6.67	0.35	27.86	68.50	3.64	11.55	98.19
2.42	5.08	0.33	30.92	64.87	4.21	8.54	99.29
2.17	3.81	0.30	34.62	60.67	4.71	7.59	98.69
2.06	3.17	0.26	37.52	57.70	4.78	6.03	99.47
1.93	2.38	0.22	42.51	52.53	4.96	6.26	98.27
1.87	2.22	0.23	43.32	51.41	5.27	5.03	99.30
1.89	1.27	0.34	54.05	36.22	9.73	5.27	98.24
1.71	1.75	0.23	46.37	47.38	6.25	4.11	99.58
2.48	1.90	0.15	54.67	41.97	3.35	4.89	99.65
2.37	1.75	0.15	55.61	40.91	3.48	7.21	97.06
2.08	1.59	0.15	54.47	41.54	3.99	4.77	99.05
1.97	1.59	0.15	53.12	42.75	4.13	4.17	99.54
2.06	1.59	0.15	54.15	41.79	4.06	3.56	100.24
1.83	1.59	0.15	51.21	44.51	4.28	4.62	98.94
1.98	1.59	0.15	53.18	42.72	4.11	4.61	99.11
1.78	1.59	0.15	50.60	45.02	4.38	3.38	100.15

Appendix 4.(b).4 30min cycling time on propene partial oxidation.

	Area Methane	Area Propene
BP1	1923544	2451781
BP2	1454144	1821958
BP3	1841878	2411621
Average	1739855	2228453

Time (min)	Area Methane	Area Propene	Area Acrolein	%CO_2	%CO	Area CO_2	Area CO
1.05	589822	644247	20741	2	0.85	47186	21904
2	570179	650559	23139	1.5	0.25	34211	6506
6.04	1252961	1461056	37938	1.2	0.06	60142	3507
8.35	1136363	1326830	33677	1	0.05	45455	2654
10	1491702	1769801	39982	0.5	0.04	29834	2832
20							
30							
40							
41	1724199	1981705	57242	1.5	0.5	103452	39634
42	1083125	1239980	34626	1.2	0.4	51990	19840
44	1183125	1339981	35627	1	0.35	47325	18760
46	1550911	1906200	43734	0.7	0.3	43426	22874
48	566386	611711	16996	0.6	0.1	13593	2447
50	764901	896767	21901	0.55	0.09	16828	3228
60							
70							
80							
82.1	949105	1133670	29789	1	0.1	37964	4535
84.02	554161	674072	17234	0.8	0.1	17733	2696
86.8	553024	663592	17435	0.7	0.09	15485	2389
86	562124	682582	18035	0.6	0.09	13491	2457
88	557024	682592	16435	0.5	0.09	11140	2457
90	941008	1182600	16435	0.5	0.09	18820	4257

Appendix 4.(b).4(Cont.) 30min cycling time on propene partial oxidation.

Yield Acrolein	Yield CO_2	Yield CO	Selectivity Acrolein	Selectivity CO_2	Selectivity CO	Conversion	%/C
2.75	6.25	2.90	23.09	52.53	24.38	14.67	97.2
3.17	4.69	0.89	36.24	53.58	10.19	10.86	97.9
2.37	3.75	0.22	37.35	59.20	3.45	8.90	97.4
2.32	3.13	0.18	41.18	55.58	3.24	8.78	96.8
2.09	1.56	0.15	55.04	41.07	3.90	7.31	96.5
2.59	4.69	1.80	28.57	51.64	19.78	10.21	98.9
2.50	3.75	1.43	32.53	48.84	18.64	10.56	97.1
2.35	3.13	1.24	35.03	46.53	18.44	11.52	95.2
2.20	2.19	1.15	39.75	39.47	20.79	3.98	101.6
2.34	1.88	0.34	51.45	41.15	7.41	15.62	88.9
2.24	1.72	0.33	52.20	40.11	7.69	8.41	95.9
2.45	3.13	0.37	41.21	52.52	6.27	6.68	99.3
2.43	2.50	0.38	45.76	47.08	7.16	4.97	100.3
2.46	2.19	0.34	49.38	43.86	6.77	6.26	98.7
2.51	1.88	0.34	53.07	39.70	7.23	5.13	99.6
2.31	1.56	0.34	54.72	37.09	8.18	4.26	99.9
1.36	1.56	0.35	41.59	47.63	10.77	1.82	101.5

APPENDIX 5 Reactor simulation.

Appendix 5A.1 The Matlab file (M-file) for solving 10 differential equations.

```
function wd=pend(t,w);
[m,n]=size(w);
wd=zeros(m,n);


%w(1) C3H6
%w(2) O2
%w(3) C3H4O
%w(4) H2O
%w(5) COx
%w(6) Os
%w(7) C3H5
%w(8) C3H5O
%w(9) OH
%w(10) V

layer = 0.005;          % 1/monolayer
V=4.52e-6;              %Volume of the reactor.
Q=116.85e-6;            %Total flowrate m^3/min.
vxx1=221;               %vxx1=Vcat/Vcstr.
vxx2=7.2*layer;         %vxx2= kg_cat/mol of sites
tau=V/Q;                %residence time

a=0.01;                 %parameter for increasing or decreasing the
                        % dynamics of the reaction.
ratio=2;                %assume that CO2 is the main product.

% Rate constannts.

  k1=10* a;
  k2=40* a;
  k3=50* a;
  k4=30* a;
  k5=50* a;
  k6=10* a;
  k7=0.001*a;

void=0.4;               %void fraction of the reactor.
```

Appendix 5A.1(Cont) The Matlab file (M-file) for solving 10 differential equations.

```
%Multistep input of propene
 w1=0 ;
if t>3600
    w1=0.20;
end

if  t>4800
    w1=0;
 end

 if    t>5400
      w1=0.2;
end

if    t>6600
     w1=0;
end

if    t>7200
    w1=0.2;
end

if    t>8400
     w1=0;
end


% Inlet conditions in the reactor
w2=0.32;
w3=0;
w4=0;
w5=0;

% Rate expressions for the single site mechanism

r1=k1*w(1)*w(6)^2;
r2=k2*w(7)*w(6);
r3=k3*w(8)*w(6);
r4=k4*w(9)^2;
r5=k5*w(7)*w(6)^2;
r6=k6*w(2)^0.5*w(10)-k7*w(6);

% Bulk species differential equations
```

Appendix 5A.1(Cont) The Matlab file (M-file) for solving 10 differential equations

```
wd(1) =(w1-w(1))/(void*tau)-vxx1*r1;                    % C3H6
wd(2) =(w2-w(2))/(void*tau)-vxx1*r6;                    % O2
wd(3) =(w3-w(3))/(void*tau)+vxx1*r3;                    % C3H4O
wd(4) =(w4-w(4))/(void*tau)+0.5*vxx1*r4;                % H2O
wd(5) =(w5-w(5))/(void*tau)+vxx1*3*r5;                  % COx


% Surface species differential equations

wd(6) =vxx2*(-2*r1-r2-r3+1/2*r4-(3*ratio+5)*r5+r6);     % Os
wd(7) =vxx2*(r1-r2-r5);                                 % C3H5
wd(8) =vxx2*(r2-r3);                                    % C3H5O
wd(9) =vxx2*(r1+r3+5*r5-r4);                            % OH
wd(10)=vxx2*(r2+r3+1/2*r4+(3*ratio+1)*r5-r6);           % V
```

Appendix 5A.2 The Matlab running file Ode23s for stiff differential equations

```
global t                          % globalising the time : M file and running file

t0=0 ;                            %Initial time.
tf=10000;                         %Final time.

w0=[0;0.32;0;0;0;0.2;0;0;0;0.8;0];  %initial conditions for differential eqn. solver.

[t,w]=ode23s('pend',t0,tf,w0);    %Ode23s solver routine.

figure                            %Ploting the figures.
subplot(2,2,1),plot(t,w(:,1)),
xlabel('t'),ylabel('propene'),grid,

subplot(2,2,2),plot(t,w(:,2)),
xlabel('t'),ylabel('O2'),grid,

subplot(2,2,3),plot(t,w(:,3)),
xlabel('t'),ylabel('Acrolein'),grid,

subplot(2,2,4),plot(t,w(:,4)),
xlabel('t'),ylabel('Water'),grid,

figure
subplot(2,2,1),plot(t,w(:,5)),
xlabel('t'),ylabel('COx'),grid,

subplot(2,2,2),plot(t,w(:,6)),
xlabel('t'),ylabel('Os'),grid,

subplot(2,2,3),plot(t,w(:,7)),
xlabel('t'),ylabel('C3H5'),grid,

subplot(2,2,4),plot(t,w(:,8)),
xlabel('t'),ylabel('C3H5O'),grid,

figure
subplot(2,2,1),plot(t,w(:,9)),
xlabel('t'),ylabel('OH'),grid,

subplot(2,2,2),plot(t,w(:,10)),
xlabel('t'),ylabel('Vacancy'),grid,

figure
subplot(2,2,1),plot(t,w(:,11)),
xlabel('t'),ylabel('Total sites'),grid,
```

Appendix5(b).1 5min cycling time simulation graphs

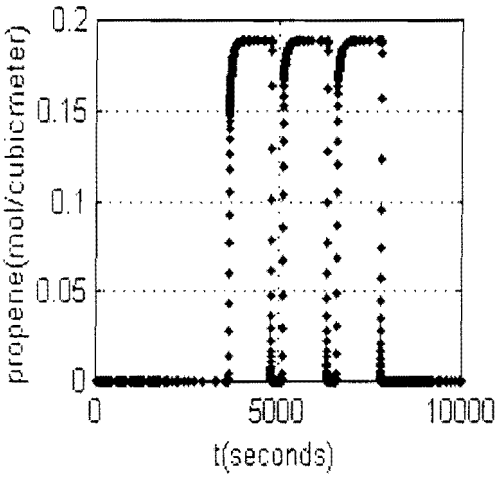

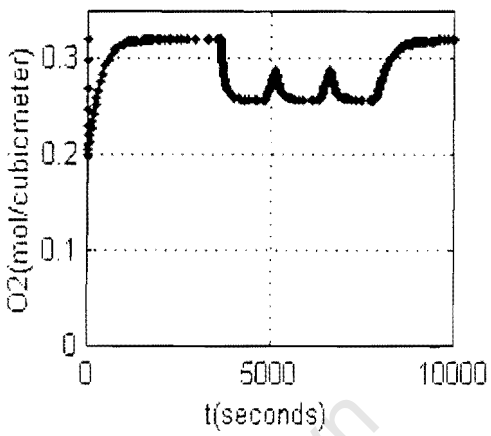

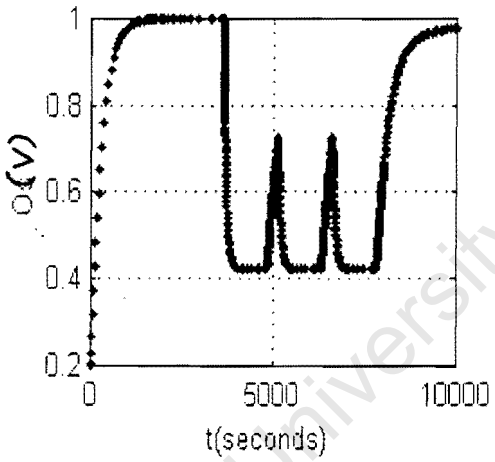

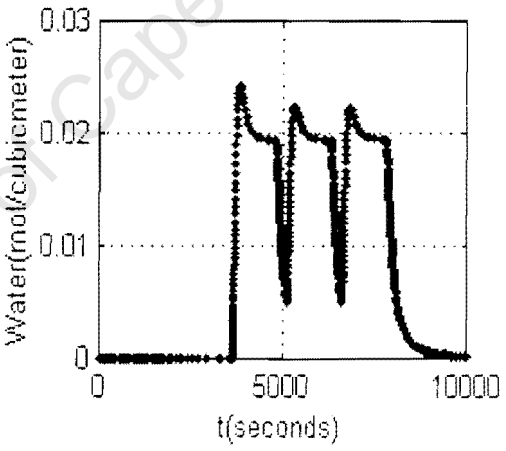

Appendix5(b).1(Cont.) 5min cycling time simulation graphs

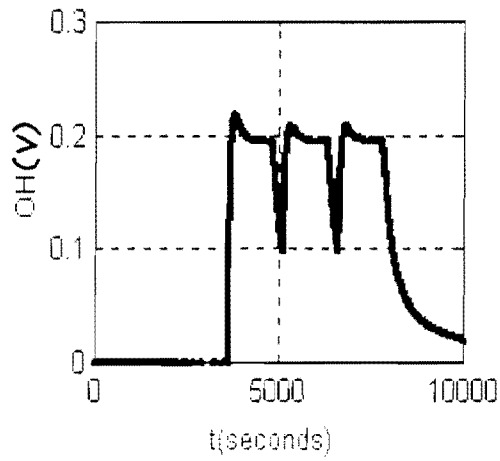

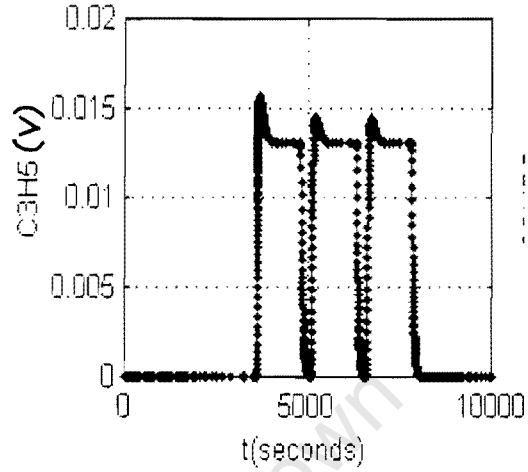

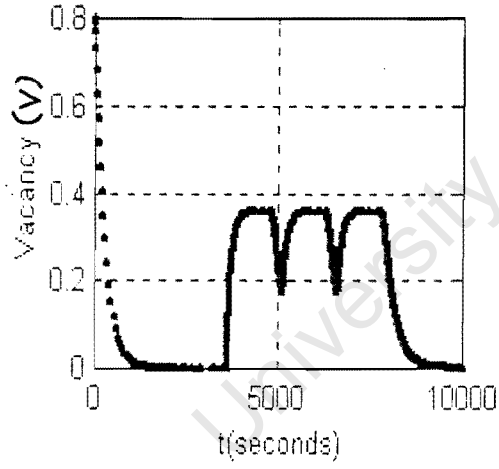

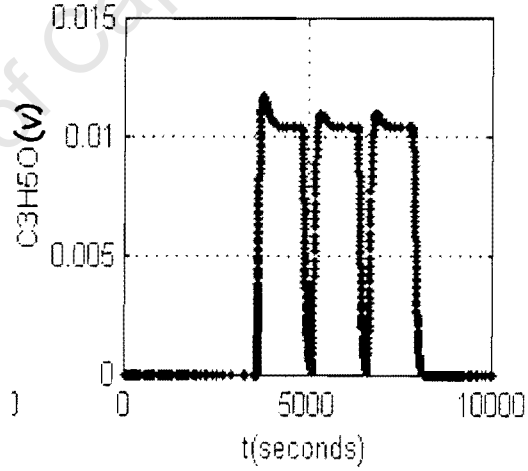

Appendix 5(b).2 10min cycling time simulation graphs

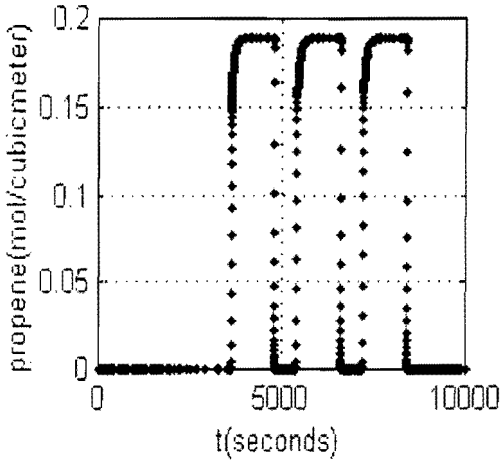

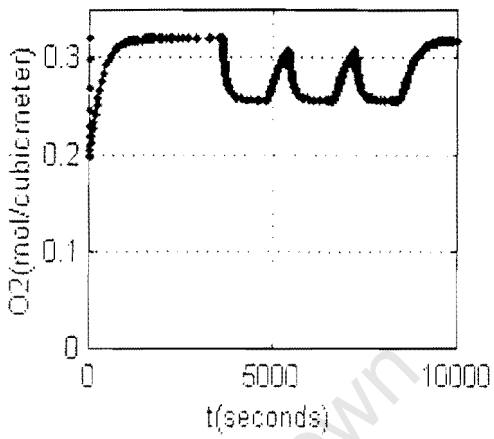

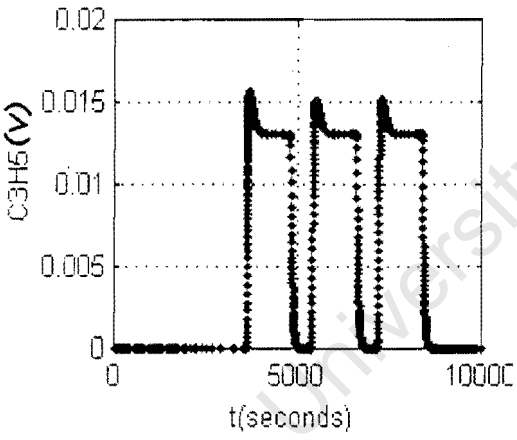

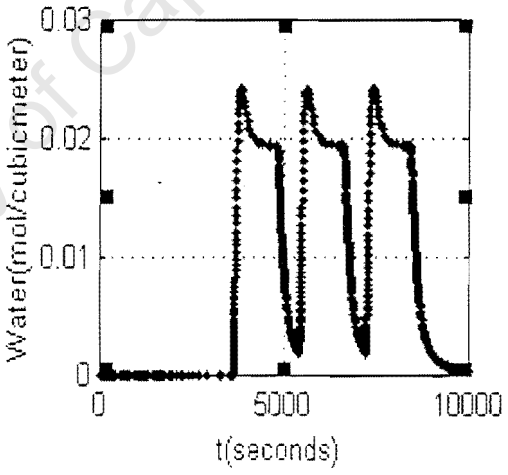

Appendix 5(b).2 (Cont.) 10min cycling time simulation graphs

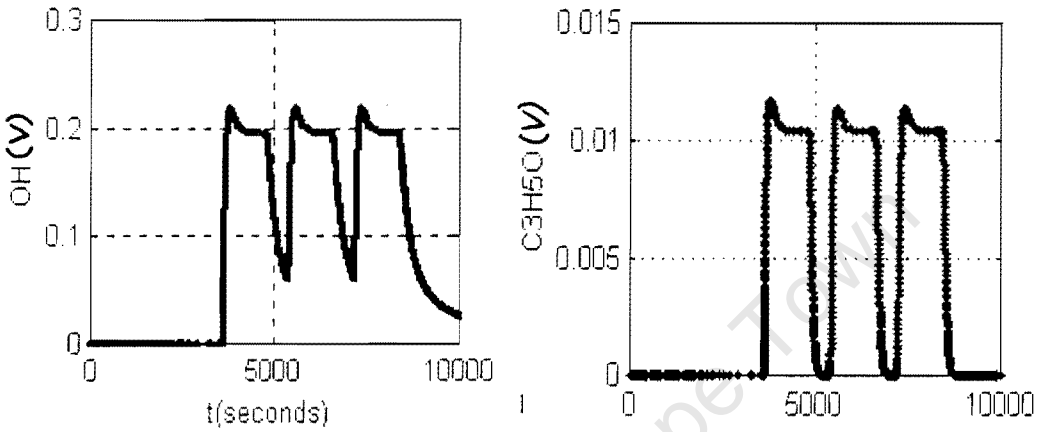

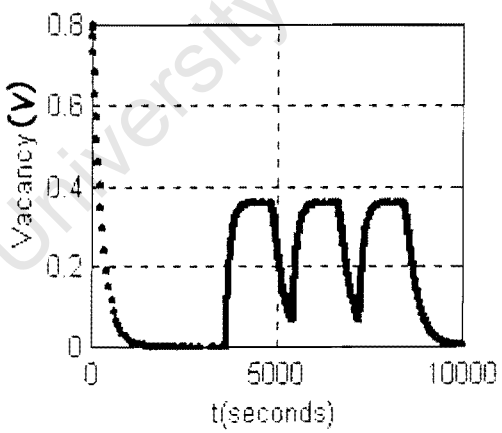

Appendix 5(b).3 20min cycling time simulation graphs

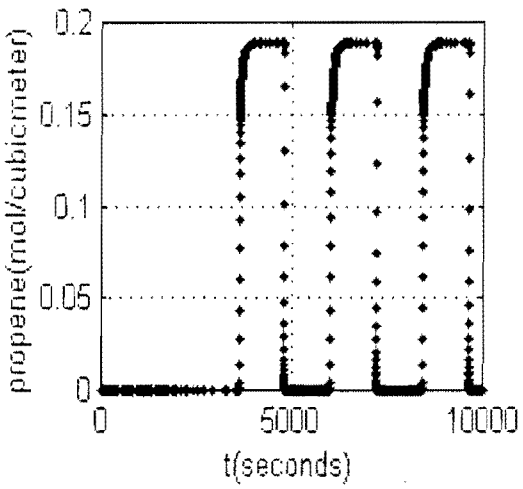

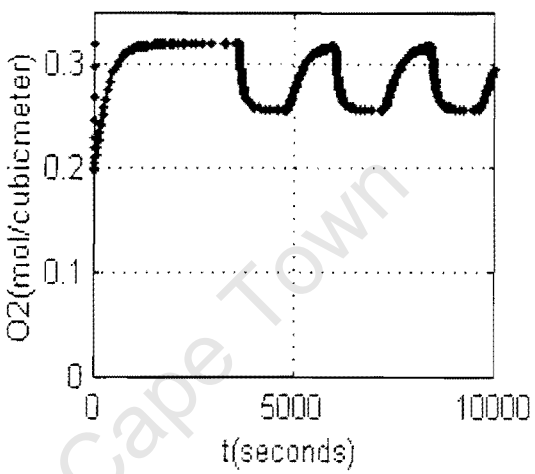

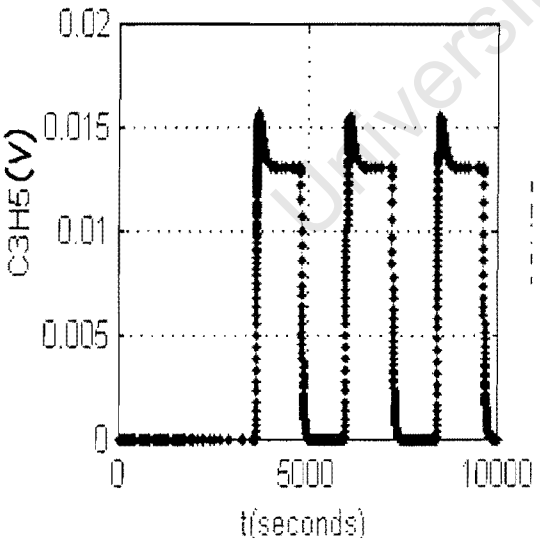

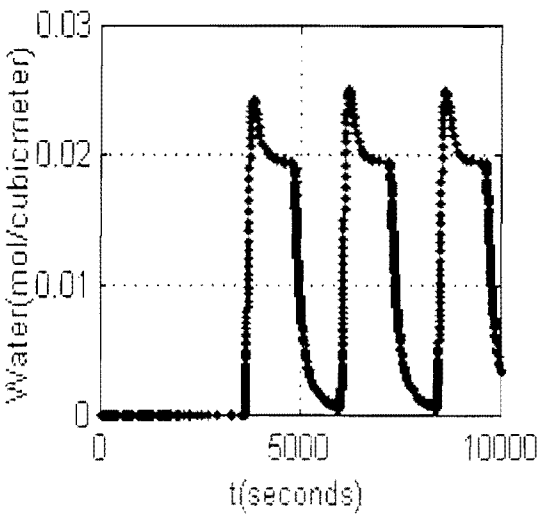

Appendix 5(b).3 (Conti.) 20min cycling time simulation graphs

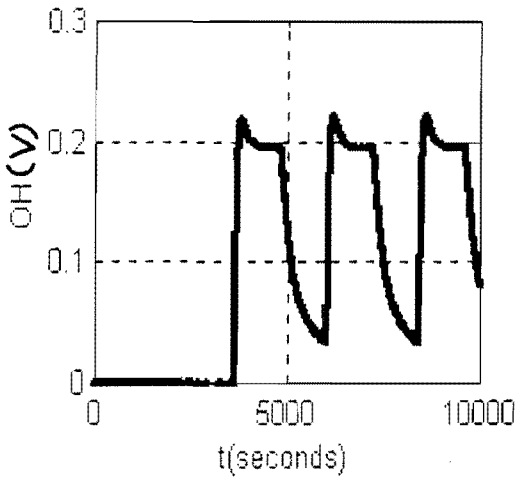

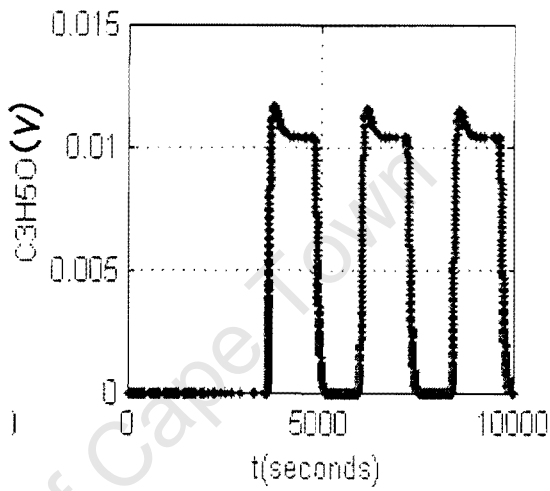

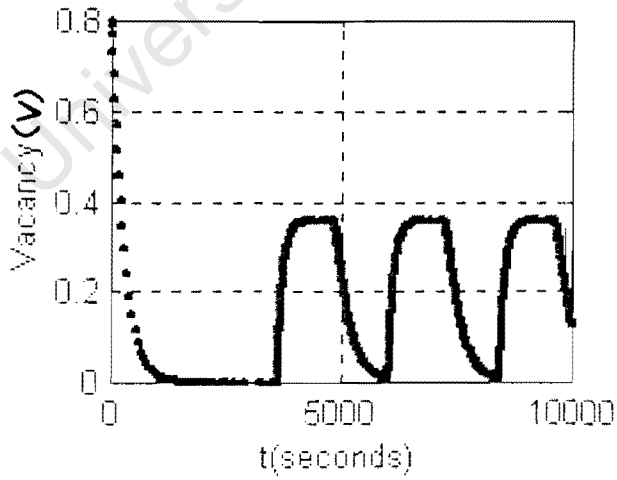

Appendix 5(b).4 30min cycling time simulation graphs

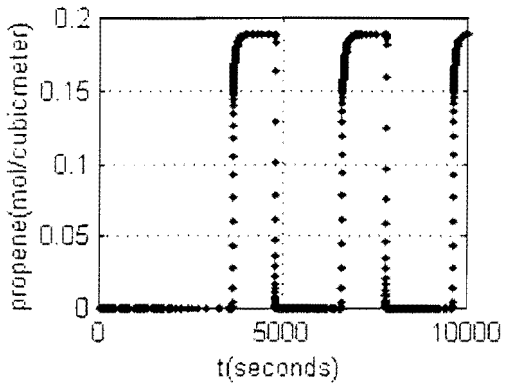

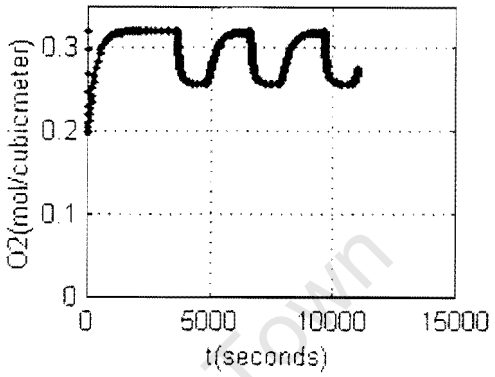

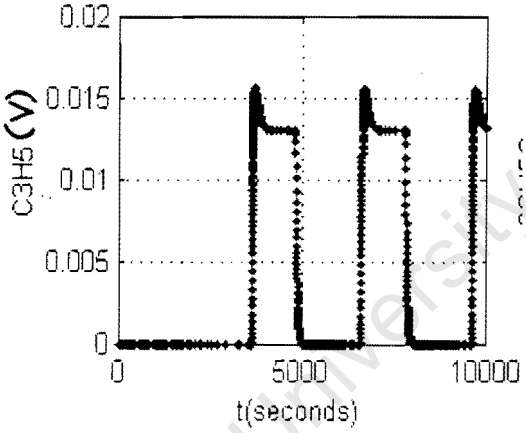

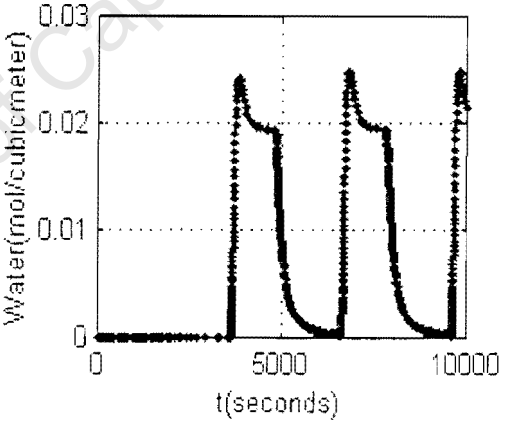

Appendix 5(b).4(Conti.) 30min cycling time simulation graphs

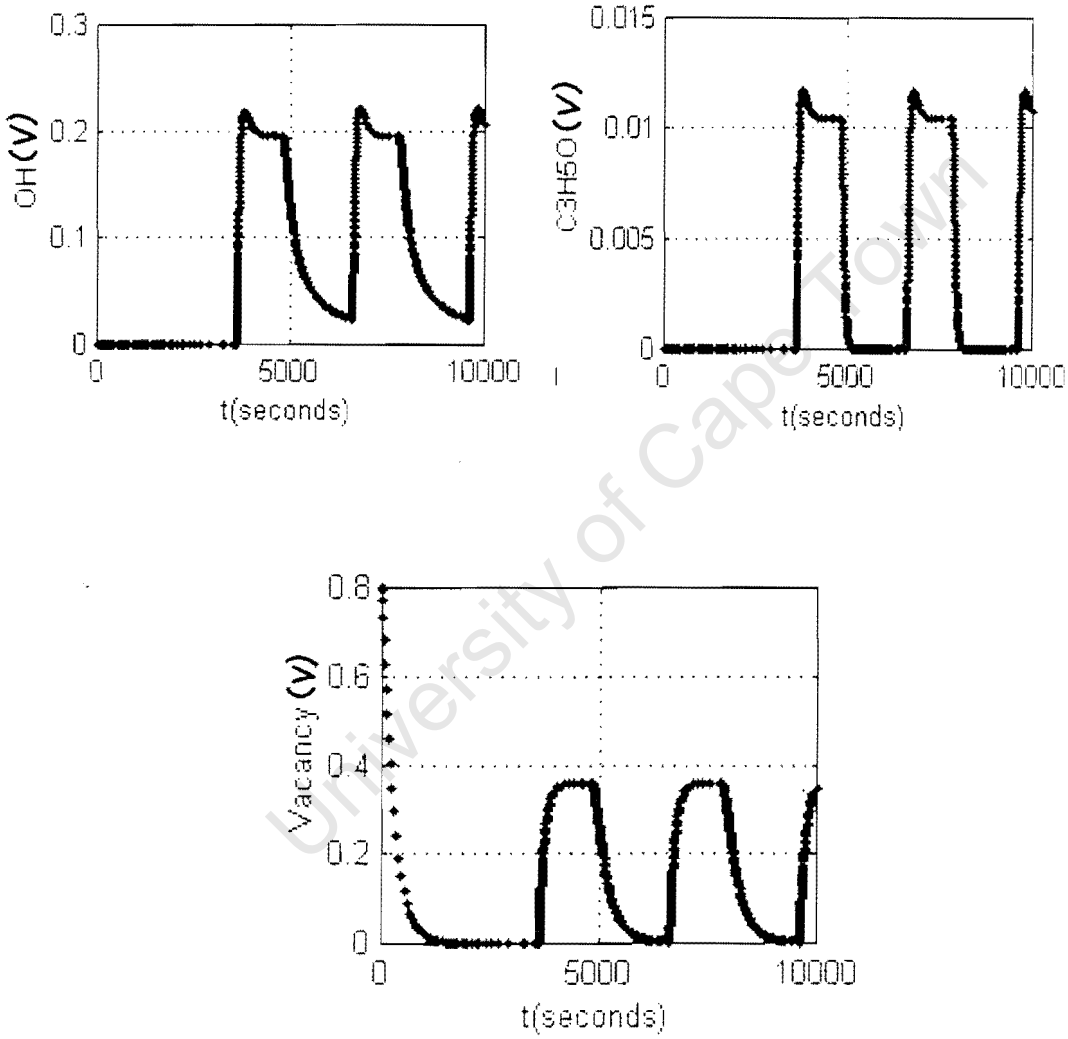

Appendix 5(c).1 10min cycling time simulation graphs n=100.

n denotes the number of monolayers.

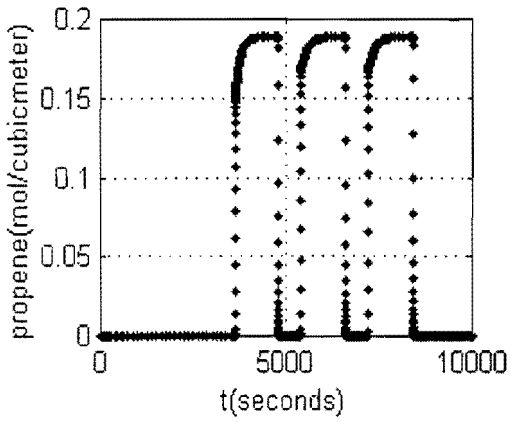

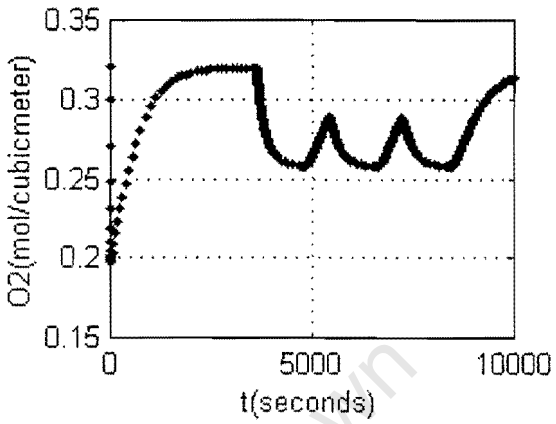

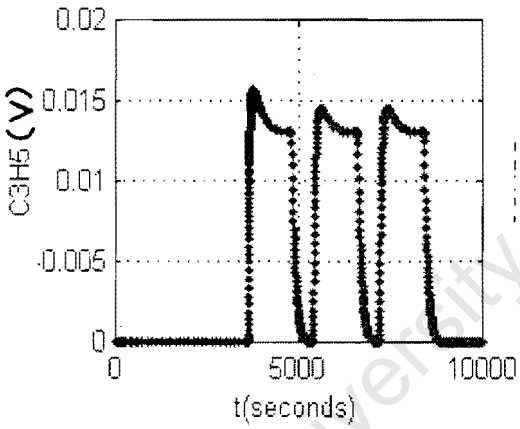

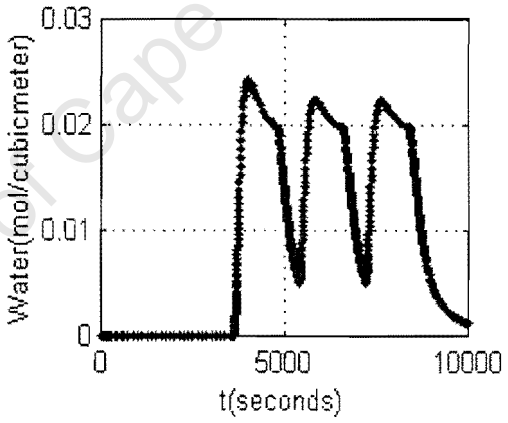

Appendix 5(c).1(Cont) 10min cycling time simulation graphs n=200.

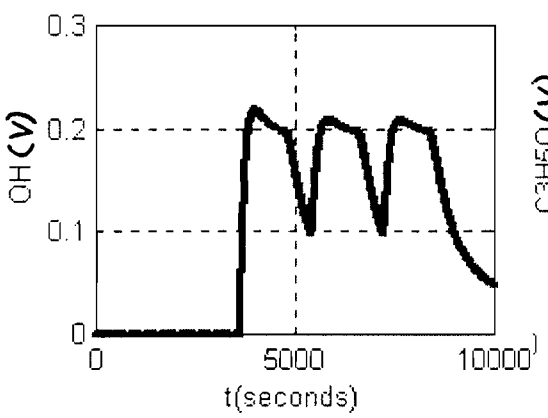

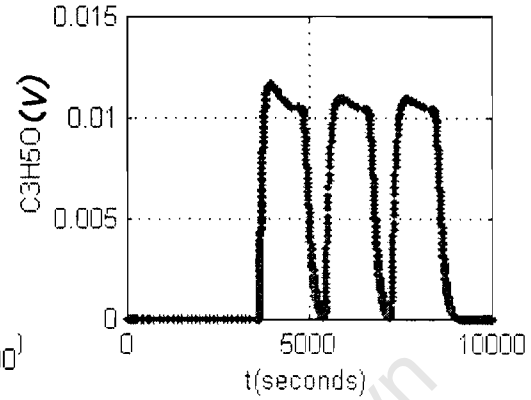

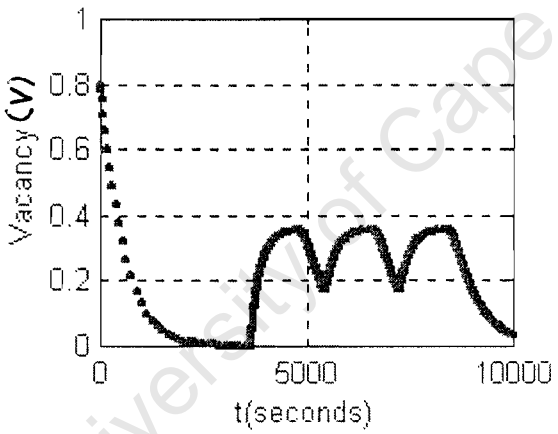

Appendix 5(c).2 10min cycling time simulation graphs n=1.

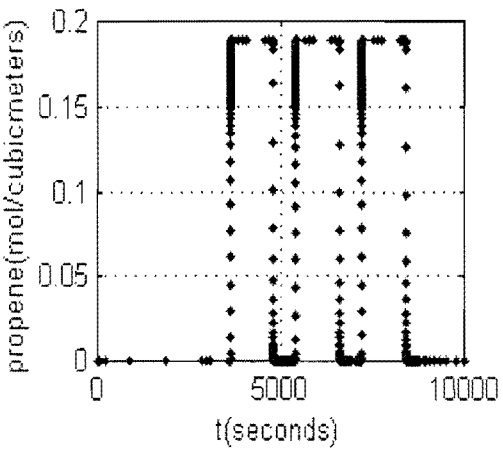

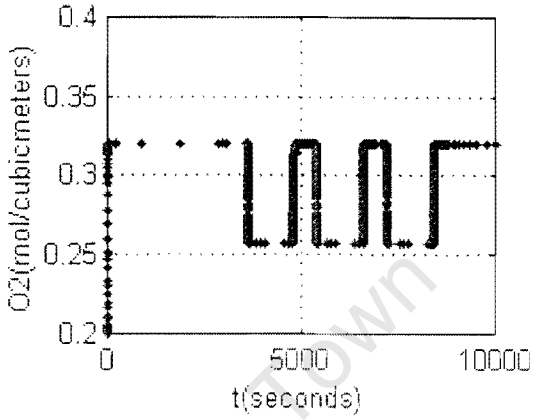

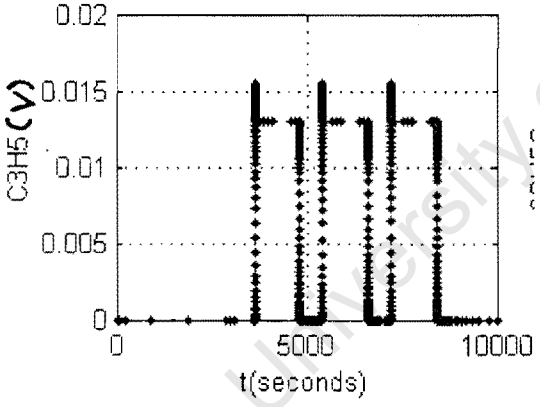

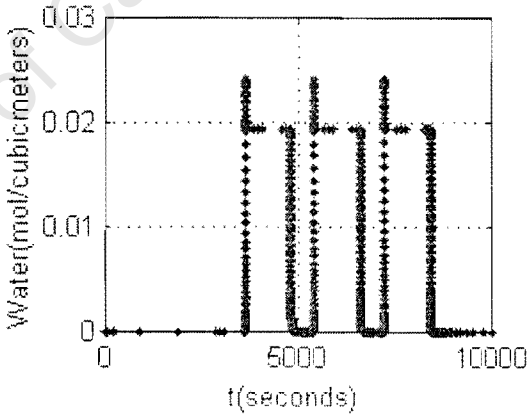

Appendix 5(c).2(Cont) 10min cycling time simulation graphs n=1.

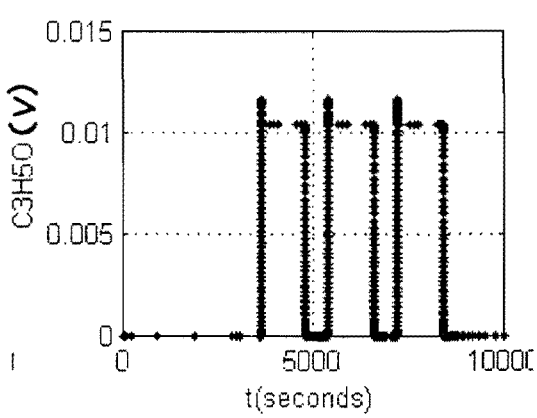

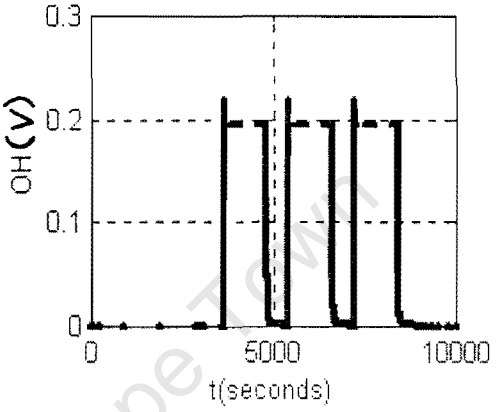

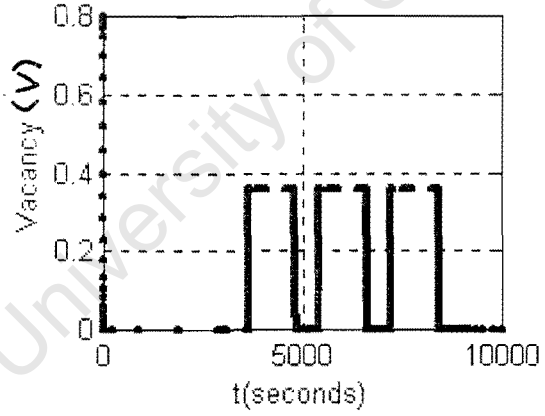

REFERENCES

Allen M. D Poulston S Bithell G E, Goringe M.J Bowker M " XPS, TEM and TPD study of the oxidation and Ammoxidation of Propene using Mixed Fe-Sb oxide Catalyst", J. of Catal. 163 (1996) pg. 204-214.

Aso I, Nakao, M, Yamazoe, N, Seiyama, T., J of Catal, 57,1979,287.

Burriesci,N Garbassi F ,Petrera M and Petrini G, Influence of the bulk and surface properties of iron –Antimony catalyst. J. Chem. Soc.,Faraday Trans. 1, 78, 1982, 817.

Burrington,J.D.,Kartisek,C.T.,Graselli,R.K.,J.Catal.87,363(1984).

Bowker M,Bicknell C.R Kerwin P," Ammoxidation of propane to acrylonitrile of $FeSbO_4$ Applied catalysis, 136,(1996) pg 205-229.

Berry J.F, Holden J.G Michael H Loretto, "Identification of the space groups and detection of cationic ordering in iron antimonate using Convergent –beam electron diffraction" J.Chem.Soc.,Faraday Trans . 1, 1987,83, 615-626.

Bielanski,A ., Haber,J.,Oxygen in Catalysis,Marcel Dekker Inc.,New York,1991,44.

Carbucicchio, M, G. Centi., F J Trifiro., J of Catal., 91,1985, 85.

Contractor, R.M, Horowitz, H.S, Sisler,G.M and Bordes, E.,Catal. Today 37(1997) 51-57.

Creaser,D. ,Andersson, B, Hudgins, R.R, Silveston,P.L.,.Chem.Eng Sci., 54(1999) pg 4437-4448

Callahan,J.L.,Foreman,R.W, Veatch,F, U.S. Pat. 2941007,June 14, (1960)

Chang,H.,Keith,J.M.,Leighton,D.T,Jr.,Ind.Eng.Chem.38(1999)pg667-682.

Dever, J.,J. R., George, K. F., Hoffman,W.C.,Soo,H., In: Kirk-Orthmer Encyclopedia of Chemical Technology , Fourth Edition, (Kroschwitz, J .I ., Howe-Grant, M.,Eds),Vol 15,John Wiley and Sons, New York,1995,903.

Devydov, A.A., Mkhaltchenko, V.G., Sokolskii, V.D., Boreskov, G.K., J. Catal, 55,299 (1978).

Felthouse,T.R ., Burnett,J.C., Mitchell, S.F., Mummey,M.J., In: Kirk-Orthmer Encyclopedia of Chemical Technology , Fourth Edition, (Kroschwitz, J .I ., Howe-Grant, M.,Eds),Vol 15,John Wiley and Sons,New York,1995,pg903.

Fattore,V. Fuhrman,Z.A, Manara,G., Notari,B.,J.Catal,37,(1975b)pg223.

Grasselli, R.K., Suresh, D. D., J. Catal, 25,1972,pg273.

Grasselli, R. K., Burrington, J. D., Adv.Catal. , 30, 1981,pg133.

Gleaves, J. T., Yablonsky,G.S. Shekhtman,S.O., Chem.Eng.Sci. 54(1999) pg4371-4378.

Grasselli, R. K., Burrington, J.D., J.D., Brazdil, J. F., Faraday Discuss. Chem.Soc .,72 , 1982,pg203.

Grasselli, R. K., Callahan, J. L., J. of Catal., 14,1969,93.

Golay,S , O Wolfrath, R Doepper , A Renken .," Model discrimination for reactions with stop effect" ., Elsevier 109(1997) 295.

Haber, J:Heterogenous Hydrocarbon oxidationn,:Warren ,B.K.,Oyama,S.T., eds ACS Symposium Series 638,American Chemical Society ,Washington,20(1996).

Haure, PM., R.R Hudgins P.L Silveston.AICHE., 35(1989)1437.

JCPDS International Centre for Diffraction Data, Swarthmore, 1980.

Keulks, G.W, M . Y . Lo ., J. Phys. Chem., 90,1986,4768.

Keulks, G.W, M . Y .Krenze, L. D., Catal, 84,38,(1983).

Keulks, G.W, Krenzke, K. D ., J.Catal., 64,295(1980).

Kapteijn, F.Moulijn,J.A. Dekker,F.H.M.,Chemical. Eng. Sci.,50(1995)pg3573-3580.

Lang, X. S, Silveston, P. L.,Hudgins,R.R. Canadian J. of Chem.Eng.,69(1991) pg1121.

Lynch, D. T., Can., J. of Chem. Eng, 61, (1983) pg183.

Magagula, Z., van Steen, E., "Time on stream behaviour in the (amm)oxidation of propene/propane over iron antimony oxide :cyclic operation"., Catalysis Today., 49 (1999) 155-160).`

Marengo,S .,Comotti,P. Vasconi,M ., Elsevier.,(1997)pg429.

Marin,G.B,Froment,G.F .,Chem. Eng.Sci.,54(1999) pg4385-4395.

Mars,P, and van Krevelen,D.W.,Chem.Eng.Sci., Suppl.3, 41(1954).

Oyama,S.T., Heterogenous Hydrocarbon Oxidation (Warren,B.K,Oyama,S.T.,eds.),ACS Symposium Series 638,American Chemical Society ,Washington,2(1996).

Pearce, R., W.R Patterson., "Catalysis and Chemical Processes".,pg294,Blackie and Son Ltd ,Bishpbriggs ,Glasgow G64 2NZ.

Rambeau, G., H . Amarigio., Appl. Catal., 1 (1981) 291.

Renken , A.,Lorenzi.M and Dubuis.S., Elserevier, (1997)pg439.

Rinker, R.G , Wilson, H.G ., Chem. Eng. Sci. 37(1980) pg343.

Snider, T. P., G.C Hill ., Catal Rev.-Sci., Eng., 31, 1989,pg-43.

Sala , F and Trifiro ,F., Excess Sb as a promoter in oxidation of Fe-Sb system J. Catal .91 , (1976),93-103.

Saleh-Alhamed.Y.A, Hudgins R.R., Sliveston, P.L., J.of Catal 161,1996 p430-440.

Saleh-Alhamed.Y.A, Hudgins, R. R, Silveston, P. L., Chem. Eng Sci.,47(1992)pg 2885-2890.

Schnobel., M "Partial Oxidation of alpha olefins over iron antimony oxide catalyst" PhD thesis .,(1997)University of Cape Town ,Department of Chemical Engineering"

Silveston, P., R. R Hudgins A Renken., " Periodic Operation of Catalytic reactors-introduction and overview"., Catalysis Today 25(1995) 91-112.

Silveston, P., M Forrissier., Ind. Eng. Chem. Prod. Res. Dev., 24(1985) 320.

Schnobel, M E van Steen., " Kinetics and Selective Oxidation of C_3-C_6 α-olefins over an Iron Antimony Oxide Catalyst., Ind. Eng. Chem. Res. 36(1997), 3568-3575.

Sala, F., Trifira, F., J.Catal.41, 1(1976)

Straguzzi, G.I, Bischoff, K.B., Koch.T.A, Schuit, G.C.A., J.Catal.103, 357(1987a)

Straguzzi, G.I, Bischoff, K.B., Koch.T.A, Schuit, G.C.A., J.Catal.103, 357(1987b)

Tomilov, V.N Zogoruiko, A.N, Kuznetsov, P.A.,Chem.Eng.Sci,54(1999)pg4359-4364

Turek, T.,Thomas, O.,Chem.Eng.Sci.,54(1999)pg4513-4520.

Teller, R.G, Brazdil, J.F, Graselli, R.K., Yelon, W.L., J.Chem. Eng. Soc.,Faraday Trans. 1,81, (1985) pg1693.

Micromeritics instrument manual , Norcross ,GA, USA.

van Steen, E Gunther, Kuwert G , Naidoo A ,Williams M "Influence of Antimony content in the iron antimony oxide catalyst and reaction conditions on the (Amm)Oxidation of propene ," Elsevier Science"p423-432.

Vesser, G., J. Frauhammer. L.D Schmidt. and G Eigenberger.," Catalytic Ignition during methane oxidation on Platinum: Experiments and Modelling., Elsevier 109(1997) 273.

Vamling, L, Technical paper, Chalmers university of Technology, Göthenburg, Sweden (1987).

van Steen,E., M . Schoebel, R Walsh, T., Riedel, Appl. Catal. A 165(1997) 349.

Weissermel.K, Arpe H.J., "Industrial organic chemistry", Third edition, Completely revised edition, VCH publishers, Inc., New York, NY (USA), 1997.

Yamazoe, N.,Aso, I.M ,Anamoto,T., Seiyama,T : New Horizons in Catalysis of the 7th International Congress on Catalysis,Tokyo,1980, Studies in Surface Science and Catalysis 7B(Seyama, T.,Tanabe, K., eds) Kodausha-Elsevier ,Tokyo-Amsterdam ,1239(1981).